



Ministério da
**Ciência, Tecnologia
e Inovação**



sid.inpe.br/mtc-m19/2012/07.31.18.22-TDI

**GEODMA: A TOOLBOX INTEGRATING DATA
MINING WITH OBJECT-BASED AND
MULTI-TEMPORAL ANALYSIS OF SATELLITE
REMOTELY SENSED IMAGERY**

Thales Sehn Korting

Doctorate Thesis at Post Graduation Course applied in Remote Sensing, advised by Drs. Leila Maria Garcia Fonseca, and Gilberto Câmara, approved in August 20, 2012

URL of the original document:

<<http://urlib.net/8JMKD3MGP7W/3CCH86S>>

INPE
São José dos Campos
2012

PUBLISHED BY:

Instituto Nacional de Pesquisas Espaciais - INPE

Gabinete do Diretor (GB)

Serviço de Informação e Documentação (SID)

Caixa Postal 515 - CEP 12.245-970

São José dos Campos - SP - Brasil

Tel.:(012) 3208-6923/6921

Fax: (012) 3208-6919

E-mail: pubtc@sid.inpe.br

BOARD OF PUBLISHING AND PRESERVATION OF INPE INTELLECTUAL PRODUCTION (RE/DIR-204):**Chairperson:**

Marciana Leite Ribeiro - Serviço de Informação e Documentação (SID)

Members:

Dr. Antonio Fernando Bertachini de Almeida Prado - Coordenação Engenharia e Tecnologia Espacial (ETE)

Dr^a Inez Staciarini Batista - Coordenação Ciências Espaciais e Atmosféricas (CEA)

Dr. Gerald Jean Francis Banon - Coordenação Observação da Terra (OBT)

Dr. Germano de Souza Kienbaum - Centro de Tecnologias Especiais (CTE)

Dr. Manoel Alonso Gan - Centro de Previsão de Tempo e Estudos Climáticos (CPT)

Dr^a Maria do Carmo de Andrade Nono - Conselho de Pós-Graduação

Dr. Plínio Carlos Alvalá - Centro de Ciência do Sistema Terrestre (CST)

DIGITAL LIBRARY:

Dr. Gerald Jean Francis Banon - Coordenação de Observação da Terra (OBT)

DOCUMENT REVIEW:

Marciana Leite Ribeiro - Serviço de Informação e Documentação (SID)

Yolanda Ribeiro da Silva Souza - Serviço de Informação e Documentação (SID)

ELECTRONIC EDITING:

Ivone Martins - Serviço de Informação e Documentação (SID)



Ministério da
**Ciência, Tecnologia
e Inovação**



sid.inpe.br/mtc-m19/2012/07.31.18.22-TDI

**GEODMA: A TOOLBOX INTEGRATING DATA
MINING WITH OBJECT-BASED AND
MULTI-TEMPORAL ANALYSIS OF SATELLITE
REMOTELY SENSED IMAGERY**

Thales Sehn Korting

Doctorate Thesis at Post Graduation Course applied in Remote Sensing, advised by Drs. Leila Maria Garcia Fonseca, and Gilberto Câmara, approved in August 20, 2012

URL of the original document:

<<http://urlib.net/8JMKD3MGP7W/3CCH86S>>

INPE
São José dos Campos
2012

Cataloging in Publication Data

K845g Korting, Thales Sehn.
Geodma: a toolbox integrating data mining with object-based and multi-temporal analysis of satellite remotely sensed imagery / Thales Sehn Korting. – São José dos Campos : INPE, 2012.
xxiv + 97 p. ; (sid.inpe.br/mtc-m19/2012/07.31.18.22-TDI)

Doctorate (Remote Sensing) – Instituto Nacional de Pesquisas Espaciais, São José dos Campos, 2012.
Advised : Drs. Leila Maria Garcia Fonseca, and Gilberto Câmara.

1. data mining. 2. image processing. 3. remote sensing. 4. computer systems. I.Título.

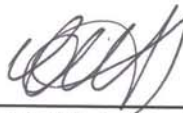
CDU 528.854

Copyright © 2012 do MCT/INPE. Nenhuma parte desta publicação pode ser reproduzida, armazenada em um sistema de recuperação, ou transmitida sob qualquer forma ou por qualquer meio, eletrônico, mecânico, fotográfico, reprográfico, de microfilmagem ou outros, sem a permissão escrita do INPE, com exceção de qualquer material fornecido especificamente com o propósito de ser entrado e executado num sistema computacional, para o uso exclusivo do leitor da obra.

Copyright © 2012 by MCT/INPE. No part of this publication may be reproduced, stored in a retrieval system, or transmitted in any form or by any means, electronic, mechanical, photocopying, recording, microfilming, or otherwise, without written permission from INPE, with the exception of any material supplied specifically for the purpose of being entered and executed on a computer system, for exclusive use of the reader of the work.

Aprovado (a) pela Banca Examinadora
em cumprimento ao requisito exigido para
obtenção do Título de **Doutor(a)** em
Sensoriamento Remoto

Dra. Claudia Maria de Almeida



Presidente / INPE / São José dos Campos - SP

Dra. Leila Maria Garcia Fonseca



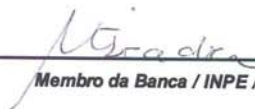
Orientador(a) / INPE / SJC Campos - SP

Dr. Gilberto Câmara



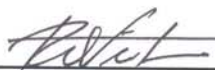
Orientador(a) / INPE / SJC Campos - SP

Dra. Maria Isabel Sobral Escada



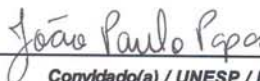
Membro da Banca / INPE / SJC Campos - SP

Dr. Raul Queiroz Feitosa



Convidado(a) / PUC- RIO / Rio de Janeiro - RJ

Dr. João Paulo Papa



Convidado(a) / UNESP / Bauru - SP

Dr. Alexandre Noma



Convidado(a) / UFABC / Santo André - SP

Este trabalho foi aprovado por:

() maioria simples

(x) unanimidade

Aluno (a): **Thales Sehn Korting**

São José dos Campos, 20 de Agosto 2012

*To my wife **Aline**, to my daughter **Lara**,
and to my parents **Elade** and **Clóvis***

ACKNOWLEDGEMENTS

In portuguese.

A minha esposa Aline Freire Korting, que me acompanhou e incentivou em todo o doutorado, com carinho, paciência e amor. A minha filha Lara Freire Korting, que em pouco tempo me cativou, emocionou e motivou a completar este doutorado. A meus pais Elade Sehn Korting e Clóvis de Lima Korting, que com amor sempre me deram forças para estudar. Ao carinho de Alba Regina Poester Freire, Vó Elga Sehn, Vó Rosa de Lima Korting, Nelsi Sehn e Delcy Oliveira Sehn.

À Dra. Leila Maria Garcia Fonseca, pela paciência, motivação, e amizade com que me acompanhou e orientou nestes anos de estudo. Ao Dr. Gilberto Câmara pelas importantes considerações sobre os métodos propostos neste trabalho.

Ao Dr. Antônio Miguel Vieira Monteiro pela amizade e incentivo. Ao CNPq, à Capes, e à Fapesp pelo apoio financeiro.

E um agradecimento geral, pois seria impossível descrever todas as importantes contribuições que recebi.



ABSTRACT

The deployment of a new generation of sensors over the last 20 years has made satellite remotely sensed imagery a very important source of spatial data available for environmental studies of large-scale geographic phenomena. The variety of spatial, temporal and spectral resolutions for remote sensing images is large, ranging from panchromatic images to polarimetric radar images. Despite the great experience in image data gathering and distribution and a diversity of image processing and analysis toolboxes, it is still difficult to find image analysis systems that provide a straightforward fully integrated environment to transform multi-temporal and multi-resolution satellite image data into meaningful information. Taking this into account, the contribution of this thesis is two-fold. Firstly, we propose and implement a new toolbox, developed under the Free and Open Source Software (FOSS) foundation, for integrating remote sensing imagery analysis methods with data mining techniques producing a user-centered, extensible, rich computational environment for information extraction and knowledge discovery over large geographic databases. The toolbox is called GeoDMA – Geographic Data Mining Analyst. It integrates techniques of segmentation, feature extraction, feature selection, classification, landscape metrics and multi-temporal methods for change detection and analysis with decision-tree based strategies adapted for spatial data mining. It gathers remotely sensed imagery with other geographic data types using access to local or remote databases. GeoDMA provides simulation methods to assess the accuracy of process models as well as tools for spatio-temporal analysis, including a visualization scheme for temporal profiles that helps users to describe patterns in cyclic events. Secondly, we develop a new approach for analyzing spatio-temporal data based on a polar coordinates transformation that allows creating a new set of features which improves the classification accuracy of multi-temporal image databases. As GeoDMA was built on top of TerraView GIS, thematic maps and other results can be produced rapidly, taking advantage of the basic GIS functionalities. To demonstrate the features of GeoDMA toolbox, five (5) case studies, applied in contexts of land use and land cover change, were carried out in different application domains. Evaluations of these experiments pointed out that the GeoDMA toolbox achieved results with a level of integration, from a user perspective, that could not be found elsewhere.

GEODMA: UMA FERRAMENTA PARA INTEGRAR MINERAÇÃO DE DADOS COM ANÁLISE MULTI-TEMPORAL E ORIENTADA A OBJETOS DE IMAGENS DE SENSORIAMENTO REMOTO

RESUMO

O desenvolvimento de uma nova geração de sensores nos últimos 20 anos consolidou as imagens de sensoriamento remoto como uma importante fonte de dados para estudos ambientais e fenômenos geográficos em larga escala. É grande a variedade de resoluções (espacial, temporal e espectral) das imagens de sensoriamento remoto, desde pancromáticas até imagens polarimétricas. Apesar da grande experiência em coleta, armazenamento e distribuição de imagens e da diversidade de ferramentas computacionais para processamento e análise, ainda é difícil de se encontrar sistemas que apresentem um ambiente integrado para transformar imagens multi-temporais e de diversas resoluções em informação útil. Tendo em vista este panorama, a contribuição desta tese é dupla. Em primeiro lugar, propomos e implementamos uma nova ferramenta, seguindo os padrões de código-fonte aberto (*Free and Open Source Software – FOSS*), para integrar métodos de análise de imagens com técnicas de mineração de dados, visando produzir um ambiente computacional extensível e focado no usuário, aplicado à extração de informações e à descoberta de conhecimento em grandes bases de dados geométricos. Esta ferramenta é chamada GeoDMA – *Geographic Data Mining Analyst* (mineração de dados geográficos). GeoDMA integra técnicas de segmentação de imagens, extração e seleção de atributos, classificação, métricas da ecologia da paisagem, métodos de análise multi-temporal para detecção de mudanças e classificação por métodos de árvores de decisão adaptados à mineração de dados espaciais. O sistema agrega imagens de sensoriamento remoto com outros tipos de dados geográficos através do acesso a bancos de dados locais ou remotos. GeoDMA também provê métodos de simulação para avaliar a acurácia dos modelos, e ferramentas para análise espaço-temporal, incluindo um esquema de visualização de perfis temporais que auxilia os usuários a descrever padrões em eventos cíclicos. Em segundo lugar, desenvolvemos um novo método para analisar dados espaço-temporais baseados na transformação dos perfis em coordenadas polares, o que permite a geração de um novo conjunto de atributos que aumenta a acurácia da classificação de imagens multi-temporais. O sistema GeoDMA foi construído como uma extensão do SIG TerraView, e por isso mapas temáticos e demais resultados são produzidos rapidamente, aproveitando-se das funcionalidades deste SIG. Para demonstrar as ferramentas do GeoDMA, cinco (5) casos de estudo, aplicados em diferentes contextos de detecção de uso e cobertura da terra, foram realizados usando dados de diferentes domínios. A avaliação destes experimentos, do ponto de vista do usuário, mostrou que a ferramenta obteve os resultados com um nível de integração não encontrado em sistemas semelhantes.

LIST OF FIGURES

	<u>Pág.</u>
2.1 Scale of objects considered in landscape ecology. Patch (left), Class (center), and Landscape (right) metrics.	8
2.2 The flowchart of KDD. DM appears as a step in the full process that transforms raw data into knowledge.	12
2.3 EVI2 profile example from 2000 to 2011, the range of values is [0,1]. . . .	15
3.1 User interface for GeoDMA.	22
3.2 User interface for Terraview.	23
3.3 GeoDMA: diagram of the main processing steps for image analysis. . . .	24
3.4 Creating input data – Multi-temporal images define cycles and segmentation defines objects from raster.	24
3.5 Interface for segmentation: the interpreter selects the algorithm and sets the thresholds. Regions obtained in the segmentation process are stored in the database as vector format.	25
3.6 Feature extraction – Spectral and Spatial features use raster and vector objects. Landscape ecology features use class information of objects. Multi-temporal features use cycles’ information.	27
3.7 Visual representation of the segmentation-based spectral and spatial features. Several features can be extracted in the highlighted region. Spectral features include metrics for maximum and minimum pixel values, or mean values. Spatial features measure the height, width, or rotation. . . .	28
3.8 Some <i>Basic</i> features obtained from time series: maximum, minimum, amplitude, integral values.	30
3.9 When the values of the cycle are associated to a certain angle (left), the closed shape is created from its polar transformation (right).	31
3.10 Relation between the four seasons and EVI2 values using polar representation.	32
3.11 Classification interface. The interpreter selects the input features, sets output parameters, and defines the classification algorithm.	33
3.12 The interface for classification. The interpreter must select the input features, set output parameters, and define the classification algorithm. .	33
3.13 Visualizing data in the feature space using a scatterplot, similar to eCognition’s module (LANG et al., 2007).	34

3.14	Spatialization of the <i>mode</i> feature. Brighter objects define regions with higher values of mode whereas darker objects define regions with lower mode values, similar to eCognition’s module (LANG et al., 2007).	35
3.15	The multi-temporal visualization module in GeoDMA. The interpreter visualizes a specific cycle and the polar transformation of the cycle by selecting a point in the image.	36
3.16	Interface for sample selection.	37
3.17	a) Splitting feature <i>pixel_mean</i> in the value of 70, and b) Splitting feature <i>area</i> in the value of 50.	39
3.18	Thematic map is the output when applying the classification model to all objects stored in the database.	43
3.19	The interface of the Monte Carlo simulation in GeoDMA.	44
4.1	Intra-urban high-resolution image for land cover classification.	48
4.2	Segmentation of high-resolution image for land cover classification with parameters of <i>scale</i> = 15, <i>compactness</i> = 40% and <i>color factor</i> = 40%.	49
4.3	The decision tree model for intra-urban land cover classification in a region of São Paulo city, Brazil.	50
4.4	Intra-urban land cover map using (top) GeoDMA and (bottom) Inter-IMAGE.	52
4.5	Study area for detecting urban landscape patterns (ULP), highlighted in yellow.	53
4.6	The decision tree model to detect the ULPs.	55
4.7	ULP map obtained by GeoDMA.	55
4.8	Study area: region of São Félix do Xingu, Pará state, Brazil.	57
4.9	Deforestation patches in São Félix do Xingu, Brazil, for 2006 (top) and 2009 (bottom).	60
4.10	The classification model for deforestation patterns.	61
4.11	Thematic map for data of 2006 and 2009 using GeoDMA. Overlapping regions define land changes occurred between 2006 and 2009.	61
4.12	Thematic map produced by eCognition. Overlapping regions define land changes occurred between 2006 and 2009. Red cells were not classified.	62
4.13	Mato Grosso state, Brazil.	63
4.14	Kappa values in the Monte Carlo simulation in the multi-temporal land cover mapping.	65
4.15	Classification model for the <i>Basic + Polar</i> set of features, with 13 leaves and Kappa = 0.81. In the nodes, (B) and (P) stand for basic and polar features, respectively.	66
4.16	Reference map (top), and land cover map (bottom).	69

4.17	Polar visualization of <i>single</i> (left) and <i>double</i> (right) classes at approximately 30 cycles per class.	70
4.18	Kappa values in the Monte Carlo simulation in the detection of single and double cropping.	70
4.19	Classification model for the <i>Basic + Polar</i> set of features, with 2 leaves and Kappa = 0.8.	70
4.20	Classification of single and double croppings for the years 2008, 2009 (top), and 2010 (bottom), in the Mato Grosso state (Lat. 11°34'23"S, Lon. 54°43'14" W).	71
4.21	Mapping the area (Km ²) of <i>single</i> and <i>double</i> croppings for the years 2008, 2009, and 2010.	72
4.22	Land change map produced from land cover maps for the years 2008, 2009 and 2010.	72
4.23	Area (Km ²) of land change patterns over a 3-year period (2008 to 2010), taking the cropland map of TerraClass as reference.	73

LIST OF TABLES

	<u>Pág.</u>
2.1 Softwares used in the remote sensing applications.	18
4.1 Typology for land cover using intra-urban imagery.	51
4.2 Typology for the 9 Urban Landscape Patterns.	54
4.3 Typology for deforestation patterns in the Brazilian Amazon.	56
4.4 Classification evaluation for GeoDMA and eCognition.	58
A.1 Segmentation-based spectral features.	93
A.2 Segmentation-based spatial features.	94
A.3 Landscape-based features. When the unit is hectares, the value is divided by 10^4	95
A.4 Temporal features for describing cyclic events.	96

LIST OF ABBREVIATIONS

BFAST	–	Breaks For Additive Seasonal and Trend
DFT	–	Discrete Fourier Transform
DM	–	Data Mining
EVI	–	Enhanced Vegetation Index
FOSS	–	Free and Open Source Software
FCM	–	Fuzzy Markov Chain
GeoDMA	–	Geographic Data Mining Analyst
GIS	–	Geographic Information Systems
GLCM	–	Gray-Level Cooccurrence Matrix
GUI	–	Graphic User Interface
KDD	–	Knowledge Discovery in Databases
LAI	–	Leaf Area Index
LCM	–	Land-cover Change Mapper
MODIS	–	Moderate Resolution Imaging Spectroradiometer
NDVI	–	Normalized Difference Vegetation Index
OBIA	–	Object-Based Image Analysis
SOM	–	Self-Organizing Maps
SVM	–	Support Vector Machines
ULP	–	Urban Landscape Pattern

LIST OF SYMBOLS

$H(p_1, p_2, \dots p_N)$	– Entropy
$info(v_1, v_2, \dots v_N)$	– Information value
μ_{pq}	– Central moment of order p and q
px	– pixel(s)
p_{ij}	– Normalized frequency of neighboring pixels, based on GLCM
w_{ij}	– Neuron from SOM at position (i, j)

CONTENTS

	<u>Pág.</u>
1 INTRODUCTION	1
1.1 Document Organization	5
2 REVIEW	7
2.1 Landscape ecology concepts	7
2.2 Object-Based Image Analysis	9
2.3 Data Mining	11
2.4 Multi-temporal analysis	13
2.5 Comments	18
3 GeoDMA – GEOGRAPHIC DATA MINING ANALYST	21
3.1 Defining the input data	24
3.1.1 Segmentation	25
3.1.2 Cycles detection	26
3.1.3 Creation of cellular space	27
3.2 Feature extraction	27
3.2.1 Segmentation-based features	28
3.2.2 Landscape-based features	29
3.2.3 Multi-temporal features	29
3.2.3.1 Basic features	29
3.2.3.2 Polar features	29
3.3 Data mining to detect land cover and change patterns	32
3.3.1 Building a training set	35
3.3.2 Classification using decision trees	36
3.3.3 Classification using self-organizing maps	41
3.4 Evaluation of classification	42
3.4.1 Accuracy assessment	43
3.4.2 Change detection	44
3.4.2.1 Direct changes	45
3.4.2.2 Trajectories of change	45
4 CASE STUDIES	47
4.1 Land cover using intra-urban imagery	47

4.2	Detection of urban landscape patterns	53
4.3	Analysis of deforestation patterns in the Brazilian Amazon	56
4.4	Exploring the multi-temporal analysis for land use and cover mapping . .	63
4.4.1	Land cover mapping	64
4.4.2	Detection of single and double cropping	66
4.4.2.1	Land change detection	67
4.5	Discussion	74
5	CONCLUSION	75
	REFERENCES	77
	APPENDIX A - TABLES OF FEATURES	93

1 INTRODUCTION

Computers are each day allowing the automation of more and more tasks that in the past were performed manually. For a large amount of data, the execution of manual tasks is difficult and time-consuming. On the other hand, in certain cases the automation appears to be stealing the place of humans in diverse aspects of the ordinary life. Hence, the balance of automating tasks seems to be coupling the human expertise with the capacity of computers to perform fast and accurate processing.

A good example of combining human knowledge with computational skills occurs in the Geographic Information Science – GIScience, where the amount of information to be gathered and analyzed is tremendous. According to Goodchild (2004), GIScience is a subfield of information science that is particularly attractive to information scientists because of the well-defined nature of geographic information. It studies how geographic knowledge is represented in the human brain, in order to make systems more readily understood and usable by humans.

GIScience addresses issues raised by the use of Geographic Information Systems (GIS) relating information technologies such as remote sensing. According to Bradley et al. (2007), remote sensing data is the only source capable of providing a continuous and consistent set of information about the Earth’s land and oceans. Combined with ecosystem models, remotely sensed data offers an unprecedented opportunity for predicting and understanding the behavior of the Earth’s ecosystem (TAN et al., 2001b). Since Landsat-1 in 1973, satellites have provided a rich data set that helps us to map land changes at the surface of our planet. Sensors with high spatial and temporal resolutions that capture precisely spatio-temporal structures in dynamic scenes are becoming more accessible. Temporal components integrating spectral and spatial dimensions also result in a valuable information source for detecting changes (BRUZZONE et al., 2003).

Remote sensing imagery provides information on land cover, which does not translate exactly into land use or land change information (MCCAULEY; GOETZ, 2004). But how to retrieve such rich information from a remotely sensed image? According to Câmara et al. (2001), despite over 30 years of experience in data gathering, processing and analysis of remote sensing imagery, it continues to be difficult to answer a basic question, “What’s in an image?”. To interpret images with the guide of a computational tool, they can be partitioned into regions, or objects, which exist only in virtue of the different sorts of demarcations effected cognitively by human beings (SMITH, 1995). These objects are explored as an instrument for capturing

landscape dynamics. Besides, there is a significant amount of reusable knowledge obtained by interpreting images which can be used to retrieve information in more images.

Although remote sensing techniques are a good alternative for mapping land use and land cover patterns, the manipulation of a great amount of data is a challenging task. According to Fayyad et al. (1996), our ability to analyze and understand massive datasets lags far behind our ability to gather and store the data. For example, the acquisition rate for IKONOS satellite is about 890 megapixels each minute (DIAL et al., 2003); for CBERS-2B it was about 120 megapixels each minute. Current human and technological resources for manual and semiautomatic data analysis are far slower than these rates (WASSENBERG et al., 2009). Besides, the pool of information provided by satellites allows revealing complex and important patterns in applications connecting environmental monitoring and analysis of land cover dynamics. In many cases, hundreds of independent features need to be simultaneously considered in order to accurately model a system’s behavior (GOEBEL, 1999). Therefore, humans need assistance in their analysis capacity. Consequently, it is necessary to have computationally efficient image analysis algorithms to manipulate and analyze the huge amount of data to better extract the information to be used in remote sensing applications.

During the 1980s and 1990s, most remote sensing image analysis techniques were based on per-pixel statistical algorithms (BLASCHKE, 2010). These techniques aimed at representing the knowledge about land cover patterns in terms of a limited set of parameters, such as average and standard deviation values of groups of individual pixels. Further research on image interpretation concluded that the set of parameters could be extended, and some techniques could be created to better represent the knowledge behind the image analysis. Recently, Object-Based Image Analysis (OBIA) has shown to be a good alternative to traditional per-pixel and region based approaches. Differently, they first identify regions in the image, extract neighborhood, spectral and spatial features and afterwards use them to classify the objects. Although segmentation has a large tradition in remote sensing (HARALICK; SHAPIRO, 1985; BINS et al., 1996), OBIA took a long time to reach mainstream users. This approach became popular when it combined image segmentation with good labeling methods that match the objects features to those of user-defined classes. Most successful software packages, either proprietary like eCognition (LANG et al., 2007) or ENVI Feature Extraction (INTERNATIONAL TELEPHONE & TELEGRAPH EXELIS, 2008), or the open source InterIMAGE (COSTA et al., 2010), have used semantic net-

works to analyze the objects. Semantic networks resemble decision trees; at each tree node there is a rule that defines the class to which the data belongs. A rule combines operation (e.g., segmentation, band ratio) with restriction on feature values (e.g., ‘select all objects with an average value greater than 100’). However, remote sensing image analysis using OBIA can be lengthy and complex because of the processing difficulties related to image segmentation, the large number of object attributes to be resolved and the many different methods needed to model the hierarchical networks (HAY; CASTILLA, 2008; PINHO et al., 2008).

Despite the success of using semantic networks in the image analysis, the main bottleneck is the feature selection phase. We have to find metrics that best describe the object properties as well as select features that best distinguish between objects. Current software extract a huge amount of statistics (mean value, standard deviation), spatial (area, perimeter, shape), color, texture, and topology (distance to neighbors, relative border) features. To obtain accurate classification, the feature selection often relies on ad hoc decisions about what should describe an object. Another problem is that land cover classes in most environments are not pure, or spatially homogeneous. Thus, scene models for classification usually present a nested structure, analyzing scenes in multiple scales (WOODCOCK; STRAHLER, 1987). An alternative is to use a theory that makes some hypothesis about the object properties defined within an application context. Such theory would provide metrics to extract object properties. Within this context, landscape ecology can help to define metrics by elaborating landscape types as *ecologically meaningful units*. Such land units can be used as the basis for analysis and assessment (GROOM et al., 2006).

Another question concerns how to build a semantic network for interpretation task. Users experience points out that there are no hard-and-fast rules for building such networks, and this task may require considerable time and expertise (LANG, 2008). On the other hand, the number of available features makes a detailed feature exploratory analysis a time-consuming task and dependent on expertise. In this case, data mining techniques can be useful to extract information from large databases where objects being classified are described through many features (TAN et al., 2001a; SILVA et al., 2008; STEIN et al., 2009; PINHO et al., 2012).

In spite of the considerable advances made over the last few years in high resolution satellite data, image analysis tools, and services, end users still lack effective and operational tools to help them manage and transform this data into useful information that can be used for decision making and policy planning purposes. For

instance, in many remote sensing applications the user needs different tools to execute the processing steps (ADDINK et al., 2007; FERRAZ et al., 2005; FROHN; HAO, 2006; HÄTTICH et al., 2009; RIBEIRO et al., 2009). This introduces more challenges for the researchers such as data integration, conversion of data format, knowledge of the software to be used, files replication, and other problems that make difficult the data analysis process. Consequently, the need of a framework capable of merging all image analysis tasks into a single platform is seen as a great demand in the remote sensing imagery analysis. Although there are some good proprietary image analysis software available, the licensing costs can be a barrier for their use. Besides, these systems cannot be studied and adapted for ones own needs. Steiniger e Hay (2009) discussed all these problems in a review about the use of geographic information tools in landscape ecology, which are critical for any application. They also advocated that sharing knowledge through the development of Free and Open Source Software (FOSS) is a requirement for technological and scientific advancement.

Considering the aforementioned questions, the contribution of this thesis is two-fold. Firstly we proposed and implemented a new toolbox, developed under the FOSS foundation, for integrating remote sensing imagery analysis methods with a repertoire of data mining techniques producing a user-centered, extensible, rich computational environment for information extraction and knowledge discovery over large geographic databases. The new toolbox is called GeoDMA – Geographic Data Mining Analyst. It integrates techniques of segmentation, feature extraction, feature selection, landscape and multi-temporal features and data mining, allowing pattern recognition tasks and multi-temporal analysis in large geographic databases. Secondly we developed a new approach for multi-temporal analysis that allowed creating a new set of features based on polar coordinates transformation to describe cyclic events such as those common in agriculture applications.

In particular, GeoDMA was thought to provide some technical capabilities, which fulfill critical requirements for geographic information tools in remote sensing applications. Below, we list the principal functionalities of GeoDMA:

- a) support for different geographic data types in local or remote database;
- b) spatio-temporal analysis tools, including visualization scheme for temporal profiles;
- c) set of features based on polar coordinates that allows describing cyclic events as well as improving the classification accuracy of multi-temporal

data;

- d) simulation to assess the accuracy of process models (e.g. using Monte Carlo methods);
- e) rapid creation of thematic maps and other results due to its integration on top of TerraView GIS (INSTITUTO NACIONAL DE PESQUISAS ESPACIAIS, 2012);
- f) detection of multi-temporal changes as well as creation of change maps, allowing to explore the causes, processes and consequences of land use and land cover change (SAITO et al., 2010).

To illustrate the potential of GeoDMA, we present 5 case studies, which analyze different land cover patterns to explore all the capabilities available in the system. One case study classify urban land cover in the Brazilian city of São Paulo; the second one explores urban landscape patterns related to the incidence of dengue fever in Rio de Janeiro, Brazil; the third one tracks the evolution of deforestation in the region of São Félix do Xingu; the fourth case classifies land cover using multi-temporal images in the northern Mato Grosso State of Brazil; the fifth case aims at distinguishing between croplands and detect direct changes considering the expansion of agriculture in the entire state of Mato Grosso.

1.1 Document Organization

This thesis is organized as follows. Chapter 2 surveys previous work in the area of land change detection, data mining, and OBIA. This chapter presents a unified taxonomy of techniques defined in a number of different domains and discusses the major approaches. Chapter 3 provides a detailed description of the GeoDMA system, highlighting its main features. Chapter 4 presents some experiments for land cover detection to show the potential of GeoDMA for image analysis. Chapter 5 concludes the thesis, providing an overview about the enhancements, advantages and drawbacks of our system.

2 REVIEW

In this Chapter we review some important topics in the literature regarding the concepts used in the development of GeoDMA. We start reviewing some concepts used by landscape ecology. Afterwards, we give a brief review about object-based image analysis and data mining techniques. Finally, we review some works related to multi-temporal analysis to detect pattern changes.

2.1 Landscape ecology concepts

Because of time and space discontinuities, the real world environments are patchy (WIENS, 1976), defining a landscape as a spatially heterogeneous area (TURNER, 2005). Associated with pattern recognition techniques, landscape ecology qualifies species, communities, and habitat patches within landscapes (READ; LAM, 2002). The landscape ecology concepts employed in this thesis are the base to analyze the structure of the landscape, defining geometric and spatial metrics for the objects present in the landscape, viewed as a *mosaic* of elements aggregated to form the pattern of *patches*, *corridors* and *matrix* on land (FORMAN, 1995).

The landscape ecology mainly considers *patches* as areas, or categories, containing habitat, and the main focus is on conservation. However, to adapt these concepts to remote sensing, *patches* are also related to other types of objects, such as a deforestation area in a forest region, or an object containing a roof in a urban imagery. Based on these considerations, 3 groups of metrics can be defined (MCGARIGAL, 2002; EL-SHAARAWI; PIEGORSCH, 2002):

- *Patch metrics* qualify individual patches and characterizes their spatial and contextual information. Examples include the area of a polygon, perimeter, and compacity. As an example, one patch can be defined as a forest fragment.
- *Class metrics* integrate all patches of a given type inside a specific area, by simple or weighted averaging. The weighted averaging scheme can reflect a greater contribution of large patches to the overall index. Instances include average shape index, and patch size standard deviation. These metrics are used to define, for instance, the amount of houses in a block, or the average size of croplands in a state.
- *Landscape metrics* concern all patch types or classes inside a specific area. These metrics are integrated by a simple or weighted averaging, and

they reflect combined patch mosaic. Landscape metrics include average perimeter-area ratio and patch size coefficient of variation.

Figure 2.1 illustrates the 3 types of landscape metrics. This Figure shows an area with 6 different land cover types, including forest, pasture and agriculture. In the Patch metrics, a single object of the class *Pasture with Regrowth* is defined. In the Class metrics, all objects of the same class are integrated. And, in the Landscape metrics, all objects belonged to the 6 classes inside the area defined by a rectangle were included.

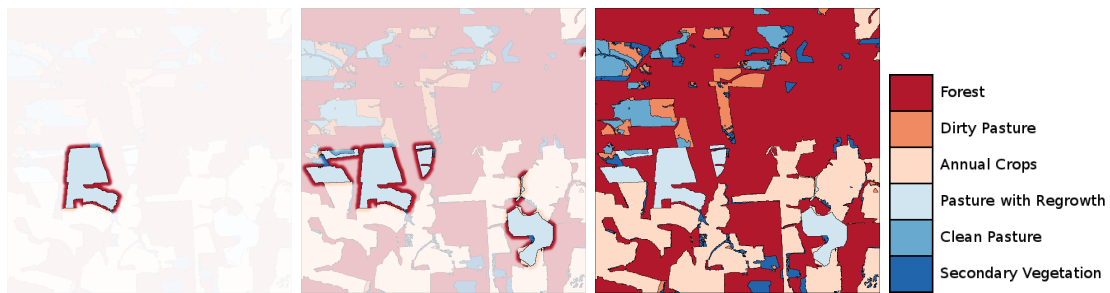


Figure 2.1 - Scale of objects considered in landscape ecology. Patch (left), Class (center), and Landscape (right) metrics.

Many works in the literature have used the landscape ecology metrics to analyze the landscape dynamics and structure. Imbernon e Branthomme (2001) modeled the ecological processes by measuring the percentage of forest cover and the resulting fragmentation. Southworth et al. (2002) used landscape metrics to describe and identify land use change patterns using Landsat imagery from 1987, 1991, and 1996.

Ferraz et al. (2005) analyzed the landscape changes in a watershed in Rondônia, Brazil, using a 18-year Landsat time series. The authors associated land cover types with metrics of size, density, connectivity, arrangement and deforested patches distribution. Ribeiro et al. (2009) evaluated landscape metrics such as edge area, connectivity and fragment size to identify species distribution in the Brazilian Atlantic Forest. They also quantified the remaining forest and suggested guidelines for conservation and preserving the functionally linked mosaics.

Frohn e Hao (2006) evaluated landscape metrics in different years of deforestation in the Brazilian Amazon. They found a set of metrics with predictable behavior, and an inverse relation to spatial aggregation. Saito et al. (2011) analyzed the sensitivity of the landscape ecology metrics when using cells of different sizes to detect deforesta-

tion patterns associated with different processes of human occupation. They used data provided by PRODES, which is a project for monitoring annual deforestation in the Amazon region (ESPACIAIS, 2012). They evaluated nine metrics that describe the landscape structure in different scales, and concluded that certain scales can favor the detection of certain patterns in despite of others. Therefore, when using a single scale for interpretation, the analyst must take this into account to choose a proper analysis scale, related to the process studied.

Gavlak et al. (2011) studied the land cover dynamics in regions with different occupation stages in an agricultural frontier in the Sustainable Forest District of BR-163 between 1997 and 2008, comparing the temporal evolution of deforestation patterns for 1997, 2000, 2003 and 2007, and secondary vegetation analysis from 2000 to 2008. They associated 6 different deforestation patterns to occupation processes. By using cells of $10 \times 10 Km$, the authors grouped the evolution of the occupation patterns into 4 groups according to different trajectories in the period of analysis.

2.2 Object-Based Image Analysis

Besides the original bands of an image, current methods for image interpretation uses additional features, such as pixel differences, ratios, band combinations, and so on. These features can also be used by segmentation algorithms to partition the image into homogeneous regions, also called segments or objects. According to Haralick e Shapiro (1985), a good segmentation should separate the image into simple regions with homogeneous behavior. In other words, segments are generated by one or more homogeneity criteria in one or more dimensions respectively (BLASCHKE, 2010). Segments have additional spectral information compared to single pixels, such as mean values per band, median values, etc. The regions with their respective features characterize the objects. The analysis of such objects, when coupled with a knowledge model with one or more segmentation levels, is called Object-Based Image Analysis – OBIA.

Image analysis usually integrates various algorithms to automate the interpretation task. Presently, the most used proprietary OBIA software is eCognition (BAATZ et al., 2008). It is based on a user-defined workflow, where the objects are modeled using interpreter’s knowledge, being afterwards classified in accord to predefined classes of interest (LANG et al., 2007). The most recent version of eCognition included a data mining module with decision trees as the underlying method for classification. Being a proprietary software package, it has stability, high performance, and a complete documentation.

ENVI Feature Extraction (INTERNATIONAL TELEPHONE & TELEGRAPH EXELIS, 2008) is also proprietary software for image analysis in the OBIA category. It performs classification using a straightforward process, and is focused on high spatial resolution imagery. The segmentation approach is called edge-based, since it suppresses weak edges according to a scale level parameter. Four types of features are computed: spatial, spectral, texture and those based on color space and band ratio. Classification algorithms include the unsupervised K-Nearest Neighbors, decision trees, and the supervised Support Vector Machines – SVM.

On the other hand, the open source InterIMAGE software integrates image processing operators in the interpretation process (COSTA et al., 2010). It offers a suit of basic operators as well, including image processing procedures like segmentation, thresholding, and filtering. The software inherits the interpretation engine and the knowledge representation scheme from geoAIDA (BÜCKNER et al., 2001). The interpreter builds manually semantic networks, in which the nodes' depths represent more generalist (root) or more specific (leaves) classes of interest.

Given an application, one important question is how to build an accurate model for interpretation. To create a proper classification model, a set of adequate features must be selected, which is not a simple task considering the complexity of classes to be analyzed as well as the large set of features to describe the objects. For large amount of data the manual analysis is unfeasible. Therefore, data mining techniques is an appealing alternative for image analysis.

Several articles relating OBIA applications have been published since around the year 2000 (BLASCHKE, 2010). Addink et al. (2007) investigated optimal object definition for biomass and leaf area index – LAI, whose fundamental objects are individual trees or shrubs. The results showed that the scale of the objects affects the prediction accuracy, and that aboveground biomass and LAI can be associated with different optimal object sizes. The study also concluded that the accuracy of parameter estimation is higher for object-oriented analysis than for per-pixel analysis.

In accord to Lackner e Conway (2008), works using procedures based on OBIA tend to rely on manual digitizing or ancillary data to delineate land use polygon boundaries. Alternatively, they used land cover information derived from IKONOS imagery to automatically delineate and classify the land use polygons in a region of Ontario, Canada. Firstly they classified land cover from IKONOS image, and then used the resultant classification as the basis for creating land use maps. The roads extracted from the land cover maps were useful in outlining land use boundaries;

however the delineation of roads in some cases produced jagged boundaries due to the spectral similarities between the roads and neighboring impervious areas, such as driveways and parking lots.

Lewinski e Bochenek (2008) classified SPOT (20 m) imagery using spectral and textural parameters to detect land cover patterns. The classification process started with recognition of water class, whose objects were delineated using multi-resolution segmentation. For the remaining land cover classes, a new segmentation was performed in order to detect urban and forest classes. Subsequently, refinement was performed to detect agriculture and grassland classes. The classification evaluation presented 89% of overall accuracy.

Zortea et al. (2012) proposed an automatic method to detect daytime cloud and cloud shadows in the context of tropical forest monitoring. The method extracted regions from the images using a region growing strategy, and then extracts features based on pixel differences, ratios, and combinations. Such features, coupled with shape matching, were employed to detect cloud and cloud shadow areas in TM and ETM+ images. The method accuracy was of 91% but it still needs improvement to be able to detect thin clouds and haze, and then to reduce the misclassification between shadows and water.

Pinho et al. (2012) mapped land cover using an OBIA approach over an IKONOS II image of southeastern Brazil city, covering an area with 50 neighborhoods. Such area contained various occupation and land use patterns, with a wide range of intra-urban targets. The interpretation combined multi-resolution segmentation, data mining and hierarchical network techniques to detect 11 classes. To select the best attributes for describing objects and then to build the hierarchical network, the authors used a classification method based on the decision tree algorithm. The final classification achieved a global accuracy of 72%.

2.3 Data Mining

Data Mining – DM – is a method to discover patterns from data. It means recovering high-level potentially useful knowledge from low-level data. The increasing volume of geoscience data makes it a perfect case for application of DM (RUSHING et al., 2005). DM deals with the challenge of capturing patterns and agents present in the geographic space, extracting specific knowledge to understand or to decide about relevant topics, including land change, climate variations and biodiversity studies.

The core of DM is the classification, which maps data into specific categories whose cardinality is fewer than the number of data objects (MILLER; HAN, 2001). Our ability to analyze and understand massive datasets is far behind our ability to gather and store the data. Therefore, a new generation of computational techniques and tools is required to support the extraction of useful knowledge from the rapidly growing volumes of data (FAYYAD et al., 1996). These techniques and tools are the subject of the emerging field of Knowledge Discovery in Databases – KDD, which contains DM as an intermediate step. In Figure 2.2 we depict the steps needed to convert raw data into useful knowledge. It is important to state that KDD is not a straightforward process, which is denoted by the interconnections between the steps. From input to output, some steps can be repeated to refine the relation between data and patterns.

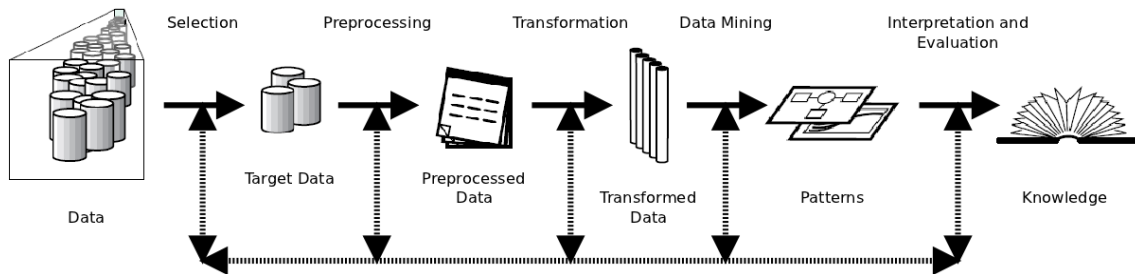


Figure 2.2 - The flowchart of KDD. DM appears as a step in the full process that transforms raw data into knowledge.

SOURCE: Adapted from Fayyad et al. (1996).

Remote sensing databases store millions of records, which hinder the detection of hidden patterns at various levels of abstraction only by visual inspection (UDELHOVEN, 2011). Stein (2008) defined the term *image mining* as “the analysis of (often large sets of) observational images to find (un)suspected relationships and to summarize the data in novel ways that are both understandable and useful to stakeholders”. In remote sensing, thematic maps define recognizable objects in satellite images, which can be either crisp or fuzzy. Crisp define entities with sharp boundaries and fuzzy holds a poor definition or a vague boundary. Examples of fuzzy include a mountain with no clear support or a city having gradual transition zones to the rural land (STEIN et al., 2009).

DM algorithms have been extensively used in remote sensing applications. Friedl et al. (1999) examined methods to increase classification accuracy using decision trees to map land cover from AVHRR multi-temporal data. The work evaluated the

inclusion of phenological metrics and geographic location as features for classification. Tan et al. (2001a) used K-means and linear correlation to measure the likeness among time series, and patterns were investigated for predicting changes in climate and carbon cycle.

Roberts et al. (2002) described land cover variation in a wide area in Amazon using a Landsat time series between 1975 and 1999. They applied DM and spectral mixture analysis to map primary forest, pasture, second growth, urban, savanna, and water. Souza et al. (2003) used decision trees and spectral mixture models to map degraded forest in the Eastern Amazon including intact forest, logged forest, degraded forest, and regeneration. McCauley e Goetz (2004) mapped residential land use in Maryland, USA, using Landsat images associated to a parcel-level database. The results showed the possibility to distinguish densities of residential development, industrial and agricultural areas. Silva et al. (2008) proposed a method to detect agents of land use change in remote sensing image databases, relating each change pattern to one of land use change.

The number of images provided daily by satellites allows research to go beyond the current achievements accomplished so far. By using a set of images acquired in different times it is possible to relate land changes to interpret images using DM and other techniques that integrate time in the analysis. According to Udelhoven (2011), there is still a need for automated methods that transform data from temporal remote sensing data into useful information and knowledge. Next, a review about some works in the area of multi-temporal analysis is presented.

2.4 Multi-temporal analysis

The growing pool of information provided by Earth satellites raised new possibilities to analyze data as image time series. The problem is that remote sensing databases store millions of temporal records, which hamper the detection of hidden patterns at various levels of abstraction only by visual inspection (UDELHOVEN, 2011). Consequently, image analysis techniques for data processing and information extraction are necessary (BOULILA et al., 2011).

In accord to Boriah et al. (2008), land change happens when the cover type at a given location switches to another type. Converting natural land cover into human-dominated cover types is a change that impacts more than locally, with many unknown environmental outcomes (POTTER et al., 2007). Remote sensing data is the only source of long-term views of the Earth's surface, which is a good alternative for

mapping land use and land cover change (BRADLEY et al., 2007).

Examples of environmental changes include land cover fragmentation, patch isolation, and a reduction in habitat and native species (METZGER et al., 2009). The climatic impacts are also significant, such as an increase in surface temperature and a decrease in the annual precipitation within tropical forests due to deforestation (NOBRE et al., 1991).

Analysts interpret the imagery and map changes by analyzing differences found in images taken in different times. Rudorff et al. (2009) related the increase in the deforestation as well as the conversion of land use from pasture and agriculture to sugarcane crops due to the biofuels expansion. Southworth et al. (2002) compared the trajectories of forest-cover change and the landscape biophysical and social characteristics using satellite images series to detect land changes. Both studies evaluated past events and the image analysis process was manually performed. However, it is a tedious and time-consuming task to interpret long series using manual methods (BOULILA et al., 2011). Various studies have used remote sensing techniques to analyze multi-temporal images and detect changes (BORIAH et al., 2008; POTTER et al., 2007; HORNSBY et al., 1999).

In agriculture applications one challenging task is to distinguish single and double croppings among the other events in satellite images (GALFORD et al., 2008). Here, single croppings stand for growing a crop once a year. Accordingly, double croppings mean growing two crops in sequence on the same field in a year, i.e. the succeeding crop is planted after the preceding crop has been harvested. As this event is cyclic, its complete characterization involves multi-temporal images analysis, the knowledge about the temporal interval that the event occurs as well as the pattern that describes such event. Studies to identify cyclic events have used images and products from the Moderate Resolution Imaging Spectroradiometer (MODIS), which is an important source of Earth data with high temporal resolution and low spatial resolution (GALFORD et al., 2008; VERBESSELT et al., 2010). This imagery records photosynthetic activity, allowing the surface analysis in time and space, and also provides vegetation index values (EVI2) in a spatial resolution of 250m (HUETE et al., 2002; JIANG et al., 2008).

By following the EVI2 values in a certain position along the time, we can define a temporal profile that has a cyclic behavior, as seen in Figure 2.3. This profile represents EVI2 values from 2000 to 2011, in a spatial resolution of 250m pixel and temporal resolution of 16 days. The cycles should not be considered change,

even though they contain different states as the variation from 0.1 to 0.75 between 2007 and 2008. However, techniques must be able to distinguish cycles to classify land cover and land change patterns. For this task, we can use temporal profiles to describe transitions between objects, and this way monitoring the land cover change dynamics (FREITAS; SHIMABUKURO, 2008). Besides, through automatic methods we can speed up the image analysis procedures and deliver results on-the-fly.



Figure 2.3 - EVI2 profile example from 2000 to 2011, the range of values is [0,1].
SOURCE: Adapted from Freitas et al. (2011).

Examples of methods to detect cycles automatically include the Discrete Fourier Transform – DFT. Methods based on DFT convert the multi-temporal profile from the time domain to the frequency domain, where it is easier to identify the frequencies that compose the signal. The peaks in the power spectrum of a time series point out the cycles (TAN et al., 2001b). The work of Galford et al. (2008) detects cycles by applying an annual standard deviation threshold. This threshold is selected each year from the local minimum in a bimodal histogram of standard deviation. Jonsson e Eklundh (2004) use a preliminary definition of the seasonality (uni-modal or bi-modal) with timings of the growing seasons.

Multi-temporal observations using remote sensing allow the analyst to recover relevant information about changes in the environment. Such information is feasible if data about objects' history is available (BITTENCOURT et al., 2011; MOTA et al., 2009). Two relevant questions are: “what has been the environment past condition?” and “when and how did such condition change?” (RASINMAKI, 2003). Change detection techniques can be used to tackle these questions.

Land change detection using remote sensing is not a new topic. However, it has received more attention due to recent advances in data gathering and storage tasks. Milne (1988) used digital imagery to calculate temporal variation between two datasets. The idea of using two instants to detect changes originated the snapshot

model, in which the methodological challenge is to compare whether objects in t_0 and t_1 are the same (BRADLEY et al., 2007). Singh (1989) evaluated several change detection methods based on snapshots. Before object-based techniques, other methods such as image differencing, regression to estimate pixels in future states, image rationing, and post-classification were employed. These methods are computationally fast but the results strongly depend on many external causes such as image registration quality, illumination effect, atmospheric conditions, and sensor calibration. Differently, Carvalho et al. (2001) proposed a method based on multi-resolution wavelet analysis to detect changes due to deforestation as well as new areas of rock exploitation in south-eastern Brazil. Regardless of accurate spatial registration or radiometric rectification, changes were found successfully while differences not related to land cover changes were bypassed.

Verbesselt et al. (2010) proposed an algorithm named Breaks For Additive Seasonal and Trend (BFAST) that integrates a decomposition of time series into trend, seasonal and noise components for detecting changes. The method iteratively estimated the time and number of changes, and characterized the change by its magnitude and direction. Changes in the trend indicated gradual and abrupt changes, while changes in the seasonal component indicated phenological changes. However, the sensitivity of the BFAST to detect seasonal changes was not extensively assessed, and it was not extended to distinguish types of changes.

Costa (2009) proposed a new multitemporal classification method based on Fuzzy Markov Chain – FCM. Training samples of change generates membership values for the object classified at times t and $t + 1$ that are defined as fuzzy label vectors. After defining a transition matrix, based on these vectors, the FCM model estimates the class membership for every new object in $t + 1$, after a defuzzification step. This approach was developed in the InterIMAGE software (COSTA et al., 2010).

Bradley et al. (2007) proposed a curve fitting method to model the average annual phenology, using a spline-based approach. The authors assumed that ecosystems have an inherent cyclicity approximated by an average annual curve. This assumption was used to fill anomalously low or missing data. The method extracted basic features from profiles such as amplitude, onset timing of greenness, intrinsic smoothness, and roughness. They evaluated the land cover variability between 1990 and 2002 from NOAA-AVHRR data (1 Km spatial resolution) in the western U.S. The method was robust to deal with unequally spaced data and reduced the influence of empty NDVI data, occurred mainly during winter. However, the curve fitting

method was sensitive to outliers, called *spikes* in the time series curve.

Castilla et al. (2009) introduced an automated change detection method called Land cover Change Mapper (LCM). LCM detects regions that undergone significant change in land cover using two or more snapshots. It is based on three steps, starting from analyzing the difference between snapshots. Afterward, they automatically detected a threshold that produces a binary image (change/no change). Finally, spurious data were removed by applying a region growing strategy in areas detected as change. The method is fast and robust to illumination differences, and was applied to track deforestation in Western Canada using SPOT imagery (2.5m spatial resolution) corresponding to years 2004 and 2006.

A more sophisticated approach to find changes in yearly time series with many observations was devised by Boriah (BORIAH, 2010). The author proposed a recursive merging algorithm to identify the scale and scope of disturbance events. It scales up to handle the large size of Earth science data, large numbers of missing and noisy values present in satellite data sets. Since any time series can be partitioned into homogeneous segments, and their boundaries represent change points, it merges the most similar pair of consecutive cycles until two cycles remain. The distance between them will indicate (or not) changes. They analyzed EVI profiles between 2000 and 2006 from MODIS sensor (250m spatial resolution) to detect land use conversion from vegetation to urban, and from barren land to vegetation. The method is fast since few processing is required but it does not tackle more sophisticated changes such as crop changes in agriculture sites.

Galford et al. (2008) first detected row crops areas by applying an annual standard deviation threshold to discriminate row crops from other land cover types. The thresholds were selected year by year from the local minimum in a bimodal histogram of standard deviation. To determine if a cropland pixel has a single or double croppings pattern, the authors detected the number of local maximums in one growing year of a wavelet-smoothed EVI time series. As mentioned by Verbesselt et al. (2010), change detection techniques need to be independent of specific thresholds or change trajectories, since finding out thresholds often produces misleading results due to different spectral and phenological characteristics of land cover types (LU et al., 2004). Moreover, manual determination of thresholds adds significant efforts to expand change detection to large areas.

Jonsson e Eklundh (2004) presented curve-fitting methods to smooth time series of satellite images. The smoothed curves are used for extracting seasonal parameters

related to growing seasons (single or double croppings). Seasonal parameters include the beginning, the mid, the end, and the amplitude of a season. Each season is detected using data from 3 years, where the central year is processed to detect growing seasons. If the amplitude of the second peak exceeds a certain fraction of the amplitude of the primary peak, double croppings are set. For cases where the amplitude of the secondary peak is low, single croppings are detected.

2.5 Comments

Several studies about land patterns analysis were presented in this Chapter. It is evident the variety of different methodologies they have used to analyze images. Concerning classification, many works have used data mining as the underlying technique for pattern recognition, and some others have still relied on the manual definition of a rule set. Table 2.1 provides a summary of some software used in the studies discussed in this Chapter.

Table 2.1 - Softwares used in the remote sensing applications.

Article	ArcGIS	eCognition	ENVI	Fragstats	R	Weka	Others	Total
Addink et al. (2007)		×			×		CAN-EYE	3
Esquerdo et al. (2009)			×					1
Ferraz et al. (2005)	×			×			SWAT2000	3
Frohn e Hao (2006)	×		×	×				3
Gavlak et al. (2011)							GeoDMA	1
Hüttich et al. (2009)		×			×		TIMESAT	3
Imbernon e Branthomme (2001)				×			ERDAS	2
Lackner e Conway (2008)		×						1
Lewinski e Bochenek (2008)		×					PCI	2
Metzger et al. (2009)	×				×			2
Novack et al. (2011)		×				×	InterIMAGE	3
Pinho et al. (2012)		×	×			×		3
Ribeiro et al. (2009)	×				×		ERDAS	3
Saito et al. (2011)							GeoDMA	1
Silva et al. (2008)				×		×	Spring	3
Southworth et al. (2002)	×			×				2

By carefully inspecting Table 2.1, it is observed that most works used more than one computational program to perform the complete image analysis. This fact introduces one more challenge for the researchers, which is the problem of data integration and the transfer of one platform to another. This includes conversion of data format, knowledge of the software to be used, files replication, and other tasks that difficult the image analysis process. Besides, in most cases such tasks are very time con-

suming, mainly due to the amount of data. Consequently, the need of an integrated framework, capable of merging all image analysis tasks into a single platform is seen as a great demand in the interpretation of remote sensing imagery.

3 GeoDMA – GEOGRAPHIC DATA MINING ANALYST

Current remote sensing research is mainly performed over GIS, since they provide the necessary functions for spatial data collection, management, analysis and representation (STEINIGER; HAY, 2009). However, advanced remote sensing research should not be limited by the basic functionality provided by a GIS platform. In particular, a tool for advanced image interpretation must include essential functionalities such as:

- a) spatio-temporal analysis tools;
- b) adequate set of features to describe patterns in spatio-temporal data;
- c) simulation methods to assess the accuracy of process models;
- d) detection of multi-temporal changes as well as creation of change maps, allowing the interpreter to understand land change patterns;
- e) options for customization and functional enhancements to advance algorithms;
- f) a proper architecture that allows experiments to be repeatable and results to be reproducible by other researchers;
- g) documentation of methods and source code, so that new researchers can learn the tools and understand or modify the underlying methods.

Taking into account these aforementioned requirements, we decided to build a FOSS for analyzing changing patterns over large remote sensing datasets, named Geographic Data Mining Analyst – GeoDMA. The basic ideas of Silva et al. (2005), who proposed a methodology for detecting deforestation patterns in the Amazon region were the starting point for our research. Therefore, GeoDMA was designed as a toolbox to integrate the most essential image analysis algorithms, landscape ecology metrics, a scheme for multi-temporal analysis, and data mining techniques to automate the analysis of large databases (KORTING et al., 2008).

Figure 3.1 shows the main interface of GeoDMA. In particular, the system supports and stores different geographic data types in local or remote databases. It integrates classification and validation tools in a friendly Graphic User Interface (GUI) based on statistics and the interpreter’s knowledge. Besides, it is a free software solution for

remote sensing applications, running in different platforms (e.g. Linux and Windows, 32 bits).

The toolbox works on top of TerraView GIS (INSTITUTO NACIONAL DE PESQUISAS ESPACIAIS, 2012), whose interface is shown in Figure 3.2. This GIS provides the interface for the interpreter to visualize the geographic information stored in databases, to control the database, and also to display the objects' properties.

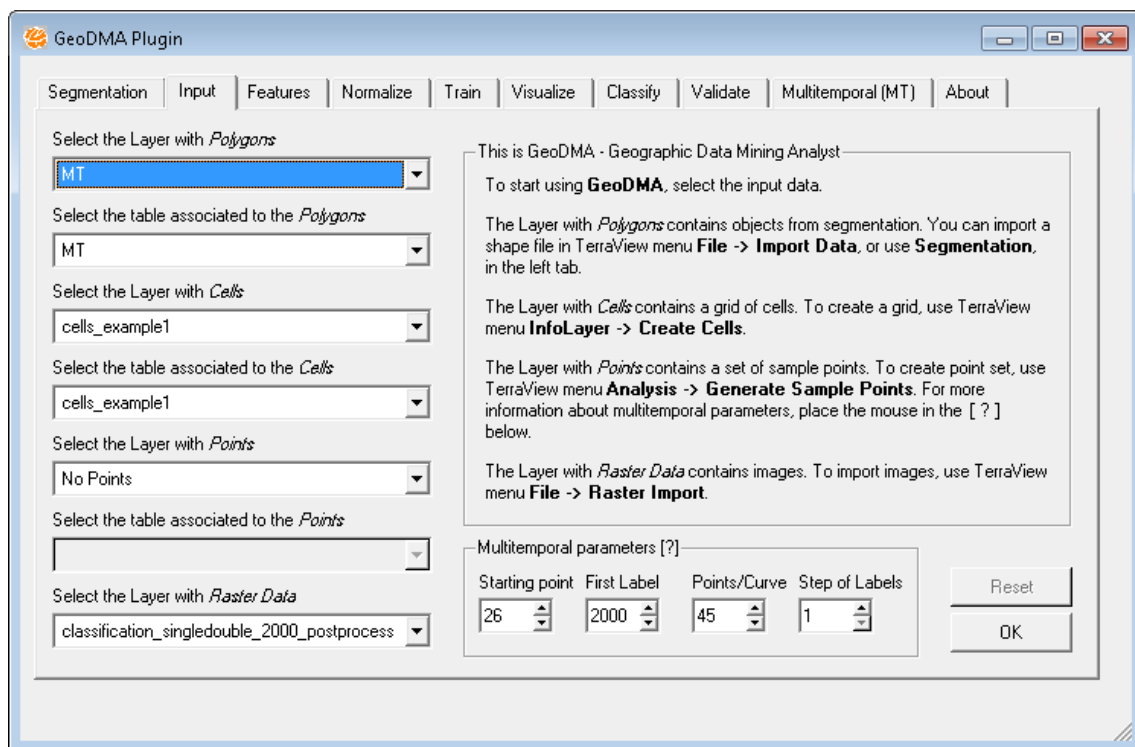


Figure 3.1 - User interface for GeoDMA.

A summary of the system is as follows:

- Software name: Geographic Data Mining Analyst – GeoDMA
- Contact: tkorting@dpi.inpe.br
- Year of first version: 2009
- Hardware: IBM compatible PC
- Operation System: Linux/Windows
- Program language: C++

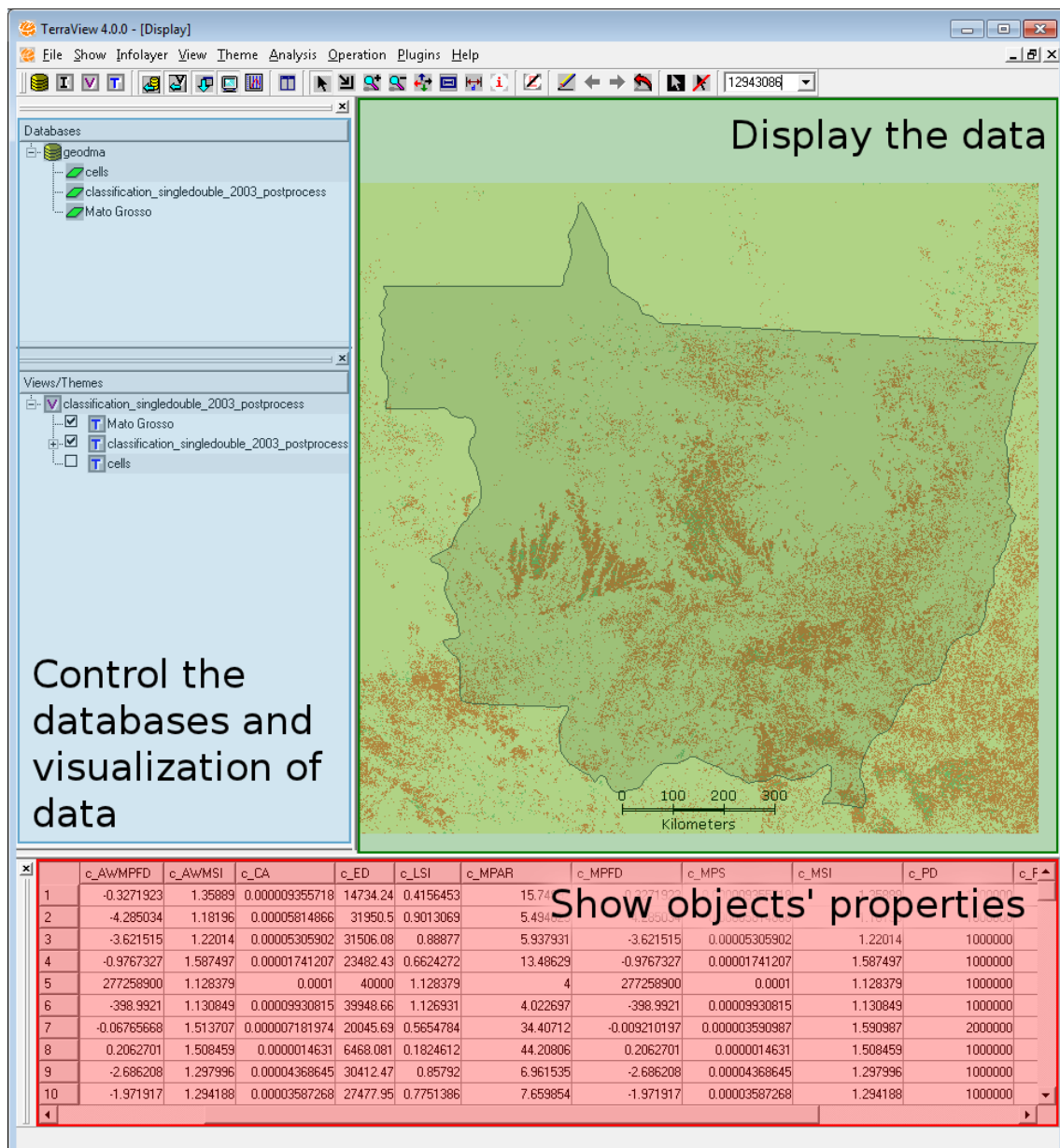


Figure 3.2 - User interface for Terraview.

- Ancillary libraries: TerraLib (CâMARA et al., 2008) and QT (BLANCHETTE; SUMMERFIELD, 2008)
- Availability: free from <http://geodma.sf.net/>
- Extra documentation: <http://geodma.sf.net/documentation>
- Data formats accepted: TIFF rasters, and ShapeFiles

Figure 3.3 shows a general diagram of the system. The processing steps start from defining the input data, going through feature extraction and the application of data mining algorithms to extract and deliver information about Earth observation. Each module in the diagram corresponds to one of the following Sections.

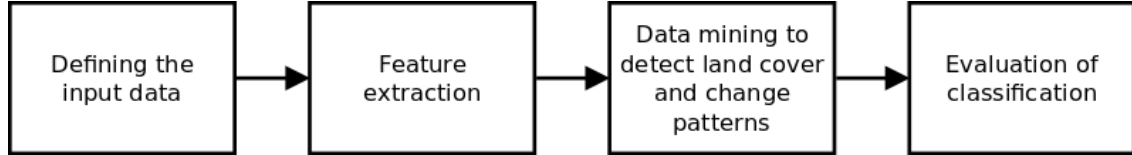


Figure 3.3 - GeoDMA: diagram of the main processing steps for image analysis.

3.1 Defining the input data

GeoDMA imports a variety of geospatial data, which are stored in a database as raster¹ or vector format. Object-based approaches use homogeneous regions from image segmentation. The regions extracted by segmentation operation, points (pixels), and cells (regular grid) define objects that are stored in database as vector information. Multi-temporal images can be represented as a sequence of snapshots in raster format, which are used to extract a sequence of values for each object in different intervals that define a curve called cycle. Figure 3.4 illustrates the relation among the input data in the system.

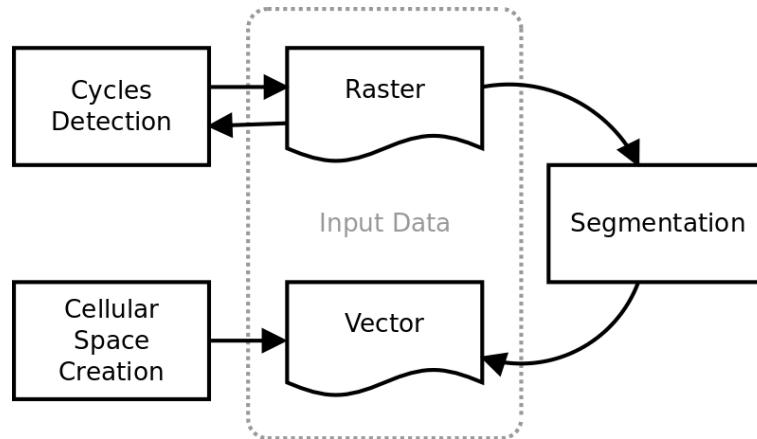


Figure 3.4 - Creating input data – Multi-temporal images define cycles and segmentation defines objects from raster.

¹Throughout the text, image and raster terms will be used interchangeably.

3.1.1 Segmentation

Image segmentation is one of the most challenging tasks in digital image processing. One simple definition states that a good segmentation should partition the image into regions with homogeneous behavior (HARALICK; SHAPIRO, 1985). Figure 3.5 shows the segmentation interface in GeoDMA.

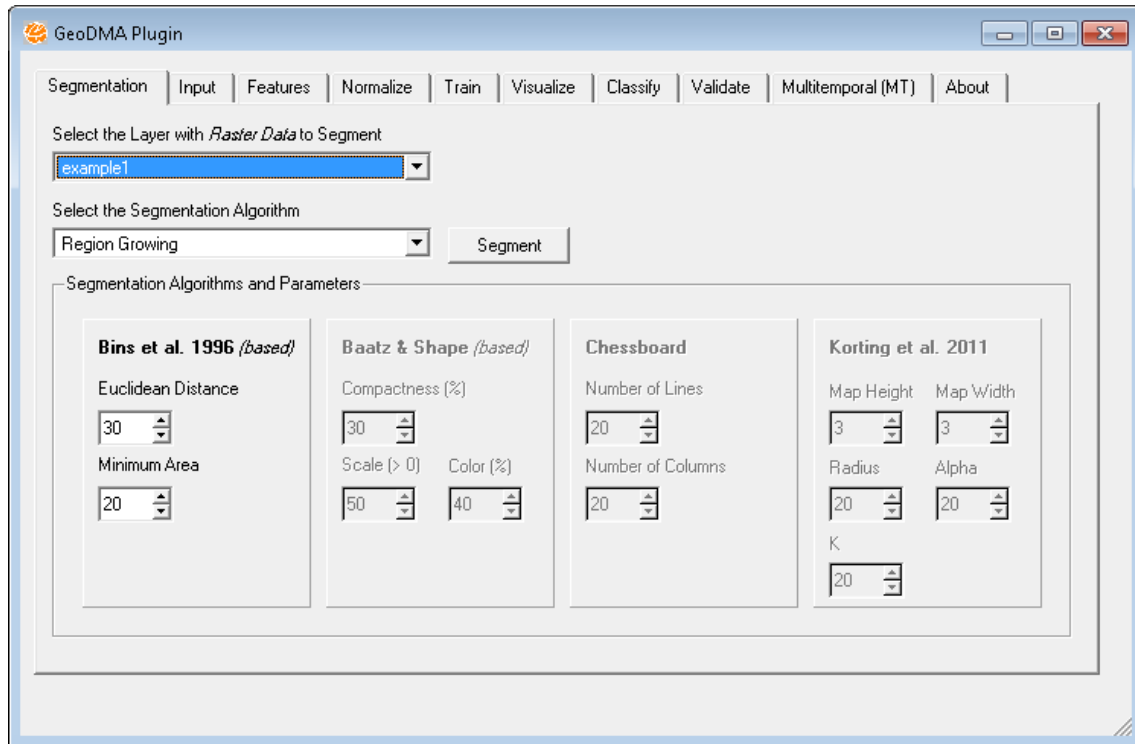


Figure 3.5 - Interface for segmentation: the interpreter selects the algorithm and sets the thresholds. Regions obtained in the segmentation process are stored in the database as vector format.

The system provides 4 segmentation algorithms:

- Region growing approach based on Bins et al. (1996). This algorithm defines random seeds over the image and merges them with neighboring pixels, according to a similarity threshold. After growing all seeds, regions with area below a threshold, which define the size of the area, are merged to the most similar neighbor. According to Meinel e Neubert (2004), this algorithm released good overall impression of results with proper delineation of homogeneous areas.
- Segmentation approach based on Baatz et al. (2000). It is based on region

growing and a multi-resolution procedure. The similarity measure depends on scale and the thresholds are weighted by the objects size. The interpreter defines the parameters for scale, band's and color weights, and weights for smoothness and compactness.

- Algorithm based on Korting et al. (2011), which classifies spectrally similar pixels according to their location, using a geographic extension of the Self-Organizing Maps (SOM). The self-organized map will cluster neighboring pixels, and these clusters will define the image segments.
- A technique of resegmentation applied to urban images based on Korting et al. (2011). Resegmentation represents the set of adjustments from a previous segmentation in which the elements are small regions with a high degree of spectral similarity (a condition known as oversegmentation). This algorithm is applied to segment the house roofs, which are assumed to have a rectangular shape. A region adjacency graph (RAG) is created to relate the border elements of the oversegmentation, and this technique splits and merges regions until they form a meaningful object.

3.1.2 Cycles detection

The land pattern detection in GeoDMA using multi-temporal images is based on cycles definition. Therefore it is important to distinguish the terms *profile* and *cycle*, although they represent the same temporal entity in some cases. Suppose we have a profile with observational data over a 5-year period while the analysis is performed yearly. In this case, the profile contains the full time series, divided into 5 cycles of 1 year. In vegetation analysis the cycles are often annual. For example, a time series with temporal resolution of 8 days defines a cycle with around 45 values per year ($\frac{365}{8} \simeq 45$). For 16 days, the number of cycles changes to 23, and so on.

The central question is how to describe each cycle. Before using data to quantify or infer spatio-temporal processes, it is crucial to understand how the processes are represented in the data. Characterization of multi-temporal imagery provides insights into how different processes are represented by the spatial, spectral and temporal sampling of the imagery (SMALL, 2011). In agriculture applications the duration of certain events is well defined, e.g. 1 year. From multi-temporal images, the user defines the initial point of a cycle and the number of points for each cycle. With this information, GeoDMA is able to extract multi-temporal features from time series.

3.1.3 Creation of cellular space

Based on the landscape ecology concepts, objects can be represented by regions obtained by segmentation (*patches*) and regions that encompass a set of objects (*landscape*). The latter is represented through a rectangular grid of cells. Such grid is defined by a resolution that indicates the size of the rectangles. The *class* and *landscape* metrics related in Section 2.1 integrate the regions inside every cell, and present metrics such as average area of the regions inside a cell, or the amount of regions for a specific class inside a cell.

As pointed by Saito et al. (2011), the interpreter must take into account the cellular space resolution and its sensitivity over the detection of different land cover patterns.

3.2 Feature extraction

Figure 3.6 describes the feature extraction module, which stores all features in a local or remote database. Several features are possible to be extracted, meanwhile according to the raster size and the quantity of objects this task can spend much time (i.e. hours) to be performed. Therefore, the creation of a feature database ensures that all features will be extracted only once.

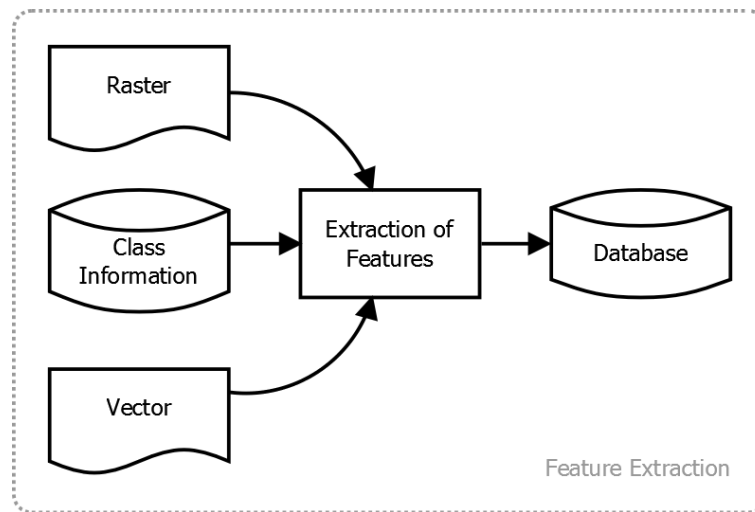


Figure 3.6 - Feature extraction – Spectral and Spatial features use raster and vector objects. Landscape ecology features use class information of objects. Multi-temporal features use cycles' information.

Features are divided into 3 groups. The *segmentation-based* features are properties obtained from the segmented objects, integrating raster and vector data types. The

landscape-based features are the landscape metrics, using vector data type. Cycles obtained from raster time series are used to extract *multi-temporal* features.

3.2.1 Segmentation-based features

The segmentation-based features include spectral (Table² A.1) and spatial (Table A.2) metrics to describe each object stored in database. The spectral features relate all pixel values inside a region, therefore include metrics for maximum and minimum pixel values, or mean values. The spatial features measure the shapes of the regions, including height, width, or rotation. Figure 3.7 shows the visual representation of both features. Some equations in Table A.1 describe features based on the Gray-Level Cooccurrence Matrix – GLCM (HARALICK et al., 1973; PACIFICI et al., 2009). The term p_{ij} is the normalized frequency in which two neighboring cells separated by a fixed shift occur on the image, one with gray tone i and the other with gray tone j . The constant D is the dimension of the GLCM, which has the same gray value range of the original image.



Figure 3.7 - Visual representation of the segmentation-based spectral and spatial features. Several features can be extracted in the highlighted region. Spectral features include metrics for maximum and minimum pixel values, or mean values. Spatial features measure the height, width, or rotation.

²All tables describing the features are in the Appendix .

3.2.2 Landscape-based features

In the Section 2.1 the concepts of landscape ecology were presented. A set of features based on this concept was implemented in GeoDMA. Such features represent the spatial relations between objects (or patches in the landscape ecology) inside a predefined landscape. Table A.3 describes these features implemented in our system.

3.2.3 Multi-temporal features

The purpose of characterizing multi-temporal data is not only to identify specific features but also to determine what can and cannot be distinguished in the data with a minimum of assumptions. Within this context, this work proposes the *Polar* representation features to better represent cyclic patterns that are common, for instance, in agriculture applications. For our purpose, we divided the set of features into 2 groups, namely *Basic* and *Polar* features, which we will describe below.

3.2.3.1 Basic features

Basic features include statistical measures and phenological metrics in case of vegetation profiles (HÜTTICH et al., 2009; JONSSON; EKLUNDH, 2004). From each cycle we trace well-known statistical features such as mean, standard deviation, minimum and maximum values, and amplitude. The phenological metrics include the timing of recurring vegetation cycles (canopy emergence and senescence), first and second slopes of the curve, integral, and distance between peaks and valleys. Hereby we define this type of feature as *Basic*. Figure 3.8 illustrates some metrics extracted from time series: maximum, minimum, amplitude, and integral values. Table A.4 presents a description of all the aforementioned features.

3.2.3.2 Polar features

According to Hornsby et al. (1999), the standard computational models of time do not consider that certain events or phenomena may be recurring. The term cycle can also be used to capture the notion of recurring events. To support cycle’s visualization, Edsall et al. (1997) proposed a time-wheel legend, resembling a clock face, divided into several wedges according to the data instances.

In our case, we adapted the time wheel legend by plotting each cycle of the profile, and by projecting values to angles in the interval $[0, 2\pi]$. Let a cycle be a function $f(x, y, T)$, where (x, y) is the spatial position of a point, and T is a time interval t_1, \dots, t_N , and N is the number of observations in such a cycle. The cycle can be

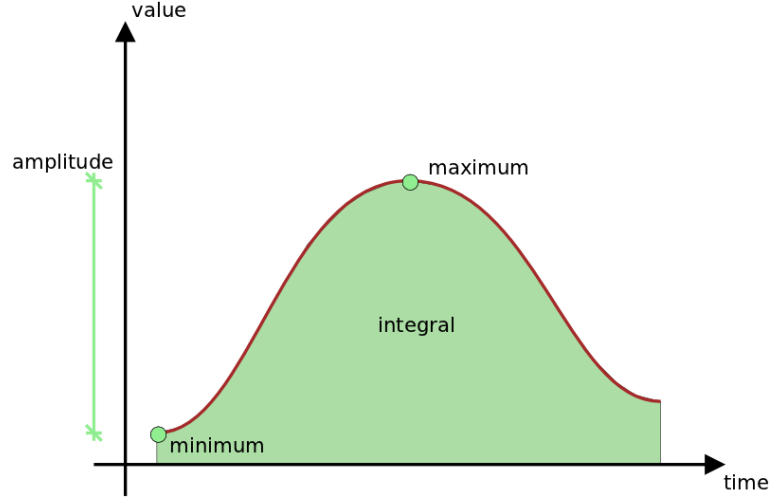


Figure 3.8 - Some *Basic* features obtained from time series: maximum, minimum, amplitude, integral values.

visualized by a set of values $v_i \in V$, where v_i is a possible value of $f(x, y)$ in time t_i . Let its polar representation be defined by a function $g(V) \rightarrow \{A, O\}$ (A corresponds to the abscissa axis in the cartesian coordinates, and O to the ordinate axis) where

$$a_i = v_i \cos\left(\frac{2\pi i}{N}\right) \in A, i = 1, \dots, N \quad (3.1)$$

and

$$o_i = v_i \sin\left(\frac{2\pi i}{N}\right) \in O, i = 1, \dots, N. \quad (3.2)$$

Considering $a_{N+1} = a_1$ and $o_{N+1} = o_1$, we can obtain the coordinates of a closed shape. Figure 3.9 illustrates a cycle and its transformation to the polar coordinate system. Given the shapes, we can extract various shape and linearity metrics, such as area, perimeter, main direction, bounding ellipse, eccentricity and radius. In this scheme, a cycle with constant values outcomes a circle, and different cycles draw different shapes according to their properties. Henceforth, this type of feature is named as *Polar*.

Moreover, polar representation provides a new visualization scheme that can help us to describe the pattern represented in the cycle. A first insight when using annual cycles suggests splitting the polar representation into 4 quadrants related to the 4 seasons. To illustrate this scheme, Figure 3.10 shows the polar representation for 2 different cycles associated to 2 land cover types (single and double croppings), divided by seasons. Most of the area that represents the single croppings class is in

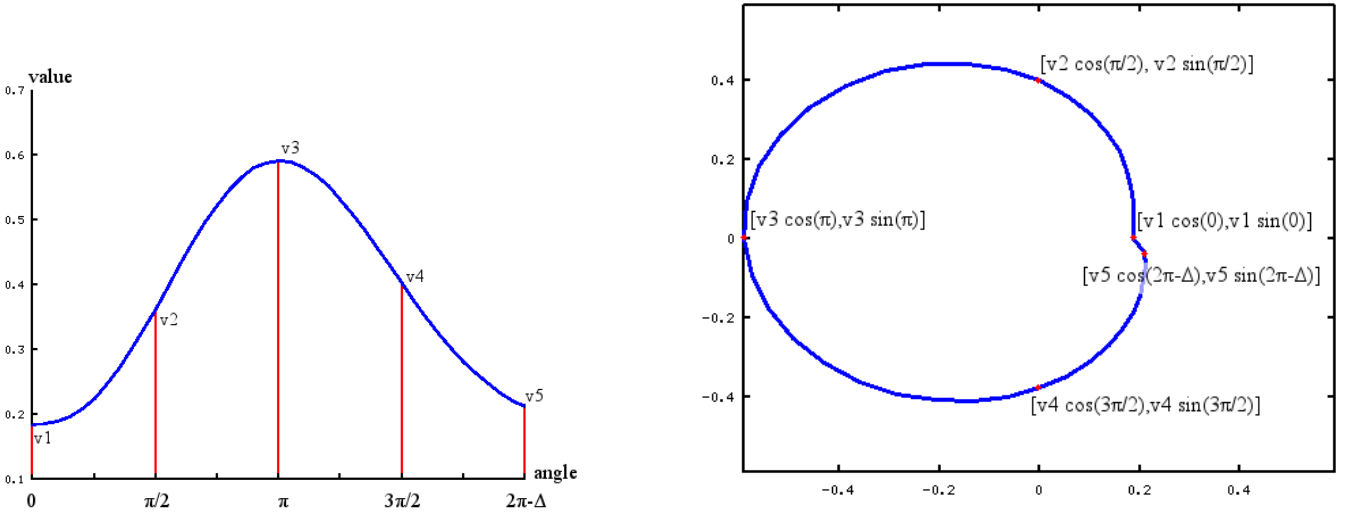


Figure 3.9 - When the values of the cycle are associated to a certain angle (left), the closed shape is created from its polar transformation (right).

the quadrant related to the summer season. In the spring and fall seasons, it is also observed that the curves have similar behaviors related to canopy emergence and senescence, respectively. Differently, the polar representation for the double crop-pings class has a small area in the winter season and similar areas in the other seasons. Hence, other features such as average values per season can also be computed. Another feature, called *Polar Balance*, calculates the standard deviation of the area per season, which indicates the stability of the profile throughout the cycles.

Given the shapes, we also extract linearity features based on geometric moments (STOJMENOVIC et al., 2008). The central moment μ , of order pq , from a set of points Q is defined as

$$\mu_{pq} = \sum_{x,y \in Q} (x - x_c)^p (y - y_c)^q \quad (3.3)$$

where (x_c, y_c) is the center of mass from Q . The feature *eccentricity* is calculated using the central moments with different orders:

$$e = \frac{\sqrt{(\mu_{20} + \mu_{02})^2 + 4\mu_{11}^2}}{\mu_{20} + \mu_{02}}. \quad (3.4)$$

The feature *angle of orientation* of Q is determined by

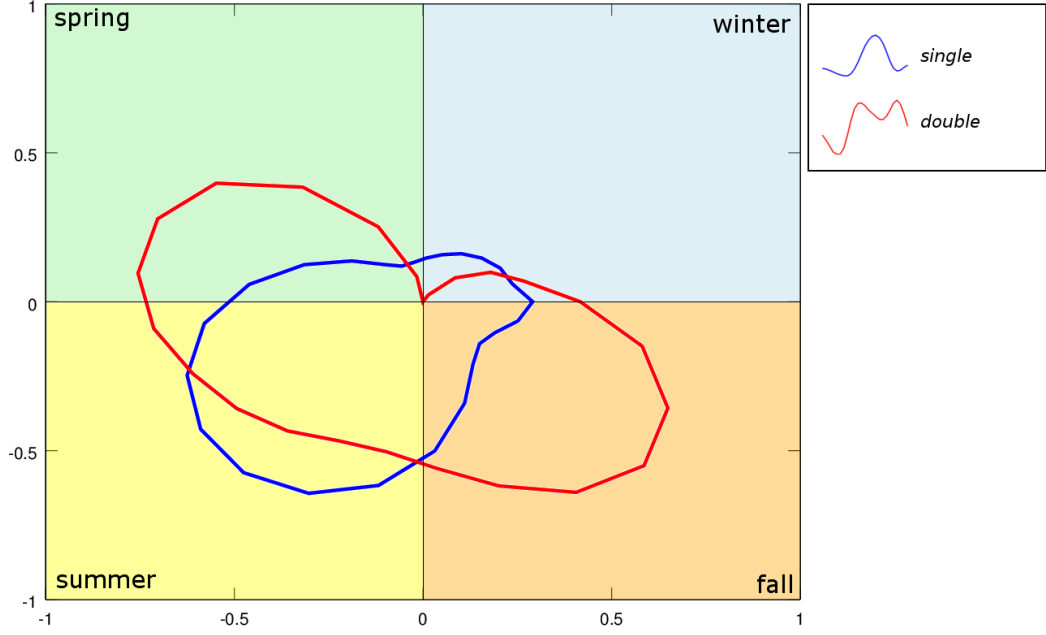


Figure 3.10 - Relation between the four seasons and EVI2 values using polar representation.

$$a = 0.5 \arctan \left(\frac{2\mu_{11}}{\mu_{20} - \mu_{02}} \right). \quad (3.5)$$

The feature *ellipse ratio* is obtained by $r = 1 - \frac{b}{a}$, where

$$a^+, b^- = \sqrt{\frac{2 \left[\mu_{20} + \mu_{02} \pm \sqrt{(\mu_{20} - \mu_{02})^2 + 4\mu_{11}^2} \right]}{\mu_{00}}}. \quad (3.6)$$

All features for describing cyclic events extracted from polar representation and implemented in the system are described in Table A.4.

3.3 Data mining to detect land cover and change patterns

In the data mining step, shown in Figure 3.11, the objects stored in a database are used by the interpreter to select representative samples for each pattern of interest. The different patterns compose the land cover typology, and some algorithms automatically build a classification model based on training samples, which can be stored for further analysis. This model shall be used to classify the entire database,

or different databases with the same typology. The classification interface is shown in Figure 3.12, where the interpreter selects the input features, sets output parameters, and defines the classification algorithm.

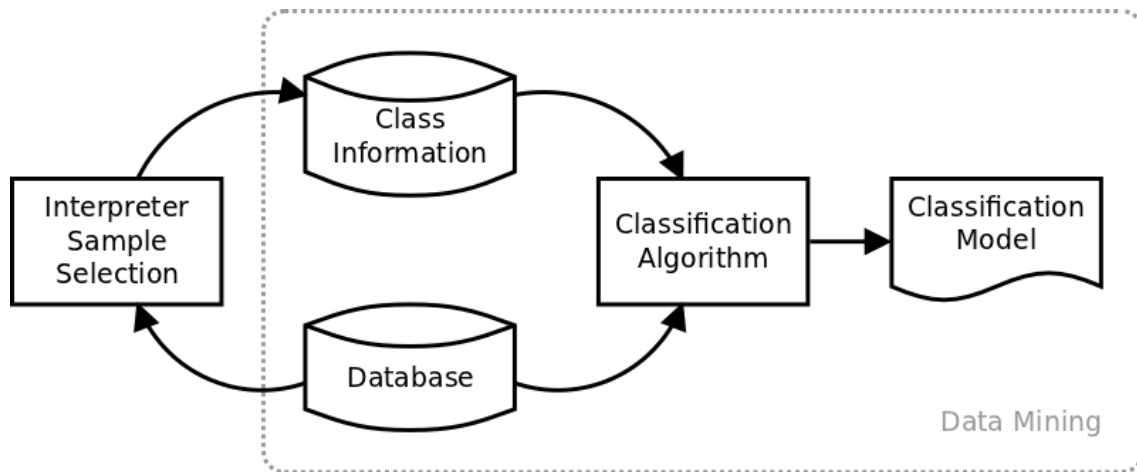


Figure 3.11 - Classification interface. The interpreter selects the input features, sets output parameters, and defines the classification algorithm.

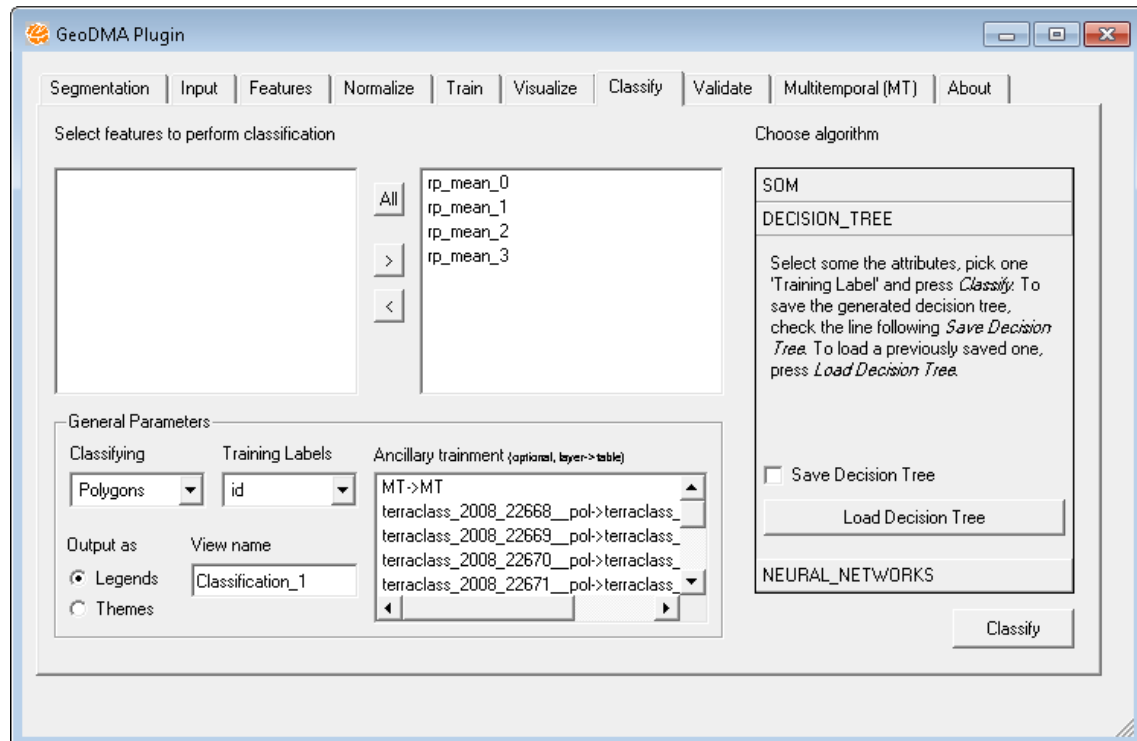


Figure 3.12 - The interface for classification. The interpreter must select the input features, set output parameters, and define the classification algorithm.

Usually, the search for patterns includes the automatic execution of a classification algorithm and a phase of feature evaluation by the interpreter. In accord to Pinho et al. (2012), the inclusion of data mining techniques in the classification process increases the speed and also reduces the empirical nature of the feature selection process and the creation of classification models. One mechanism to evaluate the features is provided in the visualization module, which displays features in a scatterplot to visualize the data distribution in the feature space, as shown in Figure 3.13.

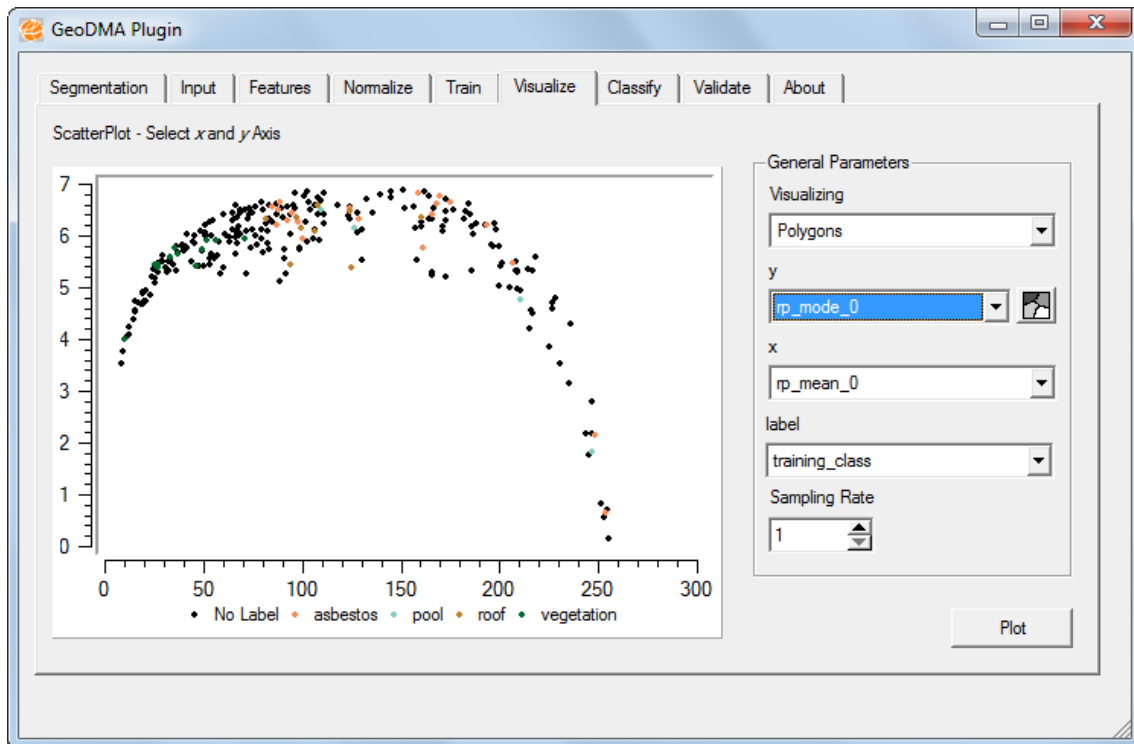


Figure 3.13 - Visualizing data in the feature space using a scatterplot, similar to eCognition's module (LANG et al., 2007).

Another visualization tool is the spatialization, which helps the interpreter to identify specific features and also to determine what can and cannot be distinguished in the data. Figure 3.14 shows the spatialization of the *mode* feature. Brighter objects define regions with higher values of mode whereas darker objects define regions with lower mode values.

When analyzing multi-temporal imagery, the interpreter needs to visualize the time series, so that a cycle can be related to a specific land pattern. GeoDMA toolbox provides the cycle's visualization as well as its polar transformation, as Figure 3.15

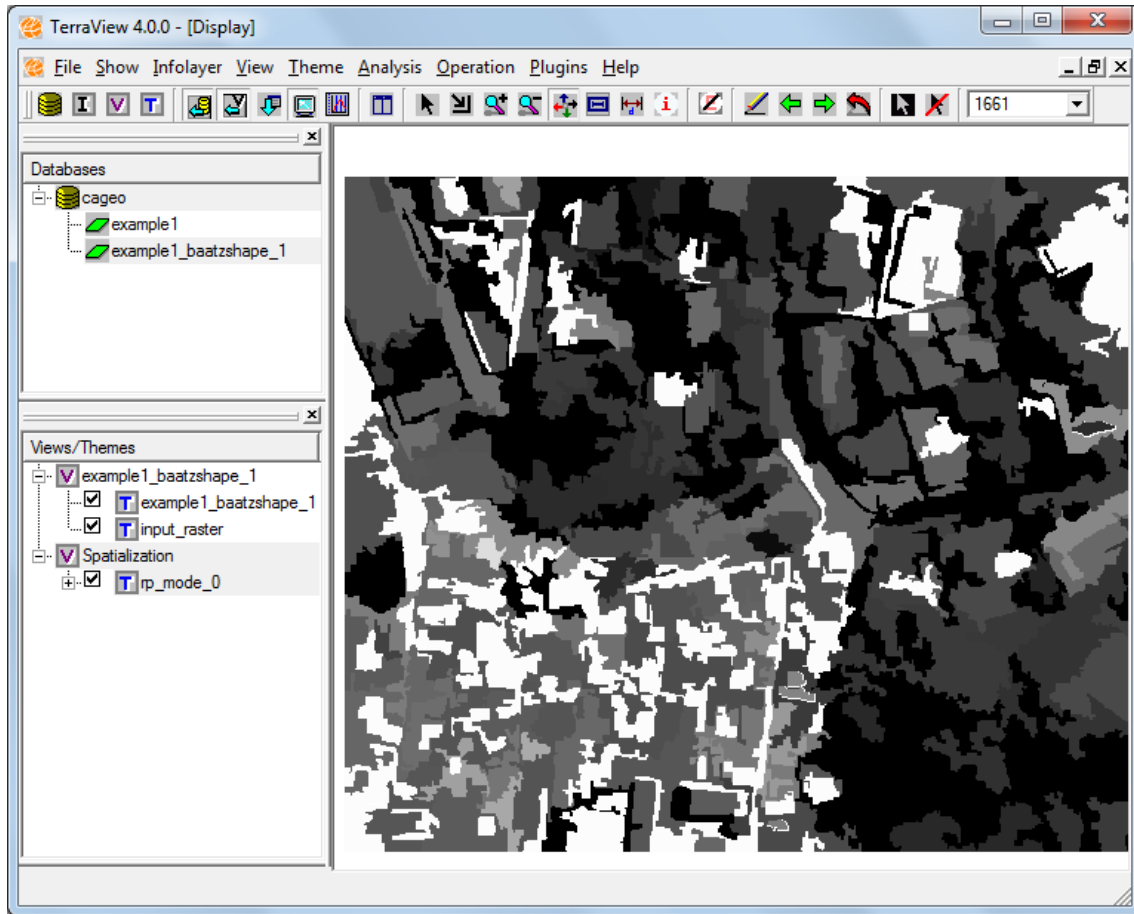


Figure 3.14 - Spatialization of the *mode* feature. Brighter objects define regions with higher values of mode whereas darker objects define regions with lower mode values, similar to eCognition’s module (LANG et al., 2007).

depicts.

3.3.1 Building a training set

Since the interpreter knows the typology behind the data he must create a description of the expected patterns by selecting training samples for each pattern, which must be representative over the images. These samples are represented by a set of features. Afterward, in the supervised classification step, the algorithm uses these training samples to build a classification model.

In GeoDMA, this step is guided by a simple interface, as shown in Figure 3.16. The interpreter creates the class typology by defining a name and a color for each pattern of interest. Subsequently, the user selects the samples in the image and associates them to each class. The information of sample selection is stored as a label in a

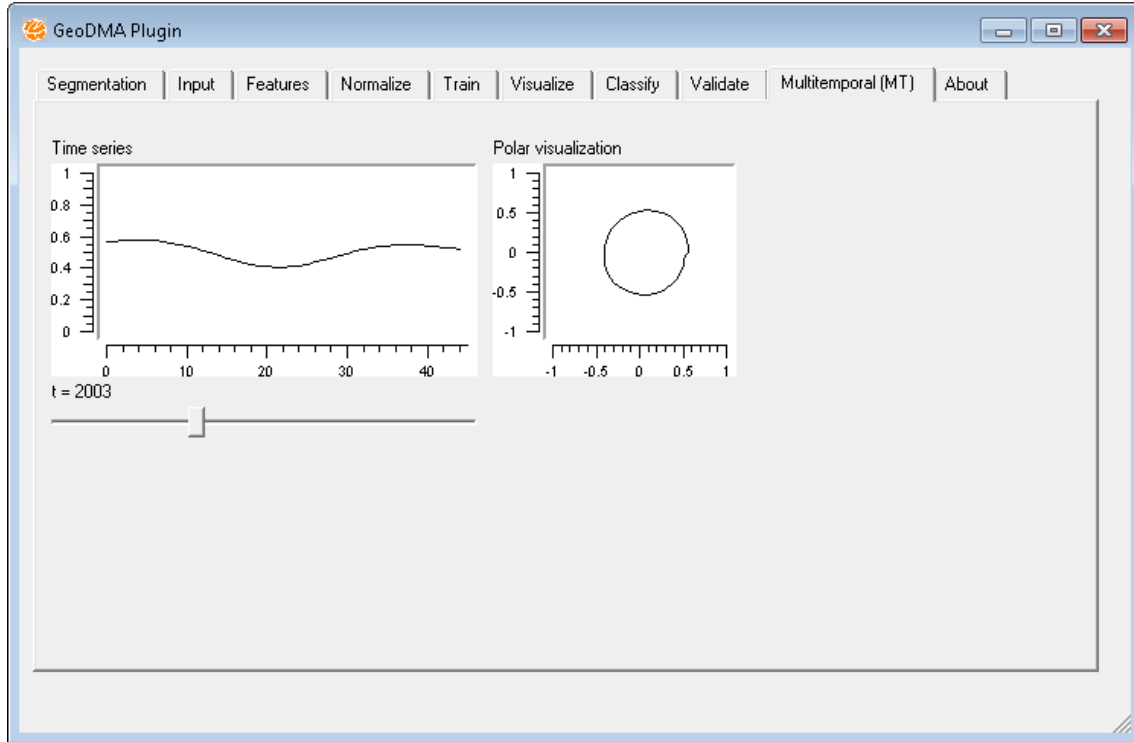


Figure 3.15 - The multi-temporal visualization module in GeoDMA. The interpreter visualizes a specific cycle and the polar transformation of the cycle by selecting a point in the image.

specific column in the objects database, and will be used to train the classification model and to evaluate the results.

3.3.2 Classification using decision trees

Statistical classifiers often assume a Gaussian distribution, which may not be adequate for remote sensing data (XU et al., 2005). On the other hand, decision trees are strictly nonparametric and do not need assumptions about the data statistical properties. According to McCauley e Goetz (2004), decision trees have an intuitive appeal because the classification is clear and easily interpretable.

In a classifier based on decision trees, thresholds are applied to object's features. Observations satisfying the thresholds are assigned to the left branch, otherwise to the right branch (HASTIE et al., 2009). In the final step, classes are assigned to the terminal nodes (or leaves) of the tree.

Forming a decision tree is a recursive problem expressed in a divide-and-conquer method. Given a set of training samples, there are three possibilities to build a

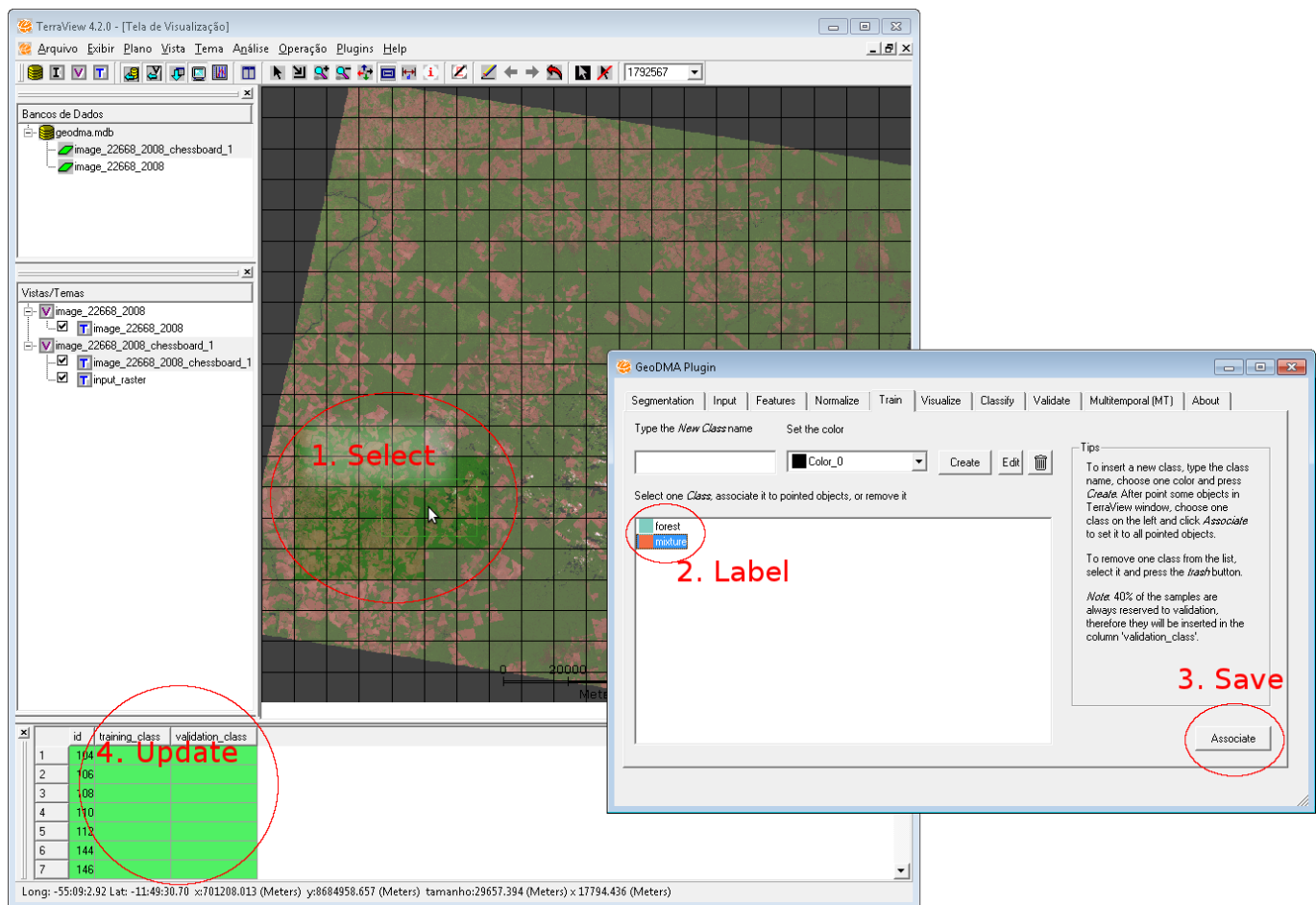


Figure 3.16 - Interface for sample selection.

decision tree (QUINLAN, 1993):

- When the set contains only samples belonging to a single class, the decision tree is composed by a leaf;
- When the set contains no samples, further information, such as the overall majority class, is necessary;
- If the set contains samples of different classes, it is refined into single class subsamples. One test based on a single feature with one or more mutually exclusive outcomes is chosen.

According to Witten e Frank (2005), a purity measure of each node improves the feature selection process that produces the purest daughter nodes. Based on information theory, the entropy relates the likelihood of a feature to be classified as a

certain pattern. The entropy aims to answer “how uncertain we are of the outcome?” (SHANNON, 1948). Suppose we have a set of possible events (features being classified as $1, 2, \dots, N$) whose probabilities of occurrence are p_1, p_2, \dots, p_N . Then the measure of entropy $H(p_1, p_2, \dots, p_N)$, is defined as follows:

$$H(p_1, p_2, \dots, p_N) = -K \sum_{i=1}^N p_i \log p_i, \quad (3.7)$$

where K is a positive constant. In the construction of a decision tree, the entropy for each possible decision (applying a threshold in some feature) is computed. The lower is the value of H , the most proper is the current decision for discriminate the classes. Briefly speaking, the problem of decision tree construction is to find the best features to discriminate the classes and to divide recursively the data into several subsets (WANG; LI, 2008).

Given this measure, one can calculate the so called *information value (info)* for the selected features, converting the occurrences of classes to a set of probabilities:

$$\begin{aligned} info([v_1, v_2, \dots, v_N]) &= H\left(\frac{v_1}{D}, \frac{v_2}{D}, \dots, \frac{v_N}{D}\right) \\ D &= \sum_{i=1}^N v_i. \end{aligned} \quad (3.8)$$

The value called *gain* measures the advantage of using a certain feature in despite to another. It is calculated by the *info* contained in all elements per sample class minus the *info* for the number of instances that go down each branch. Suppose, for example, we have two features called *pixel_mean* and *area*, and classes called *forest*, *clear_cut* and *road*, with 4 samples to *forest*, 2 samples to *clear_cut* and 3 samples to *road*. Generating a split in the *pixel_mean* feature will divide the training samples like shown in Figure 3.17a, and splitting in the *area* feature divides as indicated in Figure 3.17b. To find *gain* for both splits, one must have to calculate their *info* values:

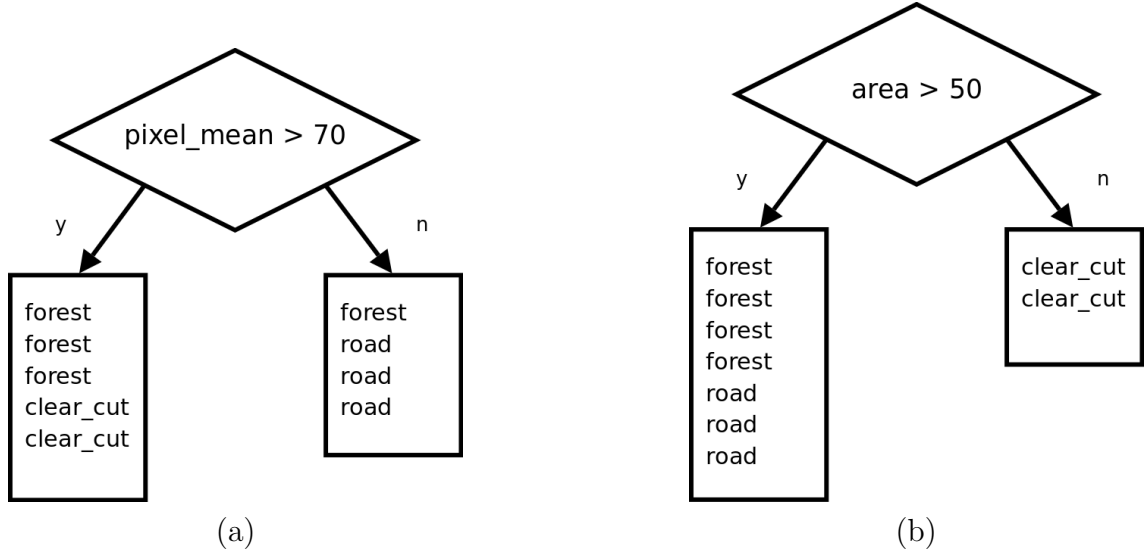


Figure 3.17 - a) Splitting feature *pixel_mean* in the value of 70, and b) Splitting feature *area* in the value of 50.

$$\begin{aligned}
 \text{gain}(\text{pixel_mean}) &= \text{info}([4, 2, 3]) - \text{info}([3, 2, 0], [1, 0, 3]) \\
 \text{gain}(\text{area}) &= \text{info}([4, 2, 3]) - \text{info}([4, 0, 3], [0, 2, 0]).
 \end{aligned}$$

The *info* value for more than one interval of values is calculated as the following:

$$\text{info}([p_1, p_2], \dots, [p_{N-1}, p_N]) = \sum_{i=1}^{N-1} \frac{p_i + p_{i+1}}{\sum_{j=1}^N p_j} H(p_i, p_{i+1}). \quad (3.9)$$

Therefore the resultant value $\text{gain}(\text{pixel_mean})$ is:

$$\begin{aligned}
 \text{info}([4, 2, 3]) &= -\frac{4}{9} \log(4/9) - \frac{2}{9} \log(2/9) - \frac{3}{9} \log(3/9) = 1.5305 \\
 \text{info}([3, 2, 0]) &= -\frac{3}{5} \log(3/5) - \frac{2}{5} \log(2/5) = 0.97095 \\
 \text{info}([1, 0, 3]) &= -\frac{1}{4} \log(1/4) - \frac{3}{4} \log(3/4) = 0.81128 \\
 \text{info}([3, 2, 0], [1, 0, 3]) &= \frac{5}{9} \times 0.97095 + \frac{4}{9} \times 0.81128 = 0.89999 \\
 \text{gain}(\text{pixel_mean}) &= 1.5305 - 0.89999 = 0.63051,
 \end{aligned}$$

and the resultant value for $gain(area)$ is:

$$\begin{aligned}
info([4, 0, 3]) &= -\frac{4}{7} \log(4/7) - \frac{3}{7} \log(3/7) = 0.98523 \\
info([0, 2, 0]) &= -\frac{2}{2} \log(2/2) = 0.0 \\
info([4, 0, 3], [0, 2, 0]) &= \frac{7}{9} \times 0.98523 + \frac{2}{9} \times 0.0 = 0.76629 \\
gain(area) &= 1.5305 - 0.76629 = 0.76421.
\end{aligned}$$

The feature *area* reached a higher value of *gain*. In this case, it would be chosen for creating a branch in the decision tree. Such feature divides better the space, since it isolates one of the classes in a single leaf (*i.e. clear_cut*), falling into the first basic assumption of decision trees, as mentioned before.

The main information used to perform splits in the decision tree is the *gain*, in which the amplitude and statistical distribution of the features values are not considered. Only the classified elements in each branch of the tree are important. This fact grants to this algorithm an independence from data standards and, therefore it becomes more flexible for classification. Particularly, in multi-temporal analysis, in which one can have many features, these facts make this algorithm more adequate for classifying change signatures than others based on mixture models, for instance.

Hastie et al. (2009) discuss the use of decision trees algorithms. Rather than splitting each node into just two groups at each stage, we might consider multiway splits into more than two groups. While it can be useful, it is not a good general strategy. The problem is that multiway splits fragment the data too quickly, leaving insufficient data at the next level down. According to the author, a major problem with trees is their high variance. Often a small change in the data can result in different series of splits, making the interpretation precarious. This happens because of the hierarchical nature of the process, in which the effect of an error in the top split is propagated down.

How far should a tree grow? Clearly, a very large tree might overfit the data, while a small tree might not capture important structures. The average size is preferred, since it does not under or overestimate the data, and it is also easily interpreted by the user. According to Witten e Frank (2005), the parameter called min_{obj} defines the minimum number of instances per leave of the tree. In other words, it has the

ability to cut out tests in which almost all training samples have the same outcome. Consequently, nodes in a tree are removed unless they have at least a minimum number of cases. High \min_{obj} values suggest a more generalist classification model, in which more objects are classified in the same tree path.

3.3.3 Classification using self-organizing maps

One unsupervised alternative for classification is also provided by GeoDMA, using the well-known algorithm of Self-Organizing Maps – SOM. SOM is a powerful tool for exploring huge amounts of high-dimensional data. It defines an elastic, topology-preserving grid of points that is fitted to the input space (LAAKSONEN et al., 2005). Proposed by Kohonen (2001) as a tool for visualization and data analysis with many dimensions, this algorithm has been used for a wide variety of applications, such as clustering, dimensionality reduction, classification, sampling, vector quantization and data-mining.

SOM is based on the idea of a set of neurons which through learning experiences specializes in identifying certain types of patterns. The basic idea of SOM is to map the data patterns onto an n -dimensional grid of neurons. That grid forms what is known as the output space. This mapping preserves topological relations, i.e. patterns that are close in the input space are mapped to close units in the output space. The neuron structure is composed by a vector of weights. The number of weights is defined by the number of input features.

The classification process involves the competition between the neurons, which occurs in several iterations, known as epochs. The training starts by initializing randomly the neurons. For each input the algorithm finds the winner neuron, which is the closest neuron to the pattern (VESANTO, 2002). The euclidean distance can be used to calculate the distances. The neighboring neurons are also updated, however using a reducing factor. While the process is repeated the neurons move in the feature space.

Let \mathbf{x} be a set of N training patterns, and \mathbf{w} the set of neurons, spread along a 2-dimensional space. Thus w_{ij} is the neuron at the (i, j) position. Let $0 \leq \alpha \leq 1$ be the learning rate, and $h(w_{ij}, w_{mn})$ the neighborhood function, varying in the $[0, 1]$ interval, closer to 0 for more distant neurons. The learning rate is usually bigger in the early epochs and smaller in the last epochs, to smooth the convergence. The basic training algorithm is described as follows:

a) Calculate the distance from pattern x_k and all neurons:

$$d_{ij} = |x_k - w_{ij}| \quad (3.10)$$

b) Find the winner neuron:

$$w_{mn} \rightarrow w_{ij} : d_{ij} = \min(d_{mn}) \quad (3.11)$$

c) Update the neural network:

$$w_{ij} = w_{ij} + \alpha h(w_{mn}, w_{ij}) |x_k - w_{ij}| \quad (3.12)$$

d) Repeat this until a stop criteria is reached.

Generally, the gaussian function is used in $h(w_{ij}, w_{mn})$ to update the neurons, according to an influence distance r , like the following:

$$h(w_{ij}, w_{mn}) = e^{-\frac{1}{2} \frac{(i-m)^2 + (j-n)^2}{r^2}}. \quad (3.13)$$

After training the neurons, each of them will be specialized in one of the expected patterns from the input data. Therefore, the resultant classifications are created by labeling each input data with the label of the winner neuron. In GeoDMA, this algorithm was implemented based on the work of Korting et al. (2008).

3.4 Evaluation of classification

The output of GeoDMA is a thematic map (Figure 3.18), obtained by applying the classification model to the database. As the KDD process suggests, from the output the interpreter can make a number of inferences besides the map evaluation.

In the decision tree classification model, it is possible to infer from the tree's nodes the most proper features for classifying each pattern. In the unsupervised classifier SOM, generally the result produces more clusters than the desired patterns. In this case, the interpreter must assign a meaning to the patterns by labeling them according to the typology. However, if the results are not satisfactory any of the previous tasks can be executed again.

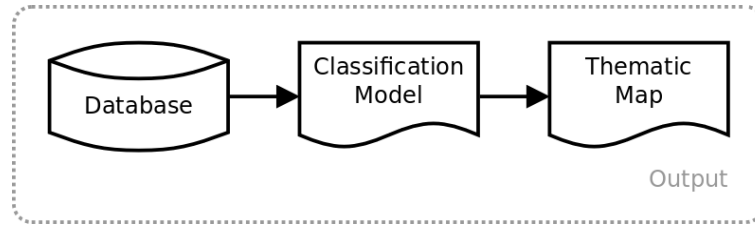


Figure 3.18 - Thematic map is the output when applying the classification model to all objects stored in the database.

3.4.1 Accuracy assessment

According to Gamanya et al. (2007), a strong and experienced evaluator of segmentation techniques is the human eye/brain combination. This statement is also supported by Baatz et al. (2000), who argued that no segmentation result – even if quantitatively proofed – will convince, if it does not satisfy the human eye. In addition, when dealing with multi-temporal analysis, the validation is often not straightforward, since independent reference sources for a broad range of potential changes must be available during the change interval (VERBESSELT et al., 2010).

However, it is always important to establish correctness measures of the results with ground truth. According to Congalton (2005), validation has become a standard component of any land cover map derived from remotely sensed data. Knowing the map accuracy is vital to any decision making performed using that map.

GeoDMA provides the calculation of the error matrix and the Kappa value for a classification. In the sample selection module the system automatically divides the samples into training and validation sets, randomly. With the validation samples, results are compared in order to create the error matrix. In cases where the sample set is reduced, GeoDMA provides an exhaustive method based on the Monte Carlo simulation using only the training samples. The base for this simulation is to perform random experiments to solve mathematical models and complex problems. The goal is to simulate a real system based on the large samples theory (RUBINSTEIN; KROESE, 2008).

To execute the Monte Carlo simulation, the training samples are subdivided N times into training and validation samples. For each subdivision, a Kappa value is calculated. In the end of the simulation, the statistics are provided, indicating maximum, minimum and average values. One example of a Monte Carlo simulation is presented in Figure 3.19.

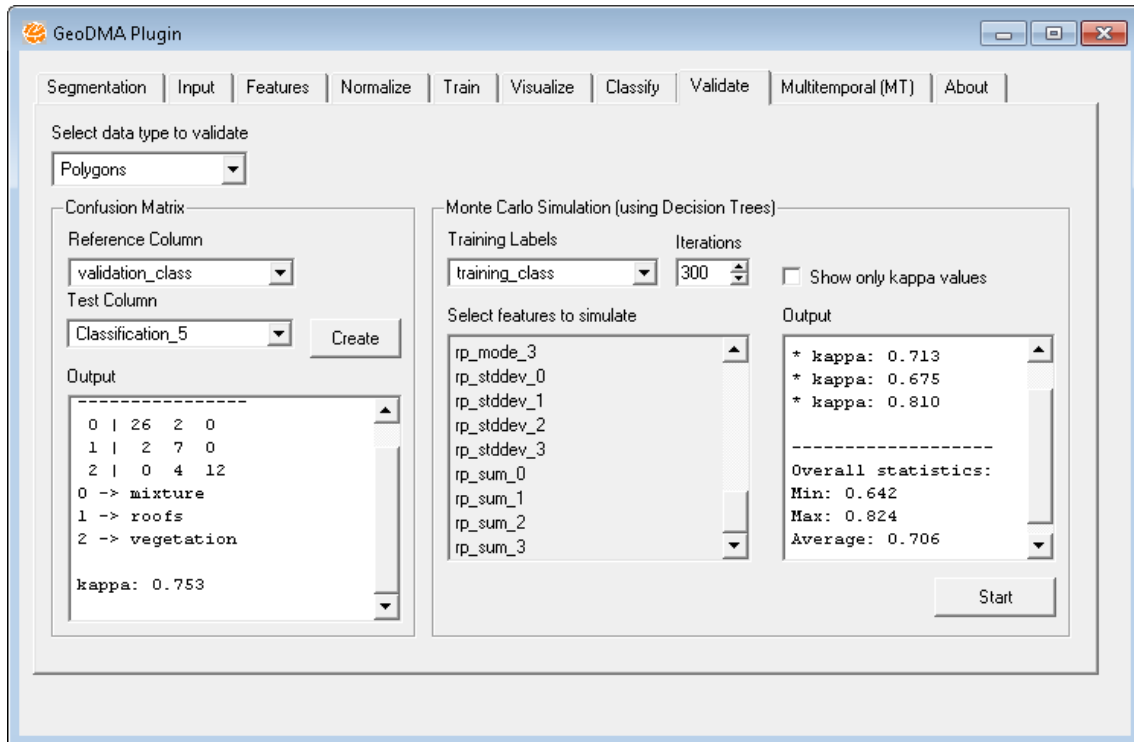


Figure 3.19 - The interface of the Monte Carlo simulation in GeoDMA.

3.4.2 Change detection

At this point, the land cover information is assumed to be available in different times. It is important to say that the time information may vary according to the available database. For example, in a multi-temporal profile of EVI2 values, every classification should represent the land cover at a predefined interval, like a single year, or a crop year. When high spatial resolution imagery is used, the classification can represent the land cover at 2 specific moments. Therefore, the interpretation should respect these intervals in this case. This means that certain aspects of change will not be correctly detected if the proper temporal resolution is not used.

Two methods for detecting change are related in this work. The first one uses 2 classification maps of the same place in different time intervals, which is called direct change. The second method creates a trajectory of change using more than 2 maps. In fact, the first method is a special case of the second. In both cases, the measure of change contains a restriction over the objects. The restriction is that maps must have the same spatial resolution, and in case where the segmentation-based approach is used, the same objects will be used for all maps. The unique variable in this case is the class typology.

3.4.2.1 Direct changes

Given the thematic maps, the method to retrieve direct changes simply evaluates the same location at 2 different times. By using this method, the resultant map will be a binary description of changed and unchanged locations. The following strategy is employed to create the direct changes map:

```

for every object in  $t_1$ 
  if the land cover class in  $t_1$  and in  $t_2$  is the same
     $label \leftarrow no\ change$ 
  else
     $label \leftarrow change$ 
  end if
  assign  $label$  to the object in the resultant map
end for

```

3.4.2.2 Trajectories of change

According to Silva et al. (2008), patterns found in one map can be linked to those in earlier and later maps, enabling a description of the objects' *trajectory of change*. In GeoDMA, the change detection method searches for trajectories of change in the classification maps. We assume that a single object belongs to a specific class on each map (cycles t_1, \dots, t_N). Within this context, the trajectory of change is defined by a sequence of land changes. It is then possible to define a label for a specific sequence, and therefore discover land change patterns.

A second important inference on trajectories is the detection of sub-trajectories where change is perceived. Suppose we have the patterns *forest*, *bare soil* and *cropland*. For instance, given 5 maps it is possible that 3 different objects behave as follows:

Object	t_1	t_2	t_3	t_4	t_5
O_1	Forest	Forest	Bare soil	Cropland	Cropland
O_2	Forest	Forest	Forest	Bare soil	Cropland
O_3	Forest	Forest	Forest	Forest	Bare soil

When analyzing the entire trajectory for the 3 objects they are different. O_1 remains unchanged in the transitions $t_1 \rightarrow t_2$ and $t_4 \rightarrow t_5$. O_2 does not change in $t_1 \rightarrow t_3$ and also O_3 does not change in $t_1 \rightarrow t_4$. However, it is noticeable the sub-trajectory *forest*, *bare soil*, *cropland* for the objects O_1 and O_2 . In this example, the only difference

is the starting points for the changes. In this case the objects O_1 and O_2 present similar behavior in terms of land change. The trajectory of O_3 can be described as *deforestation* in $t_4 \rightarrow t_5$.

4 CASE STUDIES

This Chapter presents some case studies in which GeoDMA system is applied to classify land cover patterns. Different targets are analyzed and some experiments are also performed using alternative OBIA systems such as InterIMAGE and eCognition for comparison purposes.

The first case study uses high spatial resolution images to detect automatically urban land cover patterns using segmentation-based features. The second case study exploits a set of landscape-based features to keep up a correspondence between urban patterns and incidence of diseases. The third one classifies deforestation patches using landscape-based features, and explores change detection by combining two land cover maps. To explore the multi-temporal features, the fourth and fifth case studies use polar features over an EVI time series and compare the results with experiments using only basic multi-temporal features. To evaluate the results, land cover maps produced by hand were employed as reference.

For each case study, it is provided a description about the images, the typology and the GeoDMA modules used to perform the image analysis. The number of training samples, the classification model and the accuracy assessment are provided as well.

4.1 Land cover using intra-urban imagery

Identifying changes in land cover and land use provides important information for urban planning and management (MEINEL et al., 2001). For example, this type of information can be used to plan changes in the public transportation system for areas in which the number of high-rise buildings is rapidly increasing. Such changes can be assessed using multi-temporal analyses of intra-urban land use and land cover maps, which require continuously updated, detailed and precise data (PINHO et al., 2012).

Automatic methods for urban land cover analysis face the challenge of wide intra and inter-classes spectral variability. To overcome this problem, urban applications often employs the oversegmentation strategy, which involves breaking an image into many small regions from which any sought information can be assembled with some knowledge. This strategy is recommended when the goal is object recognition (COMANICIU; MEER, 1997).

To evaluate the effectiveness of GeoDMA system for land cover classification we conduct the study for the city of São Paulo, southeast of Brazil, with a great variety

of intra-urban land cover classes, using a QuickBird imagery. The images used in this experiment consisted in an Ortho-ready Standard 2A hybrid multi-spectral set (0.6m) with 4 bands blue, green, red, infrared, and a panchromatic band (Figure 4.1). Images were acquired on March 30, 2002 with an off-nadir incidence angle of 7.0° and radiometric resolution of 11 bits.



Figure 4.1 - Intra-urban high-resolution image for land cover classification.

The class typology includes roofs (blue, bright, ceramic, dark and gray asbestos), grass, swimming pools, shadows, and trees as shown in Table 4.1. The segmentation algorithm employed is the region growing and the multi-resolution procedure based on Baatz et al. (2000). The segmentation process created 2254 objects (as shown in Figure 4.2), and the features were extracted to describe all objects. In the training step, the interpreter labeled samples according to the previously defined typology. The selection summarized 15 training samples per class and 10 validation samples per class. The parameters used in the segmentation were *scale* of 15 pixels, *compactness* of 40% and *color factor* of 40%. Such parameters are based on Novack (2009).

The classification model based on a decision tree was built using the previously selected samples which is illustrated in Figure 4.3. The features used to describe

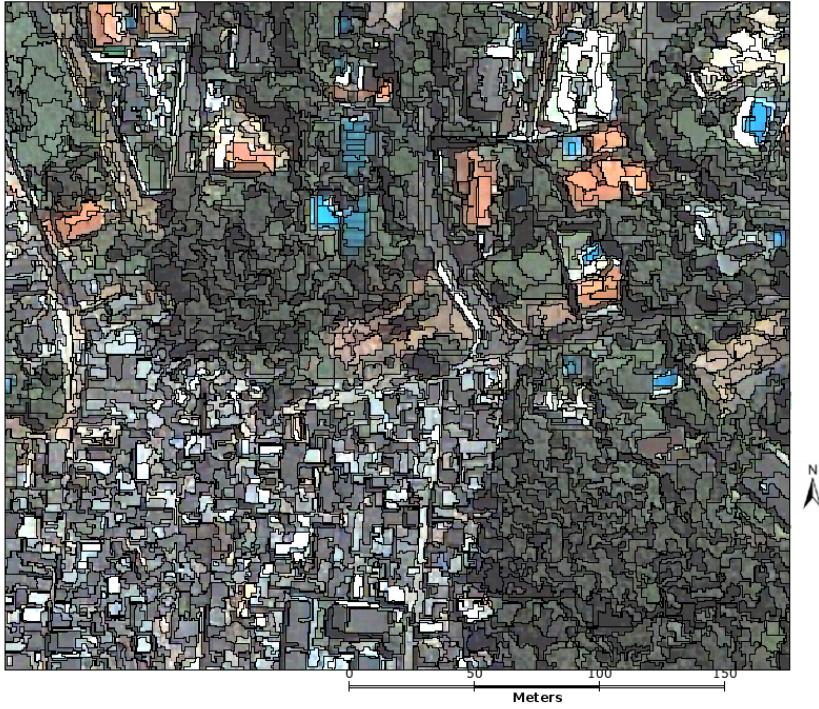


Figure 4.2 - Segmentation of high-resolution image for land cover classification with parameters of $scale = 15$, $compactness = 40\%$ and $color\ factor = 40\%$.

the patterns included spectral mean values of the 4 bands, the mode values of blue, red, and infrared bands, besides the angle, shape index, and elliptic fit from the objects. Finally, all objects in the image were classified according to the model and the top of Figure 4.4 shows the resultant thematic map. To analyze the results we selected around 10 samples per class. The land cover map was evaluated by Kappa coefficient, whose value was 0.84, with an overall accuracy of about 85%. Besides, the overall computational time to run GeoDMA was very short, around 2 hours, including the phases of segmentation, feature extraction and sample selection by the interpreter.

The same experiment was performed using the InterIMAGE system (NOVACK, 2009). Image analysis procedures included feature selection, manual histogram analysis of selected features, definition of fuzzy thresholds and semantic network. The thematic map obtained by InterIMAGE is shown in the bottom of Figure 4.4. The classification overall accuracy (85%) and Kappa value (0.84) obtained by InterIMAGE were the same as those obtained by GeoDMA.

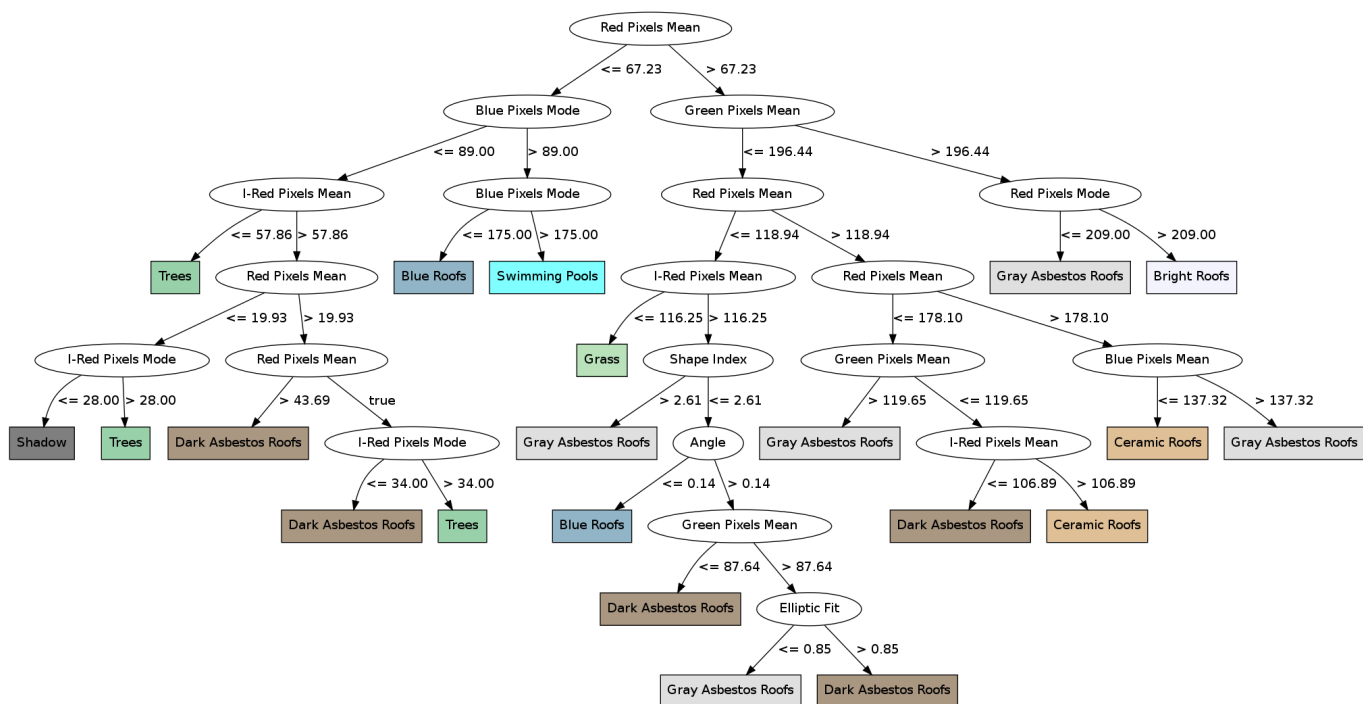


Figure 4.3 - The decision tree model for intra-urban land cover classification in a region of São Paulo city, Brazil.

Table 4.1 - Typology for land cover using intra-urban imagery.

Class	Sample	Description	Characteristics
blue roofs		Roofs with large areas, including industrial buildings.	Present smooth textures, shapes mainly rectangular and areas with a maximum of 8,000 m ² .
bright roofs		White colored roofs with large areas, including industrial buildings.	Present a smooth texture, shape mainly rectangular and areas with a maximum of 8,000 m ² .
ceramic roofs		Roofs with red or orange colors, are surrounded by vegetation and pools in richer urban areas, or clustered with different roof types in poor regions.	Shape mainly rectangular and areas with a maximum of 800 m ² .
dark roofs		Roofs with dark colors such as graphite, including industrial buildings.	Shape mainly rectangular and areas with a maximum of 8,000 m ² .
gray asbestos roofs		Roofs with large areas, including industrial buildings.	Shape mainly rectangular and areas with a maximum of 8,000 m ² .
grass		Targets with light green color, present in unoccupied areas, gardens, and soccer fields.	Often with irregular shape and variable size, and smooth or median texture.
swimming pools		Swimming pools with a light blue color, installed in residences or clubs.	Shape mainly rectangular and areas with a maximum of 250 m ² .
shadows		Targets with black color, present in regions with vegetation or high buildings.	Present an irregular shape, depending of the object that created such shadow, with a very smooth texture, and areas with a maximum of 1,800 m ² .
trees		Areas containing trees, presenting a dark green color, surrounded by shadow.	The shape is irregular when there is a cluster of trees, or circular when there is a single tree, and a rough texture.

SOURCE: Adapted from Novack (2009).

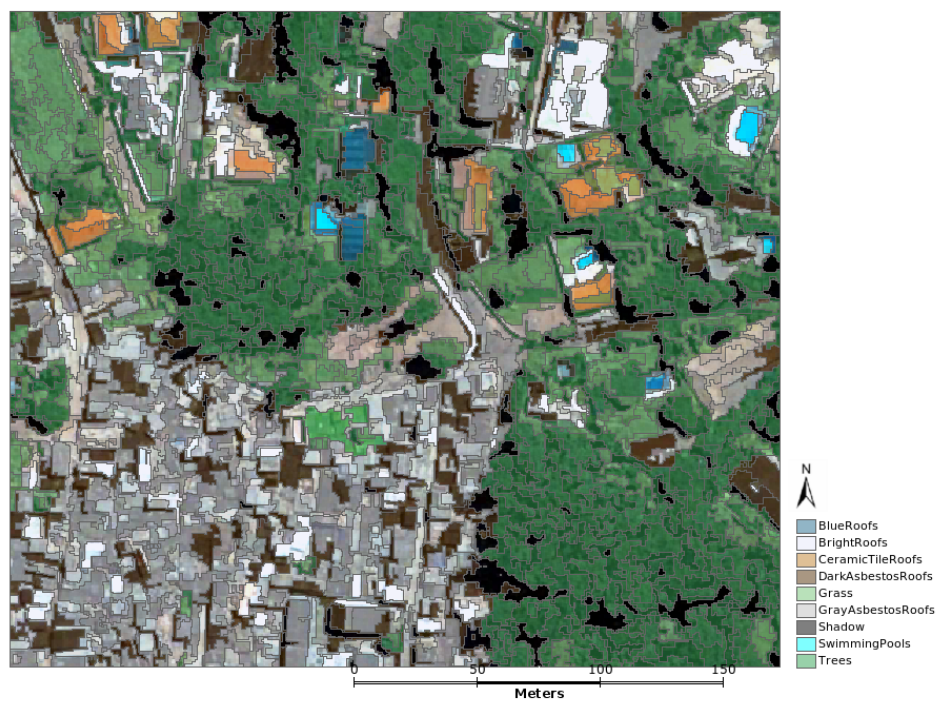


Figure 4.4 - Intra-urban land cover map using (top) GeoDMA and (bottom) InterIMAGE.

4.2 Detection of urban landscape patterns

This study aimed to detect Urban Landscape Patterns (ULP), which is based on the work of Reis (2011). Reis used GeoDMA to associate the urban environment components to the incidence of dengue fever in the Brazilian city of Rio de Janeiro. In this application the objective is to divide the landscape based on spatial distribution of the urban land use classes. For this purpose, the study area was divided into cells of $250 \times 250m$, generating about 800 cells (pixel grid), and they were classified using landscape-based features.

Figure 4.5 presents the study area highlighted in yellow and composed by 30 neighborhoods in the north of the city. The labels D, M, S, Y, and N stand for Dense, Moderate, Sparse, Yes, and No, respectively. They identify the type (D, M, S) and presence or absence (Y, N) of each urban components in the urban cells. Each cell contains a mixture of the following urban components: residential area, garden, shadow, shed, impervious area (no buildings), water body, and vegetation. Given the land cover map produced with 7 pre-defined classes (Table 4.2), each cell was classified as one of 9 possible ULP, as described in Table 4.2.

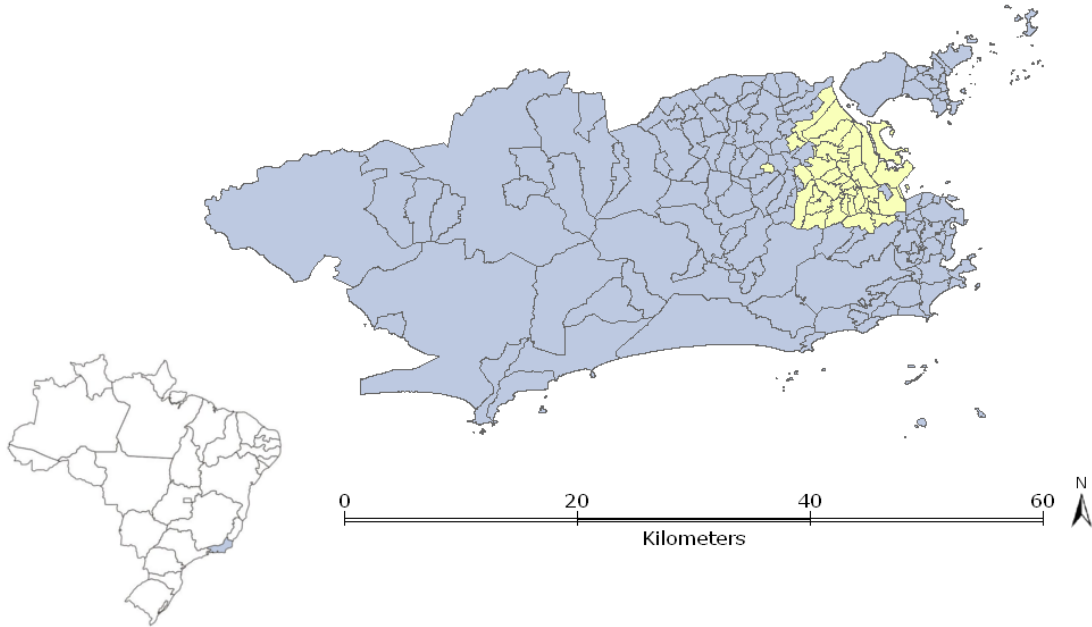


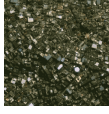








Figure 4.5 - Study area for detecting urban landscape patterns (ULP), highlighted in yellow.

In this application, GeoDMA provided the entire framework for image interpretation

Table 4.2 - Typology for the 9 Urban Landscape Patterns.

ULP	1	2	3	4	5	6	7	8	9
Samples									
Residences	D	D	D	M	M	D	D	D	S
Gardens	N	Y	N	N	N	Y	Y	N	N
Shadow	D	M	D	D	M	M	M	M	S
Sheds	N	N	N	N	N	Y	N	Y	N
Water	M	M	M	M	S	M	M	M	D
Vegetation	S	M	M	D	D	M	M	M	D
Impervious	N	N	N	N	Y	N	Y	Y	N

Labels: Dense, Moderate, Sparse, Yes, No

SOURCE: Adapted from Reis (2011).

using landscape-based features. The original image was segmented and classified by hand, and afterwards such classification was used as reference for classifying the cells into the 9 ULPs. GeoDMA extracted landscape-based features relating the incidence of land cover classes inside each cell, and the decision tree algorithm found automatically a classification model to divide the cells into the correct ULP.

The resultant classification captured key features to describe each ULP and it was simple enough to be understandable by the interpreter. The features used in the decision tree model are: (1) class area for sheds and impervious areas; (2) percentage of residential area inside the cell; (3) patch density for impervious areas and paved roads; (4) patch size standard deviation for water bodies. Figure 4.6 illustrates the decision tree model, and Figure 4.7 presents the thematic map obtained after classification process.

For evaluating the classification, a set of samples was randomly selected. The Kappa coefficient resulted in a value of 0.91. The occurrence of ULP 2 (yellow color) was higher than the remaining ones, about 30% of the total cells, as one can observe in Figure 4.7. According to the ULP typology (Table 4.2), this pattern defines a dense residential area, with gardens, moderated vegetation, and absence of impervious areas with no buildings. Reis (2011) used GeoDMA to detect automatically the spatial distribution of a landscape to infer hotspots for inserting mosquitoes egg traps inside each pattern, concluding that the environment needs to be more explored to model urban diseases.

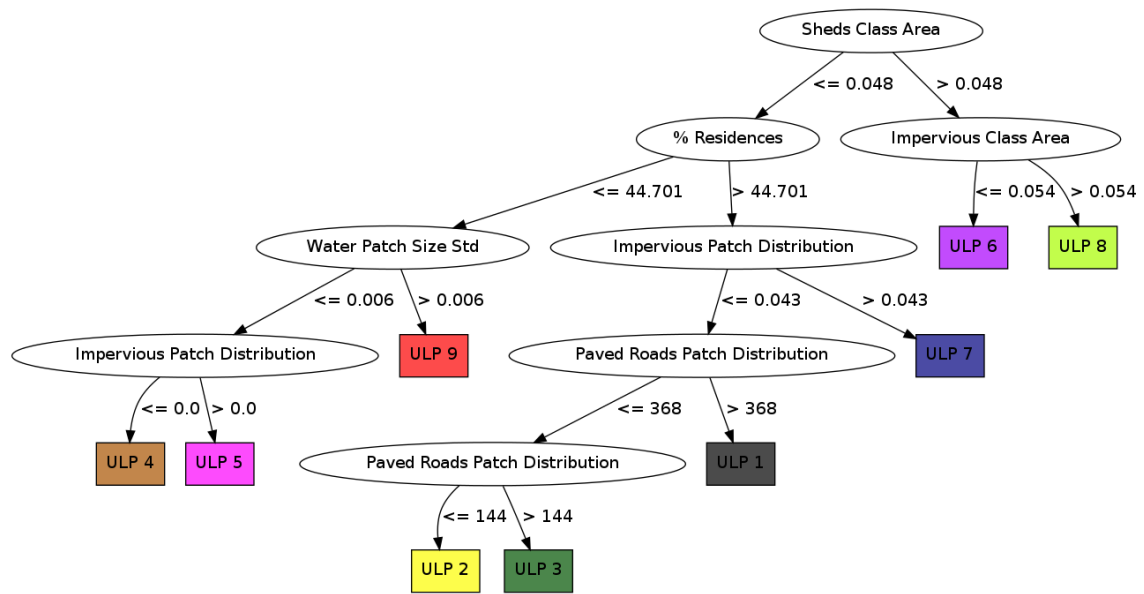


Figure 4.6 - The decision tree model to detect the ULPs.

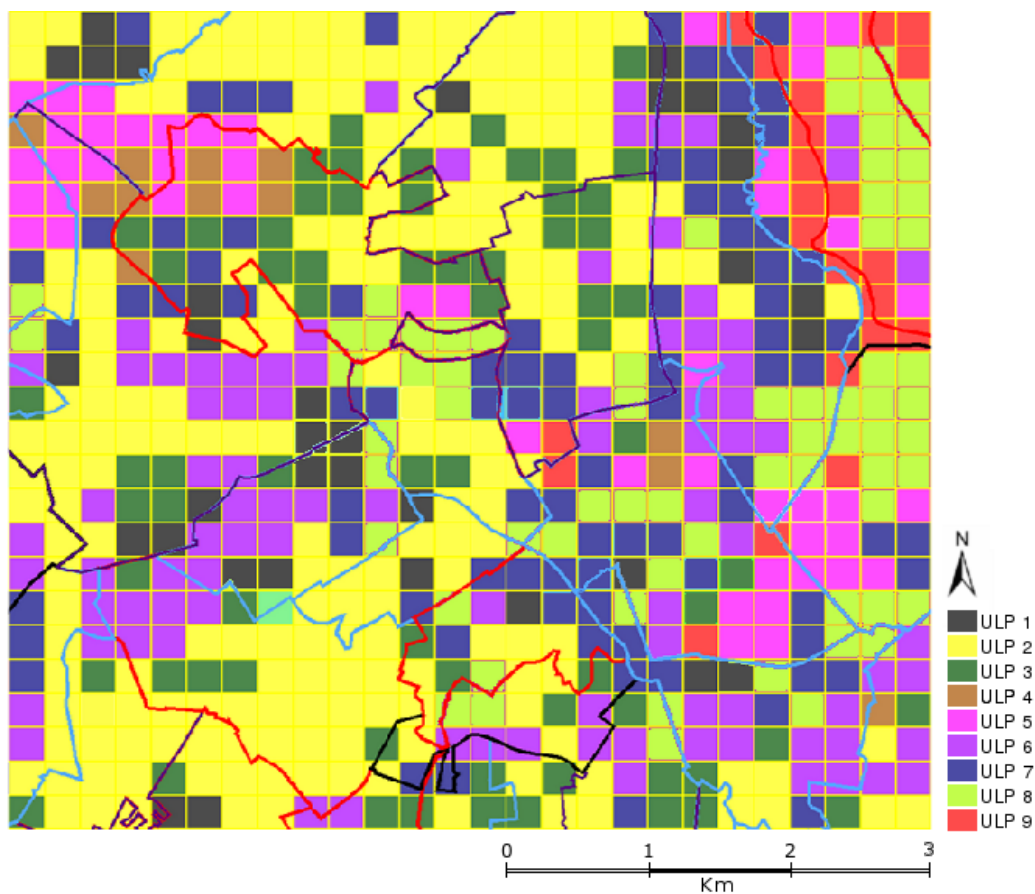
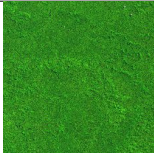
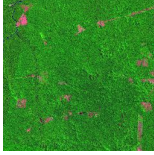




Figure 4.7 - ULP map obtained by GeoDMA.
SOURCE: Adapted from Reis (2011).

4.3 Analysis of deforestation patterns in the Brazilian Amazon

This experiment aims at classifying deforestation patterns in the Brazilian Amazon, and it is based on the works of Saito (2011) and Azeredo (2008). The study area is a deforestation region in the municipality of São Félix do Xingu, located in the southeastern region of Pará state, as shown in Figure 4.8. Deforestation maps from years 2006 and 2009 (Figure 4.9) and provided by PRODES (ESPACIAIS, 2012) were used in this study. PRODES is a methodological approach to identify and estimate deforested areas in the Brazilian Amazon. Four patterns based on Lambin et al. (2003) were used in the land cover typology: *Untouched forest*, *Diffuse*, *Geometric*, and *Consolidated*. The latest 3 classes were defined in accord to the forest occupation. The *Diffuse* pattern includes the beginning or moderate land occupation, unplanned occupation, and deforestation along rivers. The *Geometric* pattern is the beginning or intermediary stage of occupation, and medium or large farms. The *Consolidated* pattern means advanced occupation stage, land concentration composed by small, medium and large farms. This typology is summarized in Table 4.3.

Table 4.3 - Typology for deforestation patterns in the Brazilian Amazon.

Class	Sample	Description	Characteristics
Untouched forest		Areas without deforestation, containing solely forest.	A cell of untouched forest contains no internal objects of the class <i>deforestation</i> .
Diffuse		Contains areas of small and medium rural settlements, defining the initial stage of land occupation.	Isolated deforestation patches with irregular shapes.
Geometric		Describes zones with medium and large settlements, mainly devoted to agriculture or cattle ranching, defining an intermediate land occupation.	Contains areas with large settlements, and regular geometric shapes, with low or medium density of areas.
Consolidated		Defines areas with intense deforestation, devoted to agriculture and cattle ranching. The exhaustion of the forest is evident.	Defines large and homogeneous patches of deforestation, and small concentration of remaining forest.

SOURCE: Adapted from Saito (2011).

To extract landscape-based features from this data set, a regular grid with cells of $10 \times 10 Km$ was generated as shown in Figure 4.9. Following, we selected 10 samples

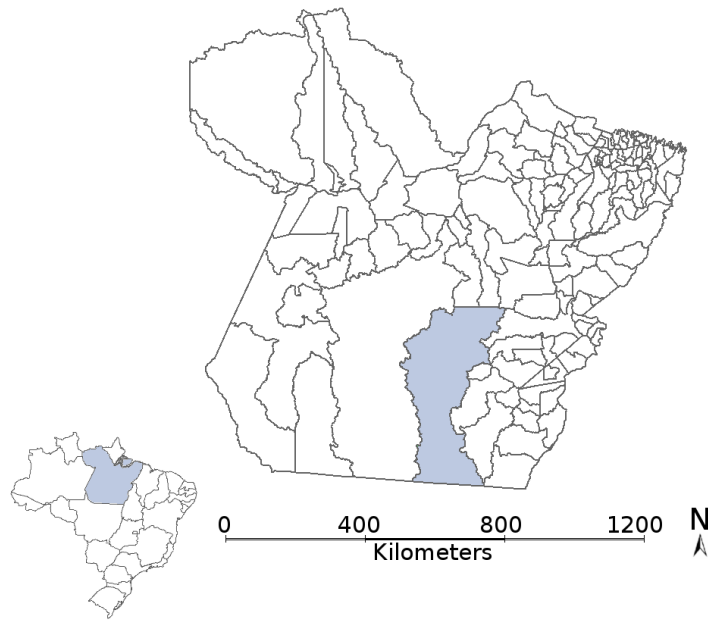


Figure 4.8 - Study area: region of São Félix do Xingu, Pará state, Brazil.

for each pattern in the year of 2006, which were employed to build the classification model as shown in Figure 4.10. We observed that only 3 landscape-based features were used in this classification model to distinguish the 4 patterns defined in Table 4.3: *percent land*, *patch density* and *class area* features. According to the model, when the value of percent land is higher than 0.96, the *Consolidated* and *Geometric* patterns are distinguished from the others. The class area feature was also used to distinguish the *Consolidated* pattern from the others, since this pattern represents the situation in which the land is completely (or almost completely) deforested. The patch density feature was included in the model to distinguish *Forest* pattern (without deforestation) from *Diffuse* (with any density of deforestation patches) pattern.

The classification model was built using training samples identified in the data of 2006, and subsequently the same model was applied in the data of 2009 to evaluate the consistency of the model in relation to temporal variation. Validation samples were selected in both years and the resultant classifications were used to detect direct land change as mentioned in Section 3.4.2.1. Figure 4.11 illustrates the thematic maps for 2006 and 2009 as well as the land changes observed in both years.

These results were compared to those obtained by using the eCognition system (version 8.64, Developer Trial) (LANG et al., 2007). Then, the landscape features as well

as two levels of segmentation were computed in eCognition. The first level included a segmentation strategy which divided the image into regular squares (Chessboard), resulting in a grid composed by objects with $10 \times 10Km$ over the deforestation patches. The second level used the deforestation patches provided by PRODES. The strategy of creating two segmentation levels in eCognition favored the calculation of ordinary class features such as *patch density* and *class area*. However, eCognition system does not rely strictly on landscape ecology concepts. Specific features had to be derived manually using the feature set available in the system, which were composed by several generic features. The supervised nearest neighbor algorithm was applied to classify the data for both years. Training samples were selected in both years, and the classification was performed individually for both years. Figure 4.12 shows the land change map produced by eCognition.

Both results, produced by GeoDMA and eCognition, described the deforestation behavior properly. Table 4.4 presents the accuracy values calculated for both systems. We can observe that the Kappa and overall accuracy values for 2009 obtained by eCognition are higher than those obtained by GeoDMA. This is explained by the fact that we did not selected training samples for data of 2009 to classify this data in GeoDMA system. This strategy was employed to test the generality of the model created by GeoDMA. Such model was trained by 2006 samples, and was used to classify 2006 and 2009 as well. Even though the accuracy for GeoDMA (86%) was a little lower than that for eCognition (88%), both systems obtained very similar results, as we can observe in Figures 4.11 e 4.12.

The use of GeoDMA in this application was straightforward, since the interpreter only loaded the deforestation patches and created a cellular grid. Afterwards, the system provided landscape-based features, a simple and intuitive interface for sample selection, and built the classification model automatically. Such model was also stored and used to classify different data, by loading deforestation patches from different years.

Table 4.4 - Classification evaluation for GeoDMA and eCognition.

	2006		2009	
	Kappa	Accuracy	Kappa	Accuracy
GeoDMA	0.87	90%	0.81	86%
eCognition	0.79	84%	0.85	88%

In this experiment, the processing time for GeoDMA was smaller than that for eCognition. One can observe that it is straightforward to build a semantic network in eCognition, which is based on a user-defined workflow (BAATZ et al., 2008). Nevertheless, several steps are necessary to accomplish the classification, including segmentation in two levels, description of new features, and the setup of the nearest neighbor algorithm.

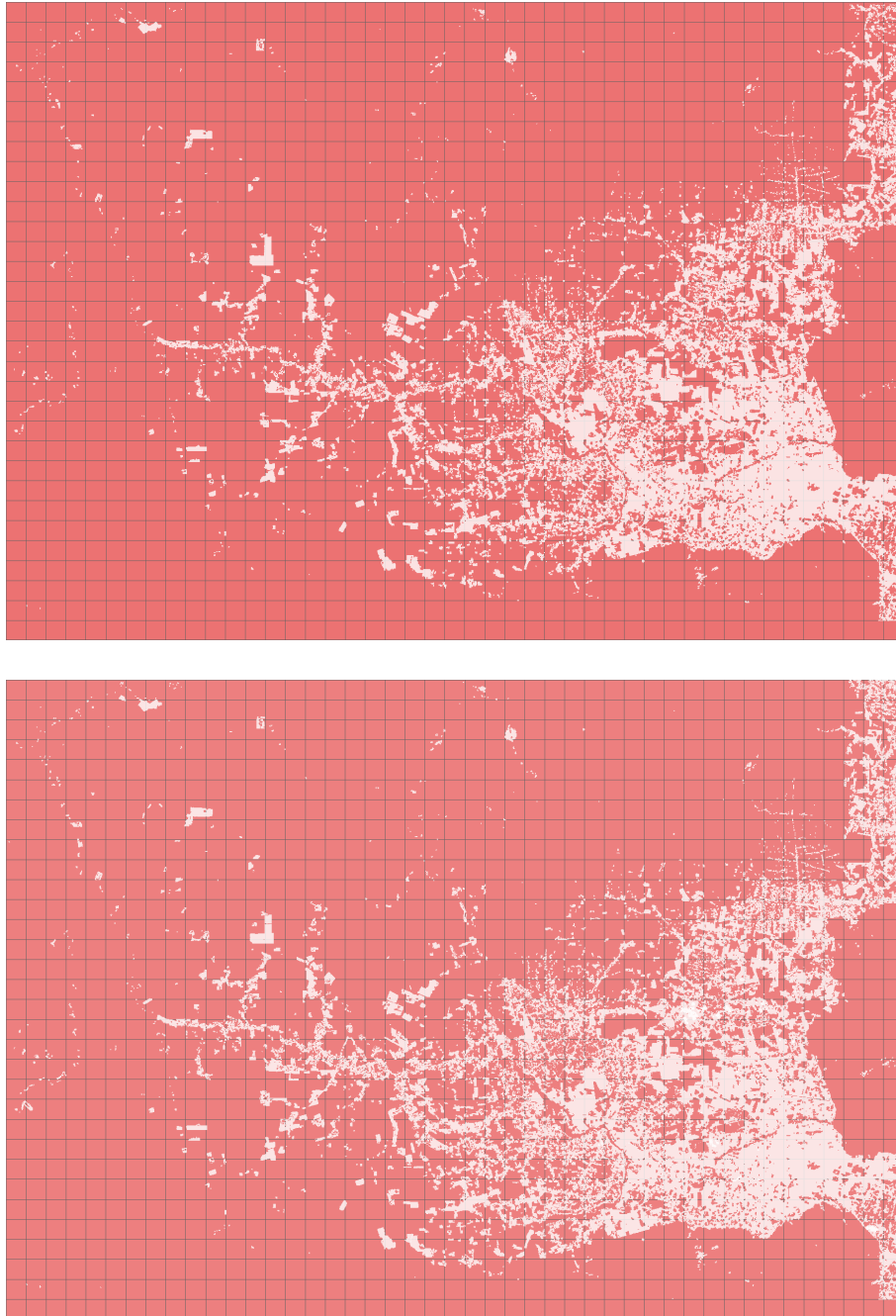


Figure 4.9 - Deforestation patches in São Félix do Xingu, Brazil, for 2006 (top) and 2009 (bottom).

SOURCE: Data provided by PRODES (ESPACIAIS, 2012).

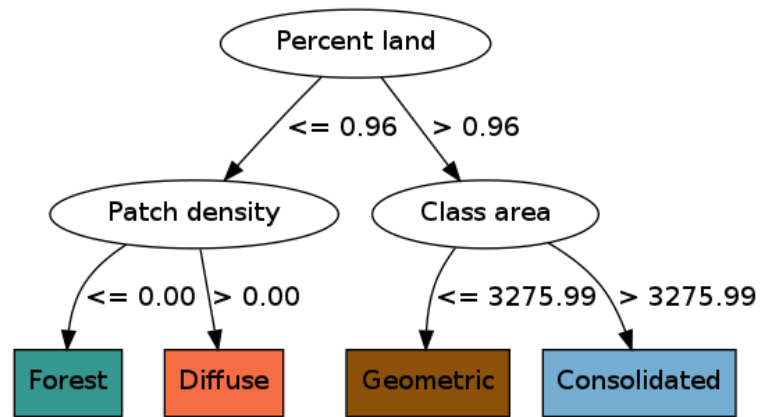


Figure 4.10 - The classification model for deforestation patterns.

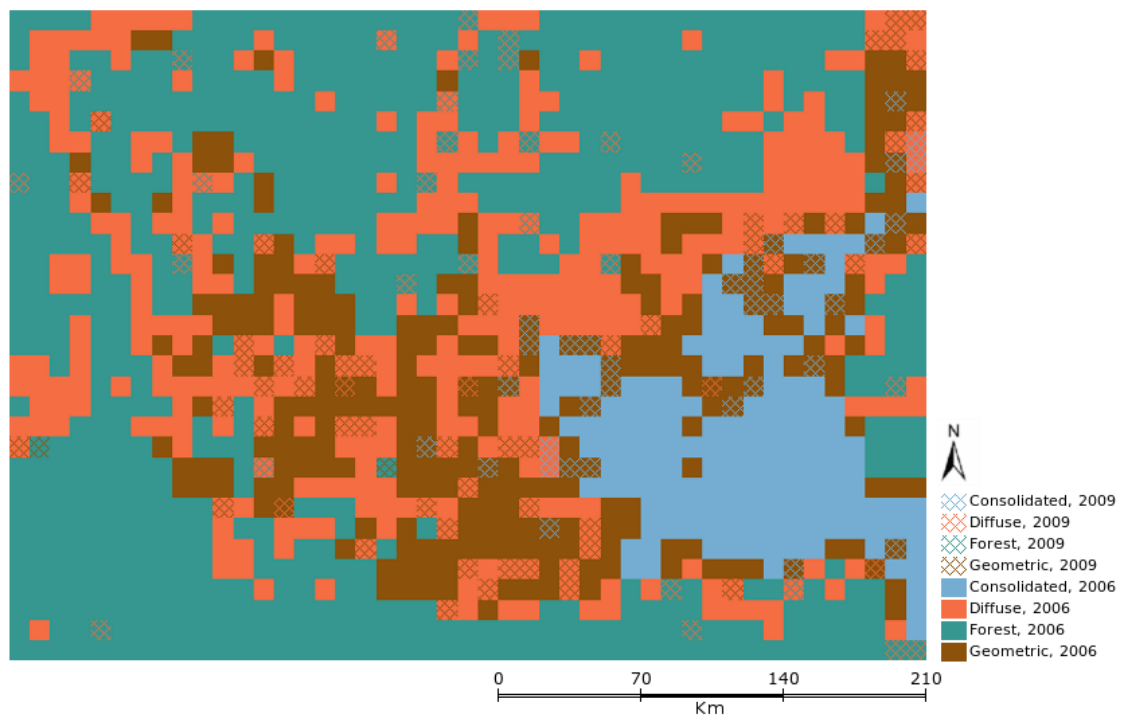


Figure 4.11 - Thematic map for data of 2006 and 2009 using GeoDMA. Overlapping regions define land changes occurred between 2006 and 2009.

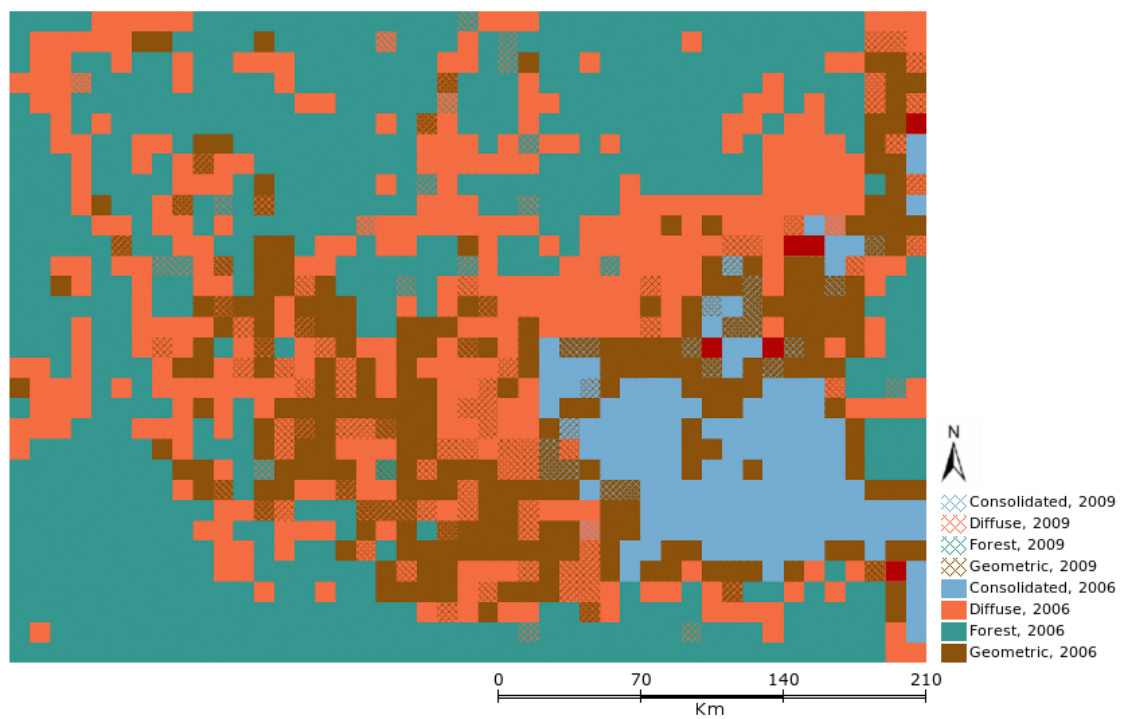


Figure 4.12 - Thematic map produced by eCognition. Overlapping regions define land changes occurred between 2006 and 2009. Red cells were not classified.

4.4 Exploring the multi-temporal analysis for land use and cover mapping

This Section presents two case studies to evaluate the effectiveness of the multi-temporal analysis scheme implemented in this thesis for distinguish between different land cover classes. The studies are primarily focused on assessing the classification accuracy improvement provided by the usage of polar features in the classification process. The first experimental study aimed at distinguishing land cover classes in the Brazilian Amazon region. The second experiment relied on detecting single and double croppings in each growing season.

The data used in the experiments consisted of 16-day EVI2 profiles from MODIS with a 250 m pixel size, which is a Level 3 product (MOD13Q1), calculated from the Level 2 daily surface reflectance product (MOD09 series) (VERMOTE et al., 2002). The criteria for the pixel selection in the composites are based on cloud screening and data quality checks. These profiles date from 2000 to 2010, with a temporal resolution of 16 days in the northern Mato Grosso state of Brazil (Lat. $11^{\circ}34'23''$ S, Lon. $54^{\circ}43'14''$ W). Mato Grosso (shown in Figure 4.13) contains the major frontier of row crops in Brazil, home to some of the largest contiguous row-crop plantations in the world (GALFORD et al., 2008).

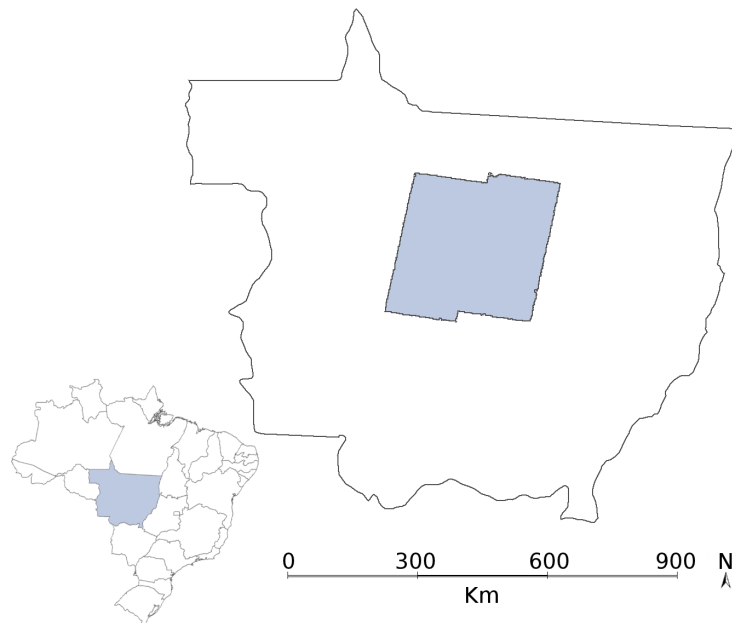


Figure 4.13 - Mato Grosso state, Brazil.

Each profile was divided into annual cycles because the biomass condition along an entire phenological cycle – the growing season – is approximately 1 year (ESQUERDO et al., 2009). Each cycle is composed of 23 values that define a temporal profile for one growing season. The cycle starts in August of one year and finishes in July of the next year. The profiles are EVI2 values in the interval $[0, 1]$, as illustrated in Figure 2.3.

In both case studies, the classification accuracy was analyzed using the cross-validation method, in which the samples are randomly divided into $n = 10$ folds of equal size. One fold was used for testing and the others $n - 1$ were used to train the model. The overall accuracy was obtained by averaging all of the folds. Furthermore, the classification accuracy between maps produced by two different sets of features was compared: only *Basic* features and a combination of *Basic* and *Polar* features (as described in Section 3.2.3).

In the evaluation process, the experiments took into account the variation of parameter \min_{obj} using the Monte Carlo simulation, which performs random experiments to solve mathematical models and complex problems. The parameter \min_{obj} stands for the minimum number of instances per leave of a decision tree. With the variation of this parameter, the model is more specialized in the training set (a small \min_{obj}), or more generalist (a big \min_{obj} value). The goal is to simulate a real system based on the large samples theory (RUBINSTEIN; KROESE, 2008). To define a credible interval, multiple classifications were performed by varying the parameter \min_{obj} . For each \min_{obj} value, 100 simulations were carried out by selecting random samples, which were approximately 30% of the total, and stored the classification accuracy for each simulation. The idea was to analyze the classification accuracy for both sets of features (*Basic* and *Polar*) in relation to the parameter \min_{obj} , allowing to find the most appropriate classification model for each application.

4.4.1 Land cover mapping

To classify land cover in the Brazilian Amazon region, five classes were defined as follows: *Croplands*, *Pasture*, *Urban area*, *Deforestation* and *Forest*. Maps produced by PRODES (ESPACIAIS, 2012) and TerraClass (ALMEIDA et al., 2009) were used as reference data to assess the classification performance when using our method. PRODES monitors the evolution of the extent and rate of total deforestation in the Brazilian Amazon and produces maps of the amount of deforested area annually (VALERIANO et al., 2012). Conversely, TerraClass maps land use and cover classes in deforested areas of the Brazilian Amazon such as Pasture, Annual Agriculture,

Forest, Non-forest, Urban, Hydrography and Secondary Vegetation, among other uses. This project started in 2009 and has delivered maps for the year 2008.

To evaluate the classification results, a stratified random selection approach was used to extract 14,088 training samples. The number of samples for each land cover class was: *Croplands* (4000), *Pasture* (4000), *Urban area* (828), *Deforestation* (1260) and *Forest* (4000). After performing the Monte Carlo simulation two credible intervals (*Basic* and *Basic + Polar*) were delivered, as shown in Figure 4.14.

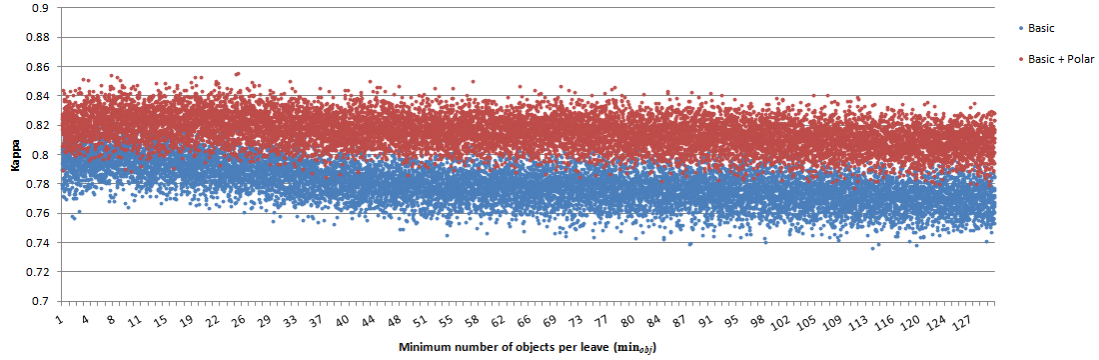


Figure 4.14 - Kappa values in the Monte Carlo simulation in the multi-temporal land cover mapping.

The experiments were simulated by changing the parameter \min_{obj} in the interval $[0, 130]$, which produced 13,000 models. In Figure 4.14, one can observe the consistency of the results, whose Kappa values maintain a quasi-constant tendency within the credible interval and show better classification accuracy for maps produced by the *Basic + Polar* set of features. The average Kappa values were 0.78 and 0.82 for maps produced by the *Basic* and *Basic + Polar* sets of features, respectively. The accuracy improvement when adding the polar features to the basic set of features was approximately 5.12%.

Figure 4.15 illustrates a classification model for the *Basic + Polar* set of features with $\min_{obj} = 100$. The Kappa value was approximately 0.81, and the decision tree contained 13 leaves. One can observe that the feature in the tree root is *area of the 1st season*. This polar feature distinguished the *Forest* class from the remaining ones. Another interesting case was the use of the *polar balance* feature to distinguish between the classes of *Forest* and *Deforestation in 2008*. When the *polar balance* feature exhibits low values, the polar visualization of the time series is more stable. Therefore, this feature explains the fact that cycles of the *Forest* class present a

constant behavior annually (*polar balance* ≤ 0.14), although, cycles of the *Deforestation* class present an abrupt change.

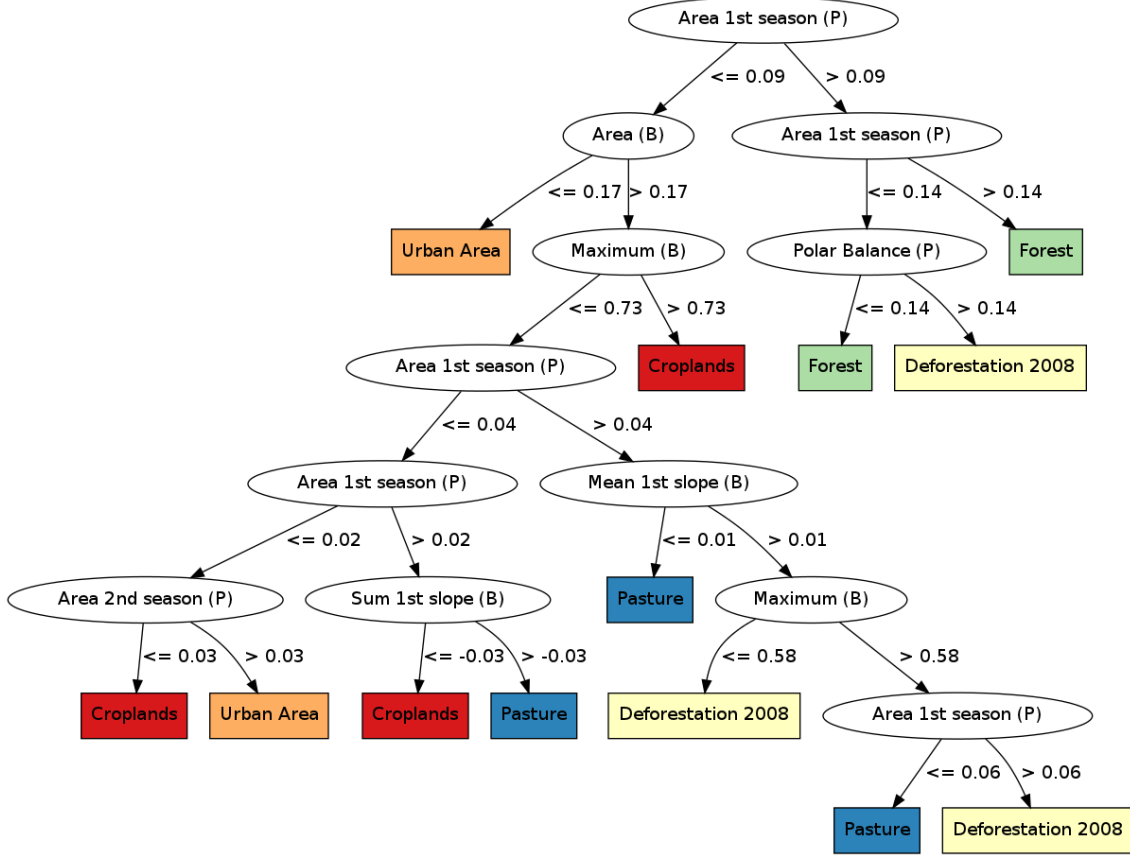


Figure 4.15 - Classification model for the *Basic + Polar* set of features, with 13 leaves and Kappa = 0.81. In the nodes, (B) and (P) stand for basic and polar features, respectively.

Finally, after applying the model to the entire database, the land cover map shown in Figure 4.16 was created. The result is visually consistent; however, it is observed confusion between some classes such as *Pasture* and *Croplands*. A possible explanation can be due to the different spatial resolutions of the data used to produce the reference (30 m) and the land cover (250 m) maps.

4.4.2 Detection of single and double cropping

This study aims at assessing the potential of the implemented toolbox for distinguishing between single and double cropping. One of the objectives for identifying these cropland classes is to detect extensification and intensification processes. According to Galford et al. (2008), extensification is the increase in total row-crop

agricultural area, which is measured as the annual increase from one growing season to the next. On the other hand, intensification describes the change from a single to double croppings pattern from one year to the next.

In this study, the objects were initially identified by hand, which were already classified as *Croplands* in the case study presented in Section 4.4.1. From those results, 578 cycle samples were randomly selected over a 3-year period. There were 225 and 353 samples for single and double cropping, respectively. The polar visualization of some cycles used in the training phase is shown in Figure 4.17. We can observe that the single and double croppings classes contain distinct behaviors, which suggests good refinement between them when using this feature space.

Using the same simulation strategy applied in the previous case study, the parameter \min_{obj} was varied in the interval $[0, 50]$. Then, 5,000 classification models were produced, and their accuracy values were simultaneously calculated and stored. The credible intervals from the two feature sets (*Basic* and *Basic + Polar*) were evaluated as well. Figure 4.18 shows the Kappa values plotted against the parameter \min_{obj} . The average Kappa values were 0.57 and 0.78 for the *Basic* and *Basic + Polar* feature sets, respectively. It was observed that for $\min_{obj} > 30$, the accuracy for the *Basic* set of features decreased, while it remained constant at approximately 0.8 for the *Basic + Polar* set of features. In Figure 4.19, we can observe that the classification model solely containing the *Gyration Radius* feature was enough to distinguish both classes, with Kappa = 0.8. Considering the average accuracy obtained using both models in the simulation, the improvement of adding polar features to the set of features was approximately 36.84%.

4.4.2.1 Land change detection

The classification model obtained in this case study was applied to a 3-year time series, creating land cover maps for the Mato Grosso state to describe the patterns of single and double croppings from years 2008 to 2010. The initial map of pattern *croplands* from TerraClass was used as reference. Therefore the objects of class *croplands* were classified as *single* or *double* croppings, for the 3 years. Figure 4.20 summarizes the classification.

The maps illustrated in Figure 4.20 show the types of cropland considering the benchmark provided by TerraClass. The classification provided in this application considered only regions labeled as cropland in 2008 by TerraClass. Therefore, in this experiment, no extensification (change from some other land cover class to cropland)

was detected. The areas (Km^2) of *single* or *double* croppings are presented in Figure 4.21. In this study region, 19237.87 Km^2 of croplands were mapped for the year 2008, of which 14097.81 Km^2 are *single* croppings, and the remaining 5140.06 Km^2 are *double* cropping. In 2009, the amount of *single* croppings increased to 15711 Km^2 (with 3526.87 Km^2 of *double* cropping), and later it decreased to 15165.06 Km^2 in 2010 (with 4072.81 Km^2 of double cropping).

When analyzing the trajectories of change from the cropland maps, 4 land change patterns were identified, as follows:

- a) *Constant*: the land cover presented no changes along over a 3-year period;
- b) *Intensification*: the land cover changed from *single* to *double* croppings;
- c) *Reduction*: the land cover changed from *double* to *single* croppings;
- d) *Interchange*: the land cover presented alternate behavior along the 3-year period (*double, single, double* or *single, double, single*).

As we can observe in Figure 4.23, the *Constant* pattern prevailed over the others, with 64.8% of the total area. The other patterns presented the following area percentages: 9.7% for *Intensification*, 15.2% for *Reduction* and 10.3% for *Interchange*. The land change map obtained from the years 2008 to 2010, took into account only the cropland classes, is shown in Figure 4.22.

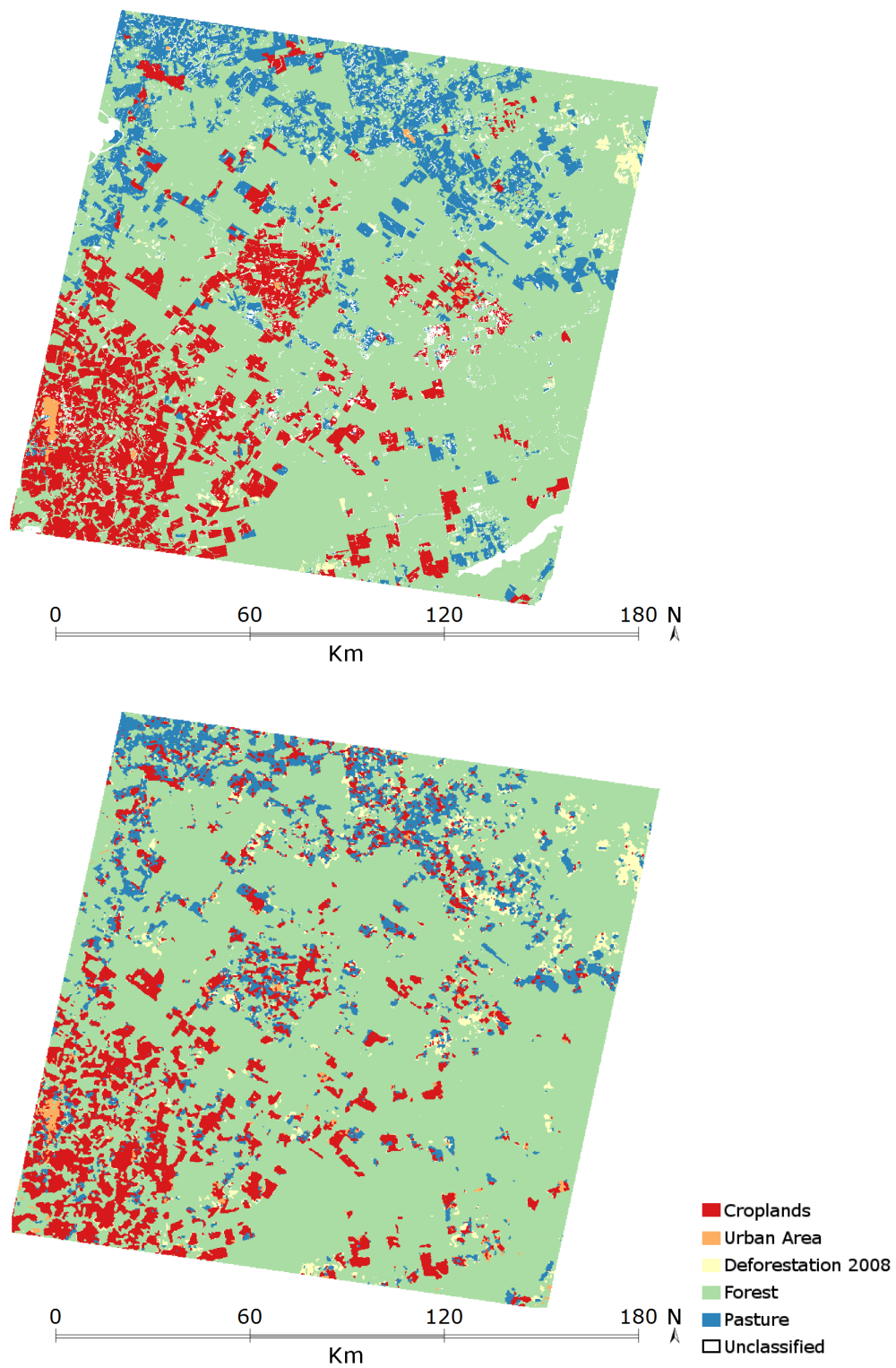


Figure 4.16 - Reference map (top), and land cover map (bottom).
 SOURCE: Reference adapted from Almeida et al. (2009).

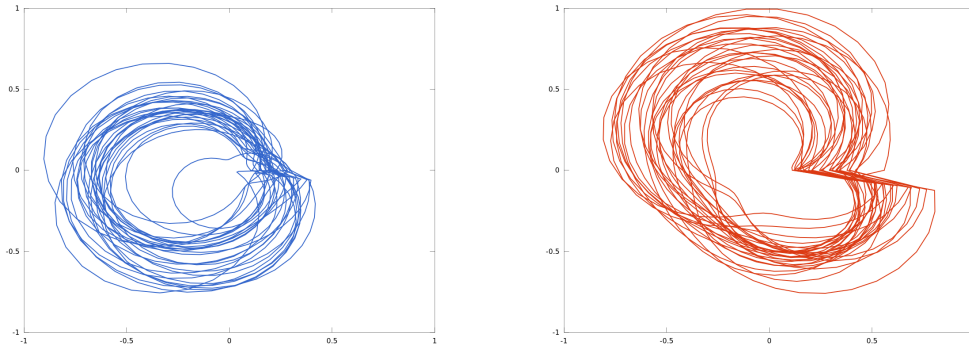


Figure 4.17 - Polar visualization of *single* (left) and *double* (right) classes at approximately 30 cycles per class.

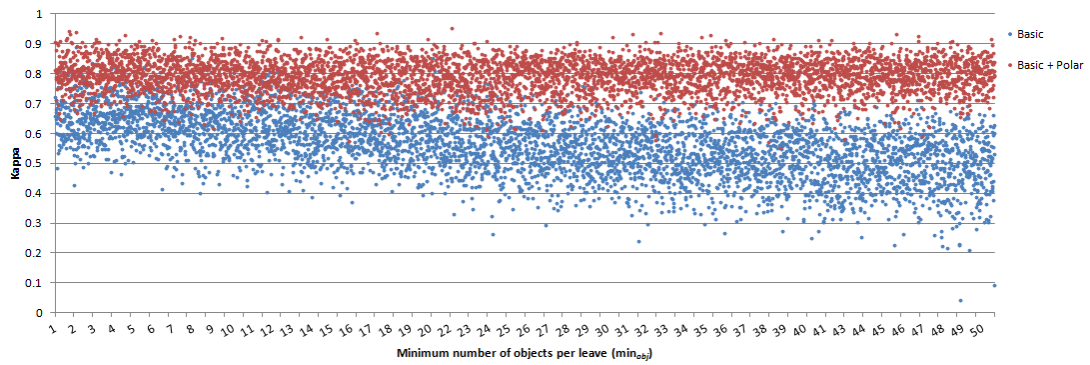


Figure 4.18 - Kappa values in the Monte Carlo simulation in the detection of single and double cropping.

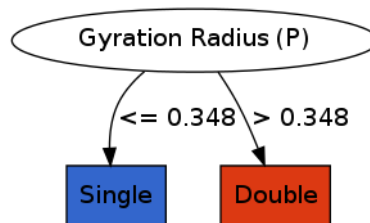


Figure 4.19 - Classification model for the *Basic + Polar* set of features, with 2 leaves and Kappa = 0.8.

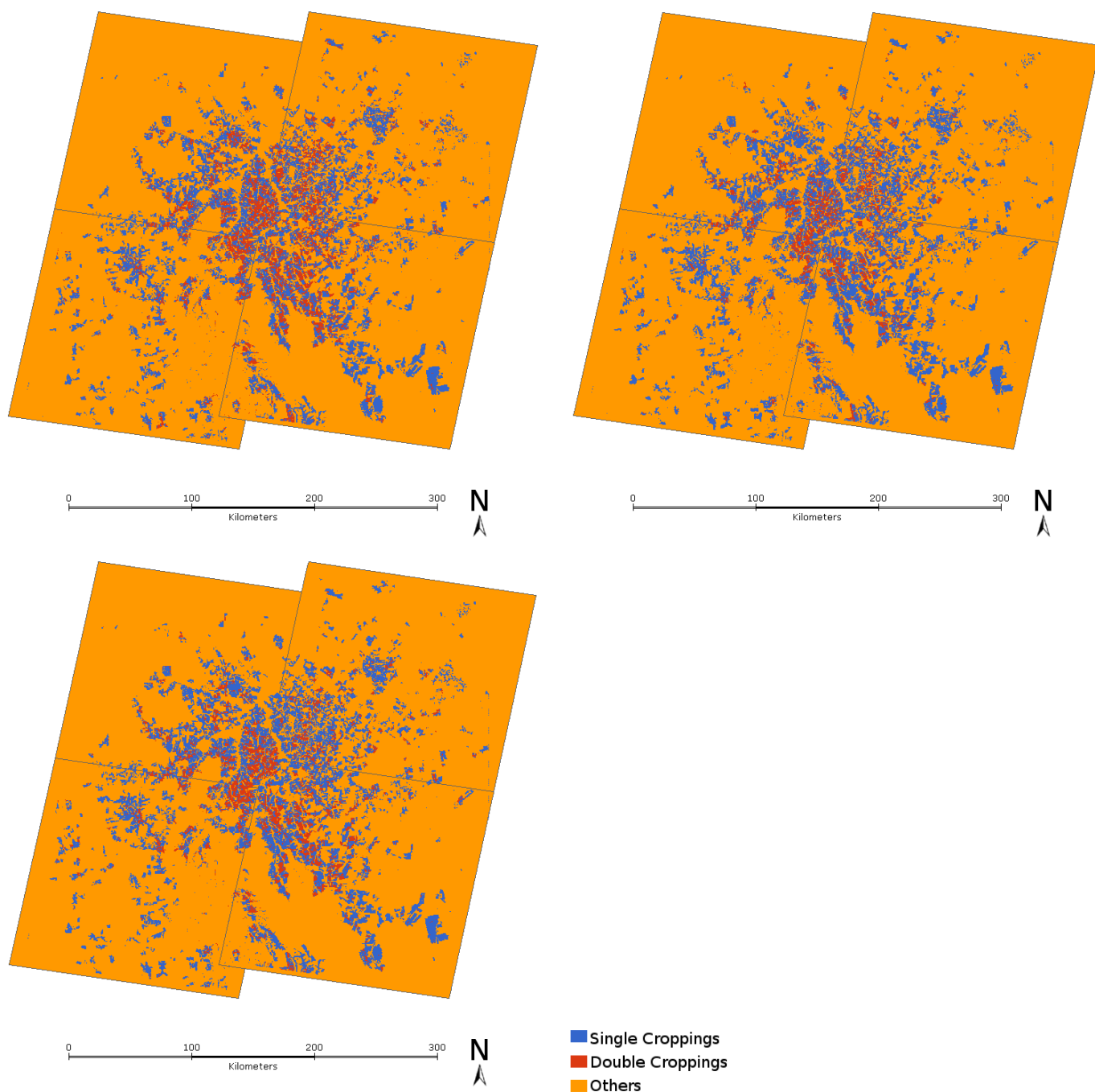


Figure 4.20 - Classification of single and double croppings for the years 2008, 2009 (top), and 2010 (bottom), in the Mato Grosso state (Lat. $11^{\circ}34'23''$ S, Lon. $54^{\circ}43'14''$ W).

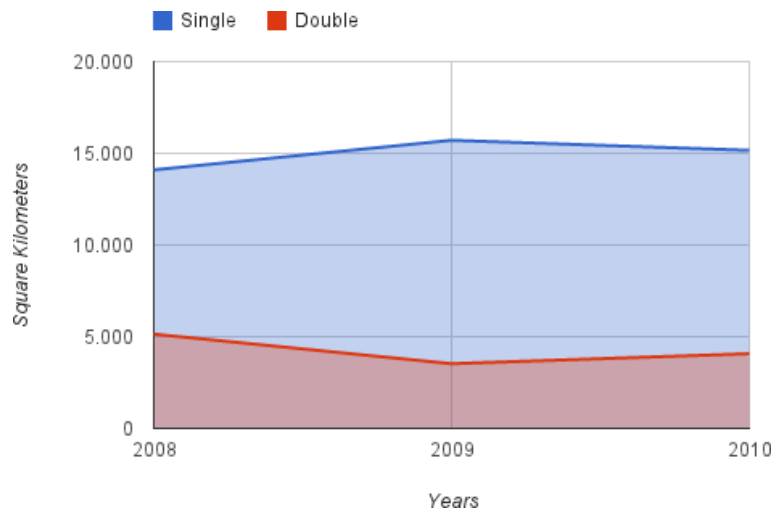


Figure 4.21 - Mapping the area (Km²) of *single* and *double* croppings for the years 2008, 2009, and 2010.

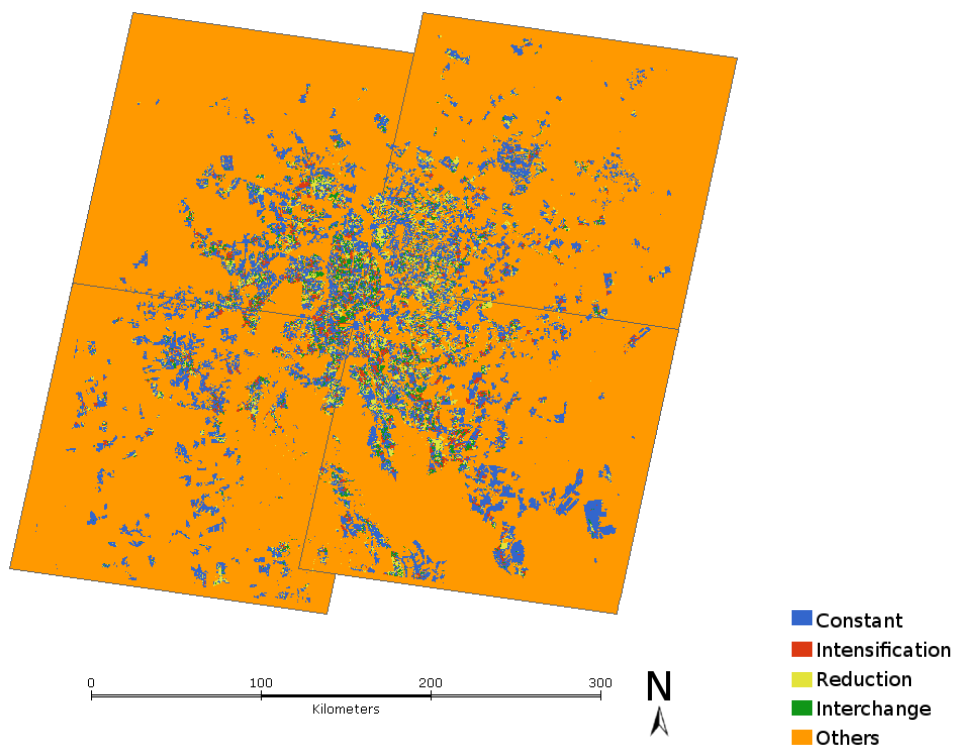


Figure 4.22 - Land change map produced from land cover maps for the years 2008, 2009 and 2010.

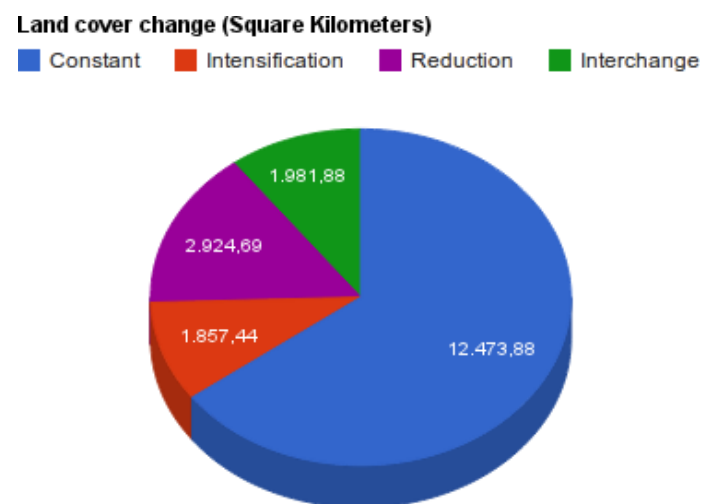


Figure 4.23 - Area (Km²) of land change patterns over a 3-year period (2008 to 2010), taking the cropland map of TerraClass as reference.

4.5 Discussion

This Chapter presented 5 case studies to show the effectiveness of using the GeoDMA toolbox. Different targets and features (segmentation-based, landscape-based, and multi-temporal) were used in each case study, which are dependent on the types of input data and application. In some studies, comparisons with other OBIA systems were also performed to evaluate the strength and weakness of GeoDMA. For every case study, we executed all processing steps using only GeoDMA functionalities, without transferring information to another platform. Due to integration of GeoDMA on top of TerraView GIS, the production of thematic maps, database management and other necessary tasks were easy and fast.

In the study cases, in which we compared GeoDMA with eCognition and InterIMAGE, our toolbox produced results in shorter time than the others. Besides, the data mining algorithm implemented in the toolbox, effectively helped the interpreter to find out the most proper features to distinguish patterns. These points are supported by Pinho et al. (2008) who used GeoDMA as well as eCognition and InterIMAGE systems for urban image analysis (COSTA et al., 2007; PINHO et al., 2008; COSTA et al., 2008; PINHO et al., 2012). In their study, GeoDMA was easy to use and provided enough generality and good accuracy for object labeling with low processing time.

5 CONCLUSION

In this thesis, two objectives were pursued: (i) the development of a free and open source toolbox, GeoDMA, which provides the functionalities needed for analysis of remote sensing imagery in large geographic databases; and (ii) the development of a scheme for multi-temporal analysis. GeoDMA integrates all processing algorithms necessary to automate the interpretation tasks such as segmentation, feature extraction, classification and data mining techniques.

In order to identify patterns, the objects in the images (pixels, regions and cells) are first detected. Next, samples are selected by the interpreter based on a predefined typology. Afterwards, features extracted from objects are then used by a classifier to build a classification model. GeoDMA also provides accuracy assessment tools allowing the interpreter to evaluate the results. We demonstrated the potential of GeoDMA in 5 case studies for detecting land patterns in a wide range of remote sensing applications. GeoDMA showed robustness and flexibility in the execution of such applications. The interpreter performed all processing steps using the toolbox, without the need to transfer information from one platform to another.

To provide the multi-temporal analysis functionalities, we developed a visualization scheme to represent the time series, and also a novel set of multi-temporal features to represent cyclic events, which are common in agriculture applications. A cyclic event involves the use of multi-temporal images, the knowledge about the temporal interval during which the event occurs as well as the patterns that describe such event. These features were employed to classify multi-temporal profiles of EVI2 from MODIS sensor in a 3-year series. When comparing the polar features to well-known features based on phenological indicators, the classification accuracy improved about 5.12% and 36.84% when coupling basic and polar features for multi-temporal land cover detection.

Further work is needed to explore the multi-temporal features for change detection and cycles detection over different periods, like seasonal or biannual. For instance, croppings can have a cycle different of one year. Besides, we also intend to work on the automatic detection of change trajectories in profiles as well as the evaluation of trends for land change based on past events.

The case studies showed that the GeoDMA performance, in terms of classification accuracy, were competitive to that achieved by other systems such as eCognition and InterIMAGE. On the other hand, in terms of computational time, GeoDMA per-

formed much better than the others. A noticeable weakness in the current processing strategy of GeoDMA is the absence of multi-resolution analysis. Various input layers can be created separately but they cannot be integrated using a hierarchical strategy, like eCognition, and InterIMAGE. This strategy would allow the computation of more features that could improve the interpretation tasks for some applications.

Another point to be addressed in the future is the definition of new features in GeoDMA. For example, if the input image has Red and Infra-red bands, it is straightforward to calculate the NDVI. Other software, such as InterIMAGE and eCognition, provide friendly interfaces for creating new features based on precomputed ones. In GeoDMA this can be done manually by editing the columns in the database, which is a tedious task, and for some users it can be hard to be accomplished.

GeoDMA proved to be an efficient alternative for image interpretation in different domains; nevertheless the tool still lacks some improvements. The data can be stored in a remote database, and the interpreter can up-to-date the interpretation wherever the work is performed. However, the storage and retrieval of large images can be time-consuming in case of remote databases. This problem happens due to the current architecture of TerraView that is being improved in the next version TerraView 5.0.

Finally, as GeoDMA is a FOSS project, it can be improved and customized by the developers, and extended to different versions according to the applications needs. The drawbacks aforementioned are related to the fact that GeoDMA is relatively young. So, we expect these drawbacks to be addressed over time, as the system matures.

REFERENCES

ADDINK, E.; JONG, S.; PEBESMA, E. The importance of scale in object-based mapping of vegetation parameters with hyperspectral imagery.

Photogrammetric Engineering & Remote Sensing, v. 73, n. 8, p. 905–912, 2007. 4, 10, 18

ALMEIDA, C.; PINHEIRO, T.; BARBOSA, A.; ABREU, M.; LOBO, F.; SILVA, M.; GOMES, A.; SADECK, L.; MEDEIROS, L.; NEVES, M.; SILVA, L.;

TAMASAUSKAS, P. **Metodologia para mapeamento de vegetação**

secundária na Amazônia Legal. São José dos Campos: Instituto Nacional de Pesquisas Espaciais, 2009. 32 p. Disponível em:

<http://www.inpe.br/cra/ingles/project_research/terraclass.php>. 64, 69

AZEREDO, M. **Mineração de dados espaciais utilizando métricas de paisagens**. São José dos Campos: Personal communication, 2008. 56

BAATZ, M.; HOFFMANN, C.; WILLHAUCK, G. Progressing from object-based to object-oriented image analysis. **Object-Based Image Analysis**, p. 29–42, 2008. Disponível em:

<<http://books.google.com.br/books?id=5ktbsV-aSBAC>>. 9, 59

BAATZ, M.; SCHAPE, A.; SCHäPE, M. Multiresolution segmentation: an optimization approach for high quality multi-scale image segmentation. In: WICHMANN-VERLAG (Ed.). **Proceedings...** Heidelberg, Germany: Herbert Wichmann Verlag, 2000. pp, p. 12–23. 25, 43, 48

BINS, L.; FONSECA, L.; ERTHAL, G.; II, F. Satellite imagery segmentation: a region growing approach. In: SIMPÓSIO BRASILEIRO DE SENSORIAMENTO REMOTO, 8. **Proceedings...** Salvador: Instituto Nacional de Pesquisas Espaciais, 1996. v. 8, p. 677–680. 2, 25

BITTENCOURT, O.; VINHAS, L.; CÂMARA, G.; COSTA, S. Extracting the evolution of land cover objects from remote sensing image series. In: GEOINFORMATIK, 11. **Proceedings...** Munster, Germany: AKA Verlag, 2011. p. 165–173. 15

BLANCHETTE, J.; SUMMERFIELD, M. **C++ GUI programming with Qt 4**. Prentice Hall, 2008. Disponível em:

<<http://portal.acm.org/citation.cfm?id=1406186>>. 23

BLASCHKE, T. Object based image analysis for remote sensing. **ISPRS Journal of Photogrammetry and Remote Sensing**, Elsevier B.V., v. 65, n. 1, p. 2–16, jan. 2010. ISSN 09242716. Disponível em:

<<http://linkinghub.elsevier.com/retrieve/pii/S0924271609000884>>. 2, 9, 10

BORIAH, S. **Time series change detection: Algorithms for land cover change**. Tese (Doutorado) — University of Minnesota, 2010. 17

BORIAH, S.; KUMAR, V.; STEINBACH, M.; POTTER, C.; KLOOSTER, S. Land cover change detection: A case study. In: ACM SIGKDD INTERNATIONAL CONFERENCE ON KNOWLEDGE DISCOVERY AND DATA MINING, 14. **Proceedings...** Las Vegas, USA, 2008. p. 857–865. 13, 14

BOULILA, W.; FARAH, I.; ETTABAA, K.; SOLAIMAN, B.; GHÉZALA, H. A data mining based approach to predict spatiotemporal changes in satellite images.

International Journal of Applied Earth Observation and Geoinformation, Elsevier B.V., v. 13, n. 3, p. 386–395, jun. 2011. ISSN 03032434. Disponível em:

<<http://linkinghub.elsevier.com/retrieve/pii/S0303243411000250>>. 13, 14

BRADLEY, B.; JACOB, R.; HERMANCE, J.; MUSTARD, J. A curve fitting procedure to derive inter-annual phenologies from time series of noisy satellite NDVI data. **Remote Sensing of Environment**, v. 106, n. 2, p. 137–145, jan. 2007. ISSN 00344257. Disponível em:

<<http://linkinghub.elsevier.com/retrieve/pii/S0034425706003014>>. 1, 14, 16

BRUZZONE, L.; SMITS, P.; TILTON, J. Foreword special issue on analysis of multitemporal remote sensing images. **IEEE Transactions on Geoscience and Remote Sensing**, v. 41, n. 11, p. 2419–2422, nov. 2003. ISSN 0196-2892. 1

BüCKNER, J.; PAHL, M.; STAHLHUT, O.; LIEDTKE, C. geoAIDA - A knowledge based automatic image data analyser for remote sensing data. In: CONGRESS ON COMPUTATIONAL INTELLIGENCE METHODS AND APPLICATIONS, 1. **Proceedings...** Bangor, Wales, UK: ICSC, 2001. Disponível em: <<http://citeseerx.ist.psu.edu/viewdoc/download?doi=10.1.1.20.5785&rep=rep1&type=pdf>>. 10

CÂMARA, G.; EGENHOFER, M.; FONSECA, F.; MONTEIRO, A. What's in an image? **Lecture Notes in Computer Science**, v. 2205, n. Spatial Information Theory, p. 474–488, 2001. Disponível em:

<<http://www.emeraldinsight.com/journals.htm?articleid=1659198>>. 1

CÂMARA, G.; VINHAS, L.; FERREIRA, K.; QUEIROZ, G.; SOUZA, R.; MONTEIRO, A.; CARVALHO, M.; CASANOVA, M.; FREITAS, U. TerraLib: An open source GIS library for large-scale environmental and socio-economic applications. **Open Source Approaches in Spatial Data Handling**, v. 2, n. Advances in Geographic Information Science, p. 247–270, 2008. Disponível em:

<<http://www.springerlink.com/index/K505665570287237.pdf>>. 23

CARVALHO, L.; FONSECA, L.; MURTAGH, F.; CLEVERS, J. Digital change detection with the aid of multiresolution wavelet analysis. **International Journal of Remote Sensing**, Taylor & Francis, v. 22, n. 18, p. 3871–3876, jan. 2001. ISSN 01431161. Disponível em:

<<http://www.tandfonline.com/doi/abs/10.1080/01431160110069836http://www.informaworld.com/openurl?genre=article&doi=10.1080/01431160110069836&magic=crossref>>. 16

CASTILLA, G.; GUTHRIE, R.; HAY, G. The Land-cover Change Mapper (LCM) and its application to timber harvest monitoring in western Canada.

Photogrammetric Engineering & Remote Sensing, v. 75, n. 8, p. 941–950, 2009. 17

COMANICIU, D.; MEER, P. Robust analysis of feature spaces: Color image segmentation. In: COMPUTER VISION AND PATTERN RECOGNITION, 8. **Proceedings...** San Juan, Puerto Rico: IEEE, 1997. p. 750–755. Disponível em:

<http://ieeexplore.ieee.org/xpls/abs_all.jsp?arnumber=609410>. 47

CONGALTON, R. Thematic and positional accuracy assessment of digital remotely sensed data. In: ANNUAL FOREST INVENTORY AND ANALYSIS SYMPOSIUM, 7. **Proceedings...** Portland, USA: USDA Forest Service, 2005. p. 149–154. Disponível em:

<http://www.nrs.fs.fed.us/pubs/gtr/gtr_wo077/gtr_wo077_149.pdf>. 43

COSTA, G. **A knowledge-based approach for automatic interpretation of multivariate remote sensing data**. 139 p. Tese (PhD) — PUC-RJ, 2009. 16

COSTA, G.; FEITOSA, R.; FONSECA, L.; OLIVEIRA, D.; FERREIRA, R.; CASTEJON, E. Knowledge-based interpretation of remote sensing data with the

interimage system: major characteristics and recent developments. In: ADDINK, E.; Van Coillie, F. (Ed.). **Proceedings...** Gent, Belgium: ISPRS Working Groups, 2010. Disponível em: <<http://geobia.ugent.be/>>. 2, 10, 16

COSTA, G.; PINHO, C.; FEITOSA, R.; ALMEIDA, C.; KUX, H.; FONSECA, L.; OLIVEIRA, D. InterIMAGE: An open source platform for automatic image interpretation. In: SIMPÓSIO BRASILEIRO DE GEOMÁTICA, 2. **Proceedings...** Presidente Prudente, 2007. p. 24–27. 74

_____. InterIMAGE: an open source cognitive platform for automatic interpretation of digital images. **Revista Brasileira de Cartografia**, v. 60, n. 04, p. 331–337, 2008. 74

DIAL, G.; BOWEN, H.; GERLACH, F.; GRODECKI, J.; OLESZCZUK, R. IKONOS satellite, imagery, and products. **Remote Sensing of Environment**, v. 88, n. 1-2, p. 23–36, nov. 2003. ISSN 00344257. Disponível em: <<http://linkinghub.elsevier.com/retrieve/pii/S0034425703002293>>. 2

EDSALL, R.; KRAAK, M.; MACEACHREN, A.; PEUQUET, D. Assessing the effectiveness of temporal legends in environmental visualization. **Proceedings of GIS/LIS**, Citeseer, p. 677–85, 1997. Disponível em: <<http://citeseerx.ist.psu.edu/viewdoc/download?doi=10.1.1.61.8955&rep=rep1&type=pdf>>. 29

EL-SHAARAWI, A.; PIEGORSCH, W. **Encyclopedia of environmetrics**. 1. ed. Sussex, England: John Wiley & Sons Inc, 2002. 7

ESPACIAIS, I. N. de P. **Deforestation estimates in the Brazilian Amazon**. 2012. Disponível em: <<http://www.obt.inpe.br/prodes/>>. 9, 56, 60, 64

ESQUERDO, J.; JUNIOR, J.; ANTUNES, J. Uso de perfis multi-tempoais de NDVI/AVHRR no acompanhamento da cultura da soja no oeste do Paraná. In: SIMPÓSIO BRASILEIRO DE SENSORIAMENTO REMOTO, 14. **Proceedings...** Natal, Brazil: Instituto Nacional de Pesquisas Espaciais, 2009. p. 145–150. 18, 64

FAYYAD, U.; SHAPIRO, G.; SMYTH, P. The KDD process for extracting useful knowledge from volumes of data. **Communications of the ACM**, ACM New York, NY, USA, v. 39, n. 11, p. 27–34, 1996. 2, 12

FERRAZ, S.; VETTORAZZI, C.; THEOBALD, D. D.; BALLESTER, M. Landscape dynamics of Amazonian deforestation between 1984 and 2002 in central

Rondonia, Brazil: assessment and future scenarios. **Forest Ecology and Management**, v. 204, n. 1, p. 69–85, jan. 2005. ISSN 03781127. Disponível em: <<http://linkinghub.elsevier.com/retrieve/pii/S0378112704006462>>. 4, 8, 18

FORMAN, R. **Land mosaics: the ecology of landscapes and regions**. 1. ed. Cambridge, England: Cambridge University Press, 1995. 7

FREITAS, R.; ARAI, E.; ADAMI, M.; SOUZA, A.; SATO, F.; SHIMABUKURO, Y.; ROSA, R.; ANDERSON, L.; RUDORFF, B. Virtual laboratory of remote sensing series: visualization of MODIS EVI2 data set over South America. **Journal of Computational Interdisciplinary Sciences**, v. 2, p. 57–64, 2011. 15

FREITAS, R.; SHIMABUKURO, Y. Combining wavelets and linear spectral mixture model for MODIS satellite sensor time-series analysis. **Journal of Computational Interdisciplinary Sciences**, v. 1, n. 1, p. 51–56, 2008. 15

FRIEDL, M.; BRODLEY, C.; STRAHLER, A. Maximizing land cover classification accuracies produced by decision trees at continental to global scales. **IEEE Transactions on Geoscience and Remote Sensing**, v. 37, n. 2, p. 969–977, mar. 1999. ISSN 01962892. Disponível em: <<http://ieeexplore.ieee.org/lpdocs/epic03/wrapper.htm?arnumber=752215>>. 12

FROHN, R.; HAO, Y. Landscape metric performance in analyzing two decades of deforestation in the Amazon Basin of Rondonia, Brazil. **Remote Sensing of Environment**, v. 100, n. 2, p. 237–251, jan. 2006. ISSN 00344257. Disponível em: <<http://linkinghub.elsevier.com/retrieve/pii/S0034425705003573>>. 4, 8, 18

GALFORD, G.; MUSTARD, J.; MELILLO, J.; GENDRIN, A.; CERRI, C.; CERRI, C. Wavelet analysis of MODIS time series to detect expansion and intensification of row-crop agriculture in Brazil. **Remote Sensing of Environment**, v. 112, n. 2, p. 576–587, fev. 2008. ISSN 00344257. Disponível em: <<http://linkinghub.elsevier.com/retrieve/pii/S0034425707002258>>. 14, 15, 17, 63, 66

GAMANYA, R.; DEMAERYER, P.; DEDAPPER, M. An automated satellite image classification design using object-oriented segmentation algorithms: A move towards standardization. **Expert Systems with Applications**, v. 32, n. 2, p. 616–624, fev. 2007. ISSN 09574174. 43

GAVLAK, A.; ESCADA, M.; MONTEIRO, A. Dinâmica de padrões de mudança de uso e cobertura da terra na região do Distrito Florestal Sustentável da BR-163. In: SIMPÓSIO BRASILEIRO DE SENSORIAMENTO REMOTO, 15.

Proceedings... Curitiba, Brazil: Instituto Nacional de Pesquisas Espaciais, 2011. p. 6152–6160. 9, 18

GOEBEL, M. A survey of data mining and knowledge discovery software tools.

ACM SIGKDD Explorations Newsletter, ACM New York, NY, USA, v. 1, p. 20–33, 1999. 2

GOODCHILD, M. GIScience, geography, form, and process. In: **Association of American Geographers**. Oxford, UK: Blackwell Publishing, 2004. v. 94, n. 4, p. 709–714. 1

GROOM, G.; MÜCHER, C.; IHSE, M.; WRBKA, T. Remote Sensing in landscape ecology: Experiences and perspectives in a european context. **Landscape**

Ecology, v. 21, n. 3, p. 391–408, abr. 2006. ISSN 0921-2973. Disponível em:

<<http://www.springerlink.com/index/10.1007/s10980-004-4212-1>>. 3

HARALICK, R.; SHANMUGAM, K.; DINSTEN, I. Textural features for image classification. **IEEE Transactions on Systems, Man and Cybernetics**,

SMC-3, n. 6, p. 610–621, 1973. Disponível em:

<http://ieeexplore.ieee.org/xpls/abs_all.jsp?arnumber=4309314>. 28

HARALICK, R.; SHAPIRO, L. Image segmentation techniques. **Applications of Artificial Intelligence II., 1985**, v. 548, p. 2–9, 1985. 2, 9, 25

HASTIE, T.; TIBSHIRANI, R.; FRIEDMAN, J. **The elements of statistical learning: data mining, inference, and prediction**. 2. ed. Stanford, CA:

Springer, 2009. 745 p. Disponível em:

<<http://books.google.com/books?id=tVIjmNS30b8C>>. 36, 40

HAY, G.; CASTILLA, G. Geographic Object-Based Image Analysis (GEOBIA): A new name for a new discipline. In: BLASCHKE, T.; LANG, S.; HAY, G. (Ed.).

Object-based image analysis. Spatial concepts for knowledge-driven remote sensing applications. Berlin, Heidelberg: Springer-Verlag, 2008. cap. 1.4, p. 75–89.

ISBN 978-3-540-77057-2. 3

HORNSBY, K.; EGENHOFER, M.; HAYES, P. Modeling Cyclic Change.

Advances in Conceptual Modeling, v. 1727/1999, n. 1, p. 98–109, 1999. 14, 29

HUETE, A.; DIDAN, K.; MIURA, T.; RODRIGUEZ, E.; GAO, X.; FERREIRA, L. Overview of the radiometric and biophysical performance of the MODIS vegetation indices. **Remote Sensing of Environment**, v. 83, n. 1-2, p. 195–213, nov. 2002. ISSN 00344257. Disponível em:

<<http://linkinghub.elsevier.com/retrieve/pii/S0034425702000962>>. 14

HÜTTICH, C.; GESSNER, U.; HEROLD, M.; STROHBACH, B.; SCHMIDT, M.; KEIL, M.; DECH, S. On the suitability of MODIS time series metrics to map vegetation types in dry savanna ecosystems: A case study in the Kalahari of NE Namibia. **Remote Sensing**, v. 1, n. 4, p. 620–643, set. 2009. ISSN 2072-4292. Disponível em: <<http://www.mdpi.com/2072-4292/1/4/620/>>. 4, 18, 29

IMBERNON, J.; BRANTHOMME, A. Characterization of landscape patterns of deforestation in tropical rain forests. **International Journal of Remote Sensing**, v. 22, n. 9, p. 1753–1765, jun. 2001. ISSN 0143-1161. Disponível em: <<http://www.informaworld.com/openurl?genre=article&doi=10.1080/01431160118426&magic=crossref||D404A21C5BB053405B1A640AFFD44AE3>>. 8, 18

INSTITUTO NACIONAL DE PESQUISAS ESPACIAIS. **TerraView**. São José dos Campos: Divisão de Processamento de Imagens, 2012. Disponível em: <<http://www.dpi.inpe.br/terraview>>. 5, 22

INTERNATIONAL TELEPHONE & TELEGRAPH EXELIS. **ENVI feature extraction module user's guide**. Gilching, Germany: Exelis Visual Information Solutions, 2008. 78 p. 2, 10

JIANG, Z.; HUETE, A.; DIDAN, K.; MIURA, T. Development of a two-band enhanced vegetation index without a blue band. **Remote Sensing of Environment**, v. 112, n. 10, p. 3833–3845, out. 2008. ISSN 00344257. Disponível em: <<http://linkinghub.elsevier.com/retrieve/pii/S0034425708001971>>. 14

JONSSON, P.; EKLUNDH, L. TIMESAT: A program for analyzing time-series of satellite sensor data. **Computers & Geosciences**, v. 30, n. 8, p. 833–845, out. 2004. ISSN 00983004. Disponível em: <<http://linkinghub.elsevier.com/retrieve/pii/S0098300404000974>>. 15, 17, 29

KOHONEN, T. **Self-Organizing Maps**. 3rd. ed. Berlin: Springer, 2001. 41

KORTING, T.; DUTRA, L.; FONSECA, L. A resegmentation approach for detecting rectangular objects in high-Resolution imagery. **IEEE Geoscience and Remote Sensing Letters**, v. 8, n. 4, p. 621–625, jul. 2011. ISSN 1545-598X.

Disponível em: <<http://ieeexplore.ieee.org/lpdocs/epic03/wrapper.htm?arnumber=5692808>>. 26

KORTING, T.; FONSECA, L.; BACAO, F. Expectation-Maximization x Self-Organizing Maps for image classification. In: IEEE INTERNATIONAL CONFERENCE ON SIGNAL IMAGE TECHNOLOGY AND INTERNET BASED SYSTEMS, 8. **Proceedings...** Bali, Indonesia, 2008. p. 359–365. 42

KORTING, T.; FONSECA, L.; CÂMARA, G. A geographical approach to Self-Organizing Maps algorithm applied to image segmentation. **Lecture Notes in Computer Science**, v. 6915, p. 162–170, 2011. 26

KORTING, T.; FONSECA, L.; ESCADA, M.; SILVA, F.; SILVA, M. GeoDMA - A novel system for spatial data mining. In: IEEE INTERNATIONAL CONFERENCE ON DATA MINING WORKSHOPS, 8. **Proceedings...** Pisa, Italy, 2008. p. 975–978. 21

LAAKSONEN, J.; VIITANIEMI, V.; KOSKELA, M. Application of Self-Organizing Maps and automatic image segmentation to 101 object categories database. In: INTERNATIONAL WORKSHOP ON CONTENT-BASED MULTIMEDIA INDEXING, 4. **Proceedings...** Riga, Latvia, 2005. 41

LACKNER, M.; CONWAY, T. Determining land-use information from land cover through an object-oriented classification of IKONOS imagery. **Canadian Journal of Remote Sensing**, v. 34, n. 2, p. 77–92, 2008. 10, 18

LAMBIN, E.; GEIST, H.; LEPEERS, E. Dynamics of land-use and land-cover change in tropical regions. **Annual Review of Environment and Resources**, v. 28, n. 1, p. 205–241, nov. 2003. ISSN 1543-5938. Disponível em: <<http://arjournals.annualreviews.org/doi/abs/10.1146/annurev.energy.28.050302.105459>>. 56

LANG, S. Object-based image analysis for remote sensing applications: modeling reality—dealing with complexity. In: **Object-Based Image Analysis**. New York: Springer, 2008. cap. 1.1, p. 3–27. 3

LANG, S.; TIEDE, D.; DEVELOPER, D. Definiens Developer. **GIS Business** 9, p. 34–37, 2007. xiii, xiv, 2, 9, 34, 35, 57

LEWINSKI, S.; BOCHENEK, Z. Rule-based classification of SPOT imagery using object-oriented approach for detailed land cover mapping. In: EARSEL SYMPOSIUM, 28. **Proceedings...** Istanbul, Turkey: EARSeL, 2008. 11, 18

LU, D.; MAUSEL, P.; BRONDIZIO, E.; MORAN, E. Change detection techniques. **International Journal of Remote Sensing**, v. 25, n. 12, p. 2365–2401, jun. 2004. ISSN 0143-1161. Disponível em: <<http://www.informaworld.com/openurl?genre=article&doi=10.1080/0143116031000139863&magic=crossref|D404A21C5BB053405B1A640AFFD44AE3>>. 17

MCCAULEY, S.; GOETZ, S. Mapping residential density patterns using multi-temporal Landsat data and a decision-tree classifier. **International Journal of Remote Sensing**, v. 25, n. 6, p. 1077–1094, mar. 2004. ISSN 0143-1161. 1, 13, 36

MCGARIGAL, K. Landscape Pattern Metrics. In: **Encyclopedia of Environmetrics**. Sussex, England: John Wiley & Sons, 2002. p. 1135–1142. 7, 94, 95

MEINEL, G.; NEUBERT, M. A comparison of segmentation programs for high resolution remote sensing data. **International Archives of Photogrammetry and Remote Sensing**, v. 35, n. Part B, p. 1097–1105, 2004. Disponível em: <<http://scholar.google.com/scholar?hl=en&btnG=Search&q=intitle:A+comparison+of+segmentation+programs+for+high+resolution+remote+sensing+data#0>>. 25

MEINEL, G.; NEUBERT, M.; REDER, J. The potential use of very high resolution satellite data for urban areas - First experiences with IKONOS data, their classification and application in urban planning and environmental monitoring. **Remote Sensing of Urban Areas/Fernerkundung in urbanen Räumen**, p. 196–205, 2001. Disponível em: <http://www2.ioer.de/recherche/pdf/2001_meinel_urs.pdf>. 47

METZGER, J.; MARTENSEN, A.; DIXO, M.; BERNACCI, L.; RIBEIRO, M.; TEIXEIRA, A.; PARDINI, R. Time-lag in biological responses to landscape changes in a highly dynamic Atlantic forest region. **Biological Conservation**, v. 142, n. 6, p. 1166–1177, 2009. ISSN 00063207. Disponível em: <<http://linkinghub.elsevier.com/retrieve/pii/S0006320709000780>>. 14, 18

MILLER, H.; HAN, J. **Geographic data mining and knowledge discovery**. CRC Press, 2001. Disponível em:

<<http://books.google.com.br/books?id=fJTD26iYxpkC>>. 12

MILNE, A. Change Direction Analysis Using Landsat Imagery: A Review Of Methodology. In: INTERNATIONAL GEOSCIENCE AND REMOTE SENSING SYMPOSIUM, 3. **Proceedings...** Edinburgh, Scotland: Ieee, 1988. p. 541–544.

Disponível em: <<http://ieeexplore.ieee.org/lpdocs/epic03/wrapper.htm?arnumber=570193>>. 15

MOTA, J.; ESCADA, M.; BITTENCOURT, O.; FONSECA, L.; VINHAS, L. Case-based reasoning for eliciting the evolution of geospatial objects. In: CONFERENCE ON SPATIAL INFORMATION THEORY, 9. **Proceedings...** Berlin, Heidelberg: Springer-Verlag, 2009. p. 88. 15

NOBRE, C.; SELLERS, P.; SHUKLA, J. Amazonian deforestation and regional climate change. **Journal of Climate**, v. 4, 1991. 14

NOVACK, T. **Classificação da cobertura da terra e do uso do solo urbano utilizando o sistema InterIMAGE e imagens do sensor QuickBird**. 214 p. Dissertação (Mestrado) — Instituto Nacional de Pesquisas Espaciais, São José dos Campos, 2009-08-18 2009. Disponível em:

<<http://urlib.net/sid.inpe.br/mtc-m18@80/2009/08.31.21.23>>. Acesso em: 13 ago. 2012. 48, 49, 51

NOVACK, T.; ESCH, T.; KUX, H.; STILLA, U. Machine learning comparison between WorldView-2 and QuickBird-2 simulated imagery regarding object-based urban land cover classification. **Remote Sensing**, v. 3, n. 10, p. 2263–2282, out. 2011. ISSN 2072-4292. Disponível em:

<<http://www.mdpi.com//2072-4292/3/10/2263/>>. 18

PACIFICI, F.; CHINI, M.; EMERY, W. A neural network approach using multi-scale textural metrics from very high-resolution panchromatic imagery for urban land-use classification. **Remote Sensing of Environment**, Elsevier Inc., v. 113, n. 6, p. 1276–1292, 2009. ISSN 0034-4257. Disponível em:

<<http://dx.doi.org/10.1016/j.rse.2009.02.014>>. 28

PINHO, C.; FONSECA, L.; KORTING, T.; ALMEIDA, C.; KUX, H. Land-cover classification of an intra-urban environment using high-resolution images and object-based image analysis. **International Journal of Remote Sensing**, v. 33, n. 19, p. 5973–5995, 2012. 3, 11, 18, 34, 47, 74

PINHO, C.; SILVA, F.; FONSECA, L.; MONTEIRO, A. Intra-urban land cover classification from high-resolution images using the C4.5 algorithm. **ISPRS Congress Beijing**, v. 7, 2008. 3, 74

POTTER, C.; GENOVESE, V.; GROSS, P.; BORIAH, S.; STEINBACH, M.; KUMAR, V. Revealing land cover change in california with satellite data. **EOS**, v. 88, n. 26, 2007. Disponível em: <<http://civil.cec.yamanashi.ac.jp/~tetsu/englishpaper/2008/2nd/2007E0260001.pdf>>. 13, 14

QUINLAN, J. **C4.5: programs for machine learning**. San Mateo, CA: Morgan Kaufmann, 1993. 302 p. Disponível em: <<http://books.google.com/books?id=HExncpjbYroC>>. 37

RASINMAKI, J. Modelling spatio-temporal environmental data. **Environmental Modelling \& Software**, v. 18, p. 877–886, 2003. ISSN 1364-8152. 15

READ, J.; LAM, N. Spatial methods for characterising land cover and detecting land-cover changes for the tropics. **International Journal of Remote Sensing**, Taylor \& Francis, v. 23, p. 2457–2474, 2002. 7

REIS, I. C. d. **Caracterização de paisagens urbanas heterogêneas de interesse para a vigilância e controle da dengue com o uso de sensoriamento remoto e mineração de padrões espaciais: um estudo para o Rio de Janeiro**. 174 p. Dissertação (Mestrado) — Instituto Nacional de Pesquisas Espaciais, São José dos Campos, 2010-12-20 2011. Disponível em: <<http://urlib.net/sid.inpe.br/mtc-m19/2010/12.06.15.22>>. Acesso em: 13 ago. 2012. 53, 54, 55

RIBEIRO, M.; METZGER, J.; PONZONI, F.; MARTENSEN, A.; HIROTA, M. The brazilian Atlantic forest: How much is left, and how is the remaining forest distributed? Implications for conservation. **Biological Conservation**, v. 142, n. 6, p. 1141–1153, 2009. ISSN 00063207. Disponível em: <<http://linkinghub.elsevier.com/retrieve/pii/S0006320709000974>>. 4, 8, 18

ROBERTS, D.; NUMATA, I.; HOLMES, K.; BATISTA, G.; KRUG, T.; MONTEIRO, A.; POWELL, B.; CHADWICK, O. Large area mapping of land-cover change in Rondônia using multitemporal spectral mixture analysis and decision tree classifiers. **Journal of Geophysical Research**, v. 107, n. D20, 2002. ISSN 0148-0227. Disponível em: <<http://www.agu.org/pubs/crossref/2002/2001JD000374.shtml>>. 13

RUBINSTEIN, R.; KROESE, D. **Simulation and the Monte Carlo method**. New Jersey: Wiley-interscience, 2008. 43, 64

RUDORFF, B.; ADAMI, M.; AGUIAR, D.; GUSSO, A.; SILVA, W.; FREITAS, R. Temporal series of EVI/MODIS to identify land converted do sugarcane. In: INTERNATIONAL GEOSCIENCE AND REMOTE SENSING SYMPOSIUM, 9. **Proceedings...** Cape Town, South Africa, 2009. 14

RUSHING, J.; RAMACHANDRAN, R.; NAIR, U.; GRAVES, S.; WELCH, R.; LIN, H. ADaM: A data mining toolkit for scientists and engineers. **Computers and Geosciences**, v. 31, n. 5, p. 607–618, jun. 2005. ISSN 00983004. Disponível em: <<http://linkinghub.elsevier.com/retrieve/pii/S009830040400233X>>. 11

SAITO, E.; FONSECA, L.; ESCADA, M.; KORTING, T. Effects of changes in scale of deforestation patterns in Amazon. **Brazilian Journal of Cartography**, v. 4, 2011. 8, 18, 27

SAITO, E.; KORTING, T.; FONSECA, L.; ESCADA, M. Mineração em dados espaciais de desmatamento do prodes utilizando métricas da paisagem caso de estudo município de novo progresso- pa. In: SIMPÓSIO BRASILEIRO DE CIÊNCIAS GEODÉSICAS, 3. **Proceedings...** Recife, Brazil, 2010. p. 001–009. 5

SAITO, É. A. **Caracterização de trajetórias de padrões de ocupação humana na Amazônia Legal por meio de mineração de dados**. 158 p. Dissertação (Mestrado) — Instituto Nacional de Pesquisas Espaciais, São José dos Campos, 2010-12-16 2011. Disponível em: <<http://urlib.net/sid.inpe.br/mtc-m19/2010/12.01.16.33>>. Acesso em: 13 ago. 2012. 56

SHANNON, C. A mathematical theory of communication. **Bell System Tech. J.**, v. 27, p. 379–423, 623–656, 1948. Disponível em: <<http://citeseerx.ist.psu.edu/viewdoc/download?doi=10.1.1.161.4366&rep=rep1&type=pdf>>. 38

SILVA, M.; CÂMARA, G.; ESCADA, M.; SOUZA, R. Remote-sensing image mining: detecting agents of land-use change in tropical forest areas. **International Journal of Remote Sensing**, Taylor & Francis, v. 29, p. 4803–4822, 2008. 3, 13, 18, 45

SILVA, M.; CÂMARA, G.; SOUZA, R.; VALERIANO, D.; ESCADA, M. Mining patterns of change in remote sensing image databases. In: IEEE

INTERNATIONAL CONFERENCE ON DATA MINING, 5. **Proceedings...** New Orleans, Louisiana, USA, 2005. 21

SINGH, A. Review Article Digital change detection techniques using remotely-sensed data. **International Journal of Remote Sensing**, v. 10, n. 6, p. 989–1003, jun. 1989. ISSN 0143-1161. Disponível em:

<<http://www.informaworld.com/openurl?genre=article&doi=10.1080/01431168908903939&magic=crossref||D404A21C5BB053405B1A640AFFD44AE3>>.

16

SMALL, C. Spatiotemporal dimensionality and time-space characterization of vegetation phenology from multitemporal MODIS EVI. In: INTERNATIONAL WORKSHOP ON THE ANALYSIS OF MULTI-TEMPORAL REMOTE SENSING IMAGES (MULTI-TEMP), 6. **Proceedings...** Trento, Italy: IEEE, 2011. p. 65–68. ISBN 9781457712036. Disponível em:

<http://ieeexplore.ieee.org/xpls/abs_all.jsp?arnumber=6005049>. 26

SMITH, B. On Drawing Lines on a Map. In: FRANK, A.; KUHN, W.; MARK, D. (Ed.). **Spatial Information Theory. Proceedings of COSIT**. Semmering, Austria: Springer Verlag, 1995. p. 475–484. 1

SOUTHWORTH, J.; NAGENDRA, H.; TUCKER, C. Fragmentation of a Landscape: incorporating landscape metrics into satellite analyses of land-cover change. **Landscape**, v. 27, n. 3, p. 253–269, 2002. 8, 14, 18

SOUZA, C.; FIRESTONE, L.; SILVA, L.; ROBERTS, D. Mapping forest degradation in the Eastern Amazon from SPOT 4 through spectral mixture models. **Remote Sensing of Environment**, v. 87, n. 4, p. 494–506, 2003. ISSN 00344257. 13

STEIN, A. Modern developments in image mining. **Science in China Series E: Technological Sciences**, v. 51, n. S1, p. 13–25, jun. 2008. ISSN 1006-9321.

Disponível em:

<<http://www.springerlink.com/index/10.1007/s11431-008-5005-6>>. 12

STEIN, A.; HAMM, N.; YE, Q. Handling uncertainties in image mining for remote sensing studies. **International Journal of Remote Sensing**, v. 30, n. 20, p. 5365–5382, 2009. ISSN 0143-1161. 3, 12

STEINIGER, S.; HAY, G. Free and open source geographic information tools for landscape ecology. **Ecological Informatics**, v. 4, n. 4, p. 183–195, set. 2009. ISSN

15749541. Disponível em:

<<http://linkinghub.elsevier.com/retrieve/pii/S1574954109000363>>. 4, 21

STOJMENOVIC, M.; NAYAK, A.; ZUNIC, J. Measuring linearity of planar point sets. **Pattern Recognition**, v. 41, n. 8, p. 2503–2511, ago. 2008. ISSN 00313203.

Disponível em:

<<http://linkinghub.elsevier.com/retrieve/pii/S0031320308000381>>. 31

TAN, P.; STEINBACH, M.; KUMAR, V.; POTTER, C.; KLOOSTER, S.; TORREGROSA, A. Clustering earth science data: Goals, issues and results. **Proc. of the Fourth KDD Workshop on Mining Scientific Datasets**, Citeseer, 2001. 3, 13

_____. Finding Spatio-Temporal Patterns in Earth Science Data. **Earth Science**, p. 1–12, 2001. 1, 15

TURNER, M. Landscape ecology: What is the state of the science? **Annual Review of Ecology, Evolution, and Systematics**, v. 36, n. 1, p. 319–344, dez. 2005. ISSN 1543-592X. Disponível em: <<http://arjournals.annualreviews.org/doi/abs/10.1146/annurev.ecolsys.36.102003.152614>>. 7

UDELHOVEN, T. TimeStats: A software tool for the retrieval of temporal patterns from global satellite archives. **Earth**, v. 4, n. 2, p. 310–317, 2011. 12, 13

VALERIANO, D.; ESCADA, M.; CÂMARA, G.; AMARAL, S.; MAURANO, L.; RENNÓ, C.; ALMEIDA, C.; MONTEIRO, A. O monitoramento do desmatamento. In: MARTINE, G. (Ed.). **População e sustentabilidade na era das mudanças ambientais globais: Contribuições para uma agenda brasileira**. Rio de Janeiro, Brazil: Associação brasileira de estudos populacionais, 2012. 64

VERBESSELT, J.; HYNDMAN, R.; NEWNHAM, G.; CULVENOR, D. Detecting trend and seasonal changes in satellite image time series. **Remote Sensing of Environment**, Elsevier B.V., v. 114, n. 1, p. 106–115, jan. 2010. ISSN 00344257.

Disponível em:

<<http://linkinghub.elsevier.com/retrieve/pii/S003442570900265X>>. 14, 16, 17, 43

VERMOTE, E.; SALEOUS, N.; JUSTICE, C. Atmospheric correction of MODIS data in the visible to middle infrared: first results. **Remote Sensing of Environment**, v. 83, p. 97–111, 2002. 63

- VESANTO, J. **Data exploration process based on the Self-Organizing Map**. Tese (Doutorado) — Helsinki University of Technology, 2002. 41
- WANG, Y.; LI, J. Feature-selection ability of the decision-tree algorithm and the impact of feature-selection/extraction on decision-tree results based on hyperspectral data. **International Journal of Remote Sensing**, Taylor \& Francis, v. 29, p. 2993–3010, 2008. 38
- WASSENBERG, J.; MIDDELMANN, W.; SANDERS, P. An efficient parallel algorithm for graph-based image segmentation. In: **COMPUTER ANALYSIS OF IMAGES AND PATTERNS, 9. Proceedings...** Muenster, Germany: Springer, 2009. p. 1003–1010. 2
- WIENS, J. Population responses to patchy environments. **Annual Review of Ecology and Systematics**, v. 7, p. 81–120, 1976. 7
- WITTEN, I.; FRANK, E. **Data Mining: Practical machine learning tools and techniques**. 2. ed. San Francisco, CA: Diane Cerra, 2005. 558 p. 37, 40
- WOODCOCK, C.; STRAHLER, A. The factor of scale in remote sensing. **Remote Sensing of Environment**, v. 21, n. 3, p. 311–332, abr. 1987. ISSN 00344257. Disponível em: <http://linkinghub.elsevier.com/retrieve/pii/0034425787900150>>. 3
- XU, M.; WATANACHATURAPORN, P.; VARSHNEY, P.; ARORA, M. Decision tree regression for soft classification of remote sensing data. **Remote Sensing of Environment**, v. 97, n. 3, p. 322–336, ago. 2005. ISSN 00344257. Disponível em: <http://linkinghub.elsevier.com/retrieve/pii/S0034425705001604>>. 36
- ZORTEA, M.; SALBERG, A.; TRIER, O. Object-based cloud and cloud shadow detection in Landsat images for tropical forest monitoring. In: **GEOGRAPHIC OBJECT-BASED IMAGE ANALYSIS, 4. Proceedings...** Rio de Janeiro, Brazil: Instituto Nacional de Pesquisas Espaciais, 2012. p. 326–331. 11

APPENDIX A - TABLES OF FEATURES

Table A.1 - Segmentation-based spectral features.

Name	Description	Formula	Range	Unit
Amplitude	Defines the amplitude of the pixels inside the object. The amplitude means the maximum pixel value minus the minimum pixel value.	$px_{\max} - px_{\min}$	≥ 0	px
Dissimilarity	Measures how different the elements of the GLCM are from each other and it is high when the local region has a high contrast.	$\sum_{i=1}^{D-1} \sum_{j=1}^{D-1} p_{ij} \cdot i - j $	≥ 0	–
Entropy	Measures the disorder in an image. When the image is not uniform, many GLCM elements have small values, resulting in large entropy.	$-\sum_{i=1}^{D-1} \sum_{j=1}^{D-1} p_{ij} \cdot \log p_{ij}$	≥ 0	–
Homogeneity	Assumes higher values for smaller differences in the GLCM.	$\sum_{i=1}^{D-1} \sum_{j=1}^{D-1} \frac{p_{ij}}{1 + (i - j)^2}$	≥ 0	–
Mean	Returns the average value for all N pixels inside the object.	$\frac{\sum_{i=1}^N px_i}{N}$	≥ 0	px
Mode	Returns the most occurring value (mode) for all N pixels inside the object. When the object is multimodal, the first value is assumed.		≥ 0	px
Std	Returns the standard deviation of all N pixels (μ is the mean value).	$\sqrt{\frac{1}{N-1} \sum_{i=1}^N (px_i - \mu)^2}$	≥ 0	px

Table A.2 - Segmentation-based spatial features.

Name	Description	Formula	Range	Unit
Angle	Represents the main angle of an object. It is obtained by computing the minimum circumscribing ellipse, and the angle of the biggest radius of the ellipse suits to the object's angle.		$[0, \pi]$	rad
Area	Returns the area of the object. When measured in pixels is equal to N .		≥ 0	px^2
Box area	Returns the bounding box area of an object, measured in pixels.		≥ 0	px^2
Circle	Relates the areas of the object and the smallest circumscribing circle around the object. In the equation, R is the maximum distance between the centroid and all vertices.	$1 - \frac{N}{\pi R^2}$	$[0, 1)$	px
Elliptic fit	Finds the minimum circumscribing ellipse to the object and returns the ratio between the object's area and the ellipse area.		$[0, 1]$	–
Fractal dimension	Returns the fractal dimension of an object.	$2 \frac{\log \frac{perimeter}{4}}{\log N}$	$[1, 2]$	–
Gyration radius	This feature equals the average distance between each pixel position in one object and the object's centroid. The more similar to a circle is the object, the more likely the centroid will be inside it, and therefore this feature will be closer to 0.	$\frac{\sum_{i=1}^N pos_i - pos_C }{N}$	≥ 0	px
Length	It is the height of the object's bounding box.		≥ 0	px
Perimeter	It is the amount of pixels in the object's border.		≥ 0	px
Perimeter area ratio	Calculates the ratio between the perimeter and the area of an object.	$\frac{perimeter}{N}$	≥ 0	px^{-1}
Rectangular fit	This feature fits a minimum rectangle outside the object and calculates the ratio between its area and the area of this rectangle. The closer to 1 is this feature, the most similar to a rectangle.		$[0, 1]$	–
Width	It is the width of the object's bounding box.		≥ 0	px

SOURCE: Some features are adapted from McGarigal (2002).

Table A.3 - Landscape-based features. When the unit is hectares, the value is divided by 10^4 .

Name	Description	Formula	Range	Unit
Class area	The metric <i>CA</i> means the sum of areas of a cell.	$\sum_{j=1}^n a_j$	≥ 0	ha
Percent land	% <i>Land</i> equals the sum of the areas (m^2) of all patches of the corresponding patch type, divided by total landscape area (m^2). % <i>Land</i> equals the percentage the landscape comprised of the corresponding patch type.	$\frac{\sum_{j=1}^n a_j}{A} \times 100$	$[0, 1]$	%
Patch density	<i>PD</i> equals the number of patches of the corresponding patch type divided by total landscape area.	$\frac{n}{A}$	≥ 0	Patches
Mean patch size	<i>MPS</i> equals the sum of the areas (m^2) of all patches of the corresponding patch type, divided by the number of patches of the same type.	$\frac{\sum_{j=1}^n a_j}{n} 10^{-4}$	≥ 0	ha
Patch size std	<i>PSSD</i> is the root mean squared error (deviation from the mean) in patch size. This is the population standard deviation, not the sample standard deviation.	$\sqrt{\frac{\sum_{j=1}^n (a_j - MPS)^2}{n}} 10^{-4}$	≥ 0	ha
Landscape shape index	<i>LSI</i> equals the sum of the landscape boundary and all edge segments (m) within the boundary. This sum involves the corresponding patch type (including borders), divided by the square root of the total landscape area (m^2).	$\frac{\sum_{j=1}^n e_j}{2\sqrt{\pi \times A}}$	≥ 1	–
Mean shape index	<i>MSI</i> equals the sum of the patch perimeter (m) divided by the square root of patch area (m^2) for each patch of the corresponding patch type.	$\frac{\sum_{j=1}^n \frac{j}{2\sqrt{\pi \times a_j}}}{n}$	≥ 1	–
Area-weighted mean shape index	<i>AWMSI</i> equals the sum, across all patches of the corresponding patch type, of each patch perimeter (m) divided by the square root of patch area (m^2).	$\sum_{j=1}^n \left[\frac{j}{2\sqrt{\pi \times a_j}} \times \frac{a_j}{\sum_{j=1}^n a_j} \right]$	≥ 1	–
Edge density	<i>ED</i> equals the sum of the lengths (m) of all edge segments involving the corresponding patch type, divided by the total landscape area (m^2).	$\frac{\sum_{j=1}^n e_j}{A} \times 10000$	≥ 0	m/ha
Mean perimeter area ratio	<i>MPAR</i> equals the sum of ratios between perimeters and areas, divided by the number of patches of the same type.	$\frac{\sum_{j=1}^n \frac{j}{a_j}}{n}$	≥ 0	m^{-1}
Patch size coefficient of variation	<i>PSCOV</i> calculates the ratio between the "Patch Size Standard Deviation" and the "Mean Patch Size".	$\frac{PSSD}{MPS} \times 100$	≥ 0	–

SOURCE: Some features are adapted from McGarigal (2002).

Table A.4 - Temporal features for describing cyclic events.

Name	Type	Description	Range
Amplitude	Basic	The difference between the cycle's maximum and minimum values. A small amplitude means a stable cycle.	$[0, 1]$
Angle	Basic	The main angle of the closed shape created by the polar visualization. A small angle defines a shape possibly stable along the seasons, whereas different angles point to EVI peaks in a specific season.	$[0, \pi]$
Area	Polar	Area of the closed shape. A higher value indicates a cycle with high EVI values.	≥ 0
Area per Season	Polar	Partial area of the closed shape, proportional to a specific quadrant of the polar representation. High value in the summer season can be related to the phenological development of a cropland.	≥ 0
Circle	Polar	Returns values close to 1 when the shape is more similar to a circle. In the polar visualization, a circle means a constant feature.	$[0, 1]$
Cycle's maximum	Basic	Maximum value of the cycle. Relates the overall productivity and biomass, but it is sensitive to false highs and noise.	$[0, 1]$
Cycle's mean	Basic	Average value of the curve along one cycle.	$[0, 1]$
Cycle's minimum	Basic	Minimum value of the curve along one cycle.	$[0, 1]$
Cycle's std	Basic	Standard deviation of the cycle's values.	≥ 0
Cycle's sum	Basic	When using vegetation indices, the sum of values over a cycle is an indicator of the annual production of vegetation.	≥ 0
Eccentricity	Basic	Return values close to 0 if the shape is a circle and 1 if the shape is similar to a line.	$[0, 1]$
First slope maximum	Basic	Maximum value of the first slope of the cycle. It indicates when the cycle presents some abrupt change in the curve. The slope between two values relates the fastness of the greening up or the senescence phases.	$[-1, 1]$
Gyration radius	Polar	Equal to the average distance between each point inside the shape and the shape's centroid. The more similar to a circle is the shape, the more likely the centroid will be inside it, and therefore this feature will be closer to 0.	≥ 0
Polar balance	Polar	The standard deviation of the areas per season, considering the 4 seasons. A small value can point to a constant cycle, such as the EVI of water (with a small value of Area), or forest (with a medium value of Area).	≥ 0

PUBLICAÇÕES TÉCNICO-CIENTÍFICAS EDITADAS PELO INPE

Teses e Dissertações (TDI)

Teses e Dissertações apresentadas nos Cursos de Pós-Graduação do INPE.

Manuais Técnicos (MAN)

São publicações de caráter técnico que incluem normas, procedimentos, instruções e orientações.

Notas Técnico-Científicas (NTC)

Incluem resultados preliminares de pesquisa, descrição de equipamentos, descrição e ou documentação de programas de computador, descrição de sistemas e experimentos, apresentação de testes, dados, atlas, e documentação de projetos de engenharia.

Relatórios de Pesquisa (RPQ)

Reportam resultados ou progressos de pesquisas tanto de natureza técnica quanto científica, cujo nível seja compatível com o de uma publicação em periódico nacional ou internacional.

Propostas e Relatórios de Projetos (PRP)

São propostas de projetos técnico-científicos e relatórios de acompanhamento de projetos, atividades e convênios.

Publicações Didáticas (PUD)

Incluem apostilas, notas de aula e manuais didáticos.

Publicações Seriadas

São os seriados técnico-científicos: boletins, periódicos, anuários e anais de eventos (simpósios e congressos). Constam destas publicações o Internacional Standard Serial Number (ISSN), que é um código único e definitivo para identificação de títulos de seriados.

Programas de Computador (PDC)

São a seqüência de instruções ou códigos, expressos em uma linguagem de programação compilada ou interpretada, a ser executada por um computador para alcançar um determinado objetivo. Aceitam-se tanto programas fonte quanto os executáveis.

Pré-publicações (PRE)

Todos os artigos publicados em periódicos, anais e como capítulos de livros.